

Topical Review

The processing and properties of bulk (RE)BCO high temperature superconductors: current status and future perspectives

Devendra K Namburi , Yunhua Shi  and David A Cardwell* 

Department of Engineering, University of Cambridge, Cambridge CB2 1PZ, United Kingdom

E-mail: dc135@cam.ac.uk

Received 12 August 2020, revised 15 October 2020

Accepted for publication 21 January 2021

Published 26 March 2021



CrossMark

Abstract

Bulk (RE)–Ba–Cu–O [(RE)BCO] cuprate HTS have been developed steadily towards a wide range of sustainable engineering and technological applications since their discovery in 1986 based primarily on their unique potential to trap very large magnetic fields (>5 T) at temperatures that are accessible potentially by thermo-electric cooling techniques. Trapped fields of ~10 T at the surface of individual (RE)BCO bulk single grains and in excess of 17 T in a reinforced two-sample stack are now being achieved reliably. This paper reviews the current state of the art of the processing of large, single grain (RE)BCO bulk superconductors required to trap fields of this magnitude, and specifically via two advanced fabrication approaches; the traditional TSMG process and the more recently developed TSIG technique. The focus of the review is on optimising the critical processing parameters to achieve high-quality, high performance single grain (RE)BCO bulk superconductors specifically for high-field applications. The review also summarises recent advances in processing, such as the integration of the so-called buffer technique into the TSMG and TSIG processing methodologies to achieve improved reliability in single grain growth with a success rate exceeding 90%, the development of a Mg-doped NdBCO generic seed crystal for the successful growth of all rare-earth and light-rare earth based bulk superconductors [(RE)BCO and (LRE)BCO] and the introduction of nano-size stable, non-superconducting phase(s) to the bulk microstructure to improve the intrinsic flux pinning strength of the material, and hence trapped magnetic field. Details of the two-step buffer-aided TSIG technique developed recently that yields dense, near-net shaped, high performance (RE)BCO bulk superconductors with improved superconducting and mechanical properties are also presented. Suitable sample-seed configurations for effective multi-seeding are discussed, which enables the production of high aspect ratio, bar-shaped (RE)BCO quasi-single grains that exhibit improved levitation forces required in Maglev-based applications, for example, are discussed. The electrical, mechanical, microstructural and

* Author to whom any correspondence should be addressed.



Original content from this work may be used under the terms of the [Creative Commons Attribution 4.0 licence](https://creativecommons.org/licenses/by/4.0/). Any further distribution of this work must maintain attribution to the author(s) and the title of the work, journal citation and DOI.

magnetic properties (including those achieved from a pulsed-field magnetisation approach) of the different (RE)BCO systems are presented and the relevant correlation in properties and performance highlighted, accordingly. Finally, a brief summary of existing applications and prospects for near-future exploitation of these remarkable, technologically important materials, and particularly in the medical and pharma-industries, is provided.

Keywords: (RE)BCO bulk superconductor, single grain growth, superconducting properties, trapped field, microstructure, mechanical properties

(Some figures may appear in colour only in the online journal)

Contents

1. Introduction	3
1.1. Superconductivity: basic concepts	4
1.2. Phase diagram, peritectic temperature and flux pinning	5
2. Practical and economic processing of (RE)BCO for engineering applications	6
2.1. Fabrication techniques based on MG: TSMG	6
2.2. Seeding	7
2.3. Isothermal vs undercooling—growth rate studies and misorientation studies	8
2.4. Growth rate studies	9
2.5. BA-TSMG	12
2.6. Generic seed crystals and the suppression of solid solution formation	13
2.7. Growth of mixed binary and ternary RE-systems (YGd, NSG, NEG, YSN)	13
2.8. Infiltration growth strategy	14
2.9. Flux pinning in (RE)BCO—peak effect	18
2.10. Multi-seeding (0–0, 45–45) and interior seeding	20
2.11. Reliability in growth, batch processing, commercial production and recycling techniques	21
3. Microstructure and properties	23
3.1. Influence of microstructure on the properties of (RE)BCO	23
3.2. Other microstructure-related studies	26
3.3. Electrical properties	28
3.4. Magnetic properties	29
3.5. Mechanical properties	32
4. Applications of (RE)BCO bulk superconductors	35
4.1. Static/dynamic applications	35
4.2. Medical-based applications	36
4.3. Shielding based applications	37
5. Superconducting wires, magnets and joining techniques	39
5.1. Superconducting wires and tapes	39
5.2. Superconducting magnets	40
5.3. Superconducting joints	41
6. Summary and conclusions	41
References	42

Acronyms—expansions and symbols, as they appear in the article

TSMG	top seeded melt growth
TSIG	top-seeded infiltration and growth
HTS	high temperature superconductors
H_{irr}	irreversibility field
(RE)BCO	RE–Ba–Cu–O
T_c	critical temperature
J_c	critical current density
H_c	critical magnetic field
λ	penetration depth
ξ	coherence length
κ	Ginzburg–Landau parameter
BCS theory	Bardeen–Cooper–Schrieffer theory
Y-211	Y_2BaCuO_5
Y-123	$\text{YBa}_2\text{Cu}_3\text{O}_{7-\delta}$
T_p	peritectic temperature
QMG	quench melt growth
MPMG	melt powder melt growth
OCMG	oxygen controlled melt growth
MG	melt growth
RE-123	$\text{REBa}_2\text{Cu}_3\text{O}_{7-\delta}$
RE-211	$\text{RE}_2\text{BaCuO}_5$
IG	infiltration and growth
T_{max}	maximum processing temperature
T_{iso}	isothermal temperature
T_{g1}	growth start temperature
T_{g2}	growth final temperature
T_g	growth temperature
R or R^*	single-grain growth rate
ΔT	undercooling temperature
L	single grain length
R_a	single grain growth rate along a/b -axis
R_c	single grain growth rate along c -axis
Y-2411	$\text{Y}_2\text{Ba}_4\text{Cu}_1\text{M}_1\text{O}_y$
t_s and t_f	are the growth time(s) associate with start and end of the continuous cooling period, respectively
R_{cc}	single grain growth rate during continuous cooling
R_{ih}	single grain growth rate during isothermal hold period
CCIH	continuous cooling and isothermal holding
BA-TSMG	buffer-assisted top-seeded melt-growth
(NSG)BCO	$(\text{Nd,Sm,Gd})_1\text{Ba}_2\text{Cu}_3\text{O}_7$
(NEG)BCO	$(\text{Nd,Eu,Gd})_1\text{Ba}_2\text{Cu}_3\text{O}_7$
(SEG)BCO	$(\text{Sm,Eu,Gd})_1\text{Ba}_2\text{Cu}_3\text{O}_7$
(YSN)BCO	$(\text{Y,Sm,Nd})_1\text{Ba}_2\text{Cu}_3\text{O}_7$
(YGd)BCO	$(\text{Y}_{0.5}\text{Gd}_{0.5})_1\text{Ba}_2\text{Cu}_3\text{O}_7$
LA-TSMG	liquid-assisted top-seeded melt growth
I_c	critical current
APC	artificial pinning centres
TEM	transmission electron microscopy
$J_c(H)$	field dependence of J_c
B_t	trapped field
H_p	peak field
Φ_0	flux quantum ($=h/2e$)
h	Planck's constant ($6.62 \times 10^{-34} \text{ m}^2 \text{ kg s}^{-1}$)
e	charge of electron ($1.6 \times 10^{-19} \text{ C}$)

a_f	Vortex lattice spacing
F_d	drag force
F_i	interfacial force
$\Delta\sigma_o$	interfacial energy
$\Delta\sigma_{\text{SP}}$	surface energy at the solid/particle interface
$\Delta\sigma_{\text{LP}}$	surface energy at the liquid/particle interface
$\Delta\sigma_{\text{SL}}$	surface energy at the solid/liquid interface.
r^*	critical size of the RE-211 particle
η	viscosity of the melt
ρ	electrical resistivity
FC	field-cooling
ZFC	zero-field cooling
PFC	pulsed-field cooling
PFM	pulsed field magnetisation
σ	tensile stress
B_0	maximum trapped field in the sample
μ_0	permeability of space/vacuum permeability ($4\pi \times 10^{-7} \text{ H m}^{-1}$)
Gd210	Gd_2BaO_4
RT	room temperature
K_{IC}	fracture toughness
LNT	liquid nitrogen temperature
MRI	magnetic resonance imaging
NMR	nuclear magnetic resonance
MAGLEV	magnetic levitation
LTS	low temperature superconductor
F	magnetic force
B	magnetic induction
F_L	Lorentz force
U	mean flow velocity of the liquid/fluid
V	Characteristic volume.
SF	shielding factor
B_{lim}	threshold induction or limiting field
B_{appl}	applied magnetic field
B_{in}	induced field
RABiTS	rolling-assisted biaxially textured substrate
MOCVD	metal-organic chemical-vapor deposition
PLD	pulsed laser deposition
LHC	Large Hadron Collider
ITER	international thermonuclear experimental reactor
FCC	future circular colliders
SAED	selected area electron diffraction

1. Introduction

HTS fabricated in the form of large, single grain bulk samples have the potential to carry large macroscopic currents and therefore to generate some of the largest magnetic fields ever recorded in the history of the planet. This makes these technologically important materials particularly attractive for wide variety of engineering applications, including trapped field magnets, flywheel energy storage, magnetic separation and compact motors and generators [1]. The magnetisation of bulk, single grain superconductors scales with sample volume, unlike conventional permanent magnet materials, such as Sm–Co or Nd–Fe–B, for which magnetisation is generally independent of sample size. As a result, the larger the single grain

and the higher its current carrying ability, the greater the magnitude of magnetic field the material can trap. Furthermore, and interestingly, the potential of a bulk superconductor for trapping magnetic field increases significantly as temperature is reduced due to its enhanced associated superconducting properties. One key figure of merit that determines generally the overall potential of a superconducting material for practical applications at a given temperature, and particularly in the presence of applied magnetic field, is its so-called irreversibility field, H_{irr} . The temperature dependence of H_{irr} , $H_{\text{irr}}(T)$, is referred to conventionally as the ‘irreversibility line’. The irreversibility lines for a selection of high-temperature superconductors are shown in figure 1, which shows clearly that (RE)–Ba–Cu–O ((RE)BCO, where RE is a rare earth element or Y) materials are operable practically at LNTs (77 K) and offer a significant performance advantage over other HTS materials [2]. This review focusses on the processing, properties and applications of bulk high temperature superconducting materials with a particular emphasis on the (RE)BCO family of superconductors.

1.1. Superconductivity: basic concepts

Superconductivity, which was first discovered in mercury [3] by the Dutch Physicist Heike Kammarlingh-Onnes in 1911 at 4.2 K, is now observed in many thousands of metals and alloys [4–6]. A material is classed as superconducting if it exhibits two basic properties; zero resistance to the flow of dc electrical current and complete magnetic flux expulsion at low magnetic fields, leading to perfect diamagnetism (the latter is known as the Meissner effect). The superconducting state is known to exist below certain thermodynamic limits defined by T_c , J_c , and H_c . The quest to enhance the magnitude of these critical parameters, and therefore to improve the potential for practical applications employing superconducting materials in their various forms has been on-going since their discovery more than 100 years ago.

Superconductors, in general, are classified as either type-I or type-II based on their intrinsic properties such as magnetic λ and ξ . In practice, the ratio $\frac{\lambda}{\xi}$, referred to as Ginzburg–Landau parameter and denoted as ‘ κ ’, determines the class into which superconductors fall. Typically, if $\kappa > \frac{1}{\sqrt{2}}$ then the material is classified as type-II, otherwise it is type-I. Typical values of T_c , H_c , λ and ξ of some type-I and type-II superconducting materials are shown in table 1, with other basic properties of superconducting materials reported elsewhere [7–9]. The evolution with time of the discovery of various superconducting materials with respect to T_c is shown in figure 2.

Prior to 1986, the compound Nb_3Ge exhibited the maximum T_c of 23 K [11] of any known superconductor, which is consistent with the limit of the popular and successful Bardeen–Cooper–Schrieffer theory (the so-called BCS theory) [12]. The discovery of superconductivity in the barium-lanthanum-cuprate oxide system by Bednorz and Müller in 1986 [13] with a relatively high T_c of ~ 33 K, however,

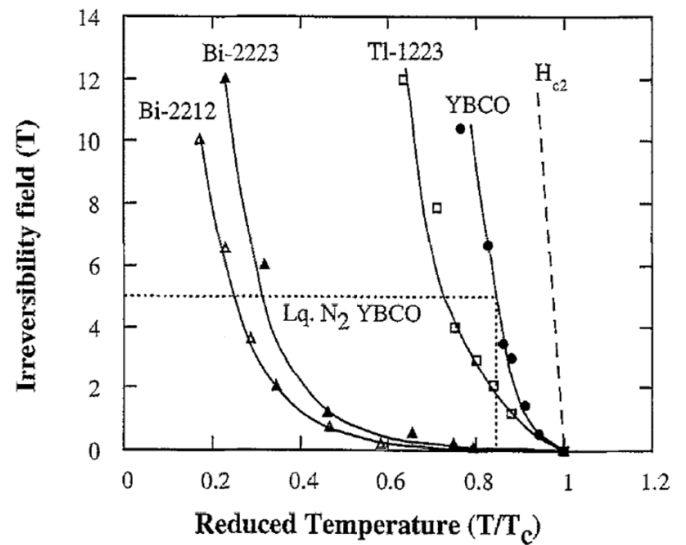
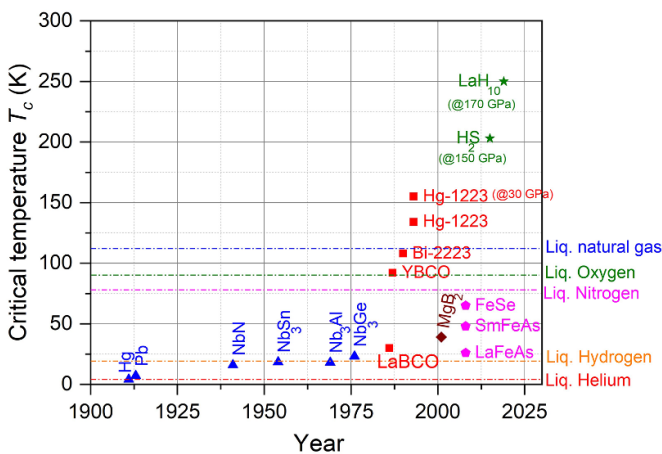


Figure 1. H_{irr} as a function of reduced temperature ‘ T/T_c ’ (i.e. the so-called irreversibility line) for selected high-temperature superconducting materials [2]. Here T_c indicates critical temperature. Reprinted from [2], with the permission of IOP Publishing.

exceeded significantly the theoretical BCS limit and produced great excitement broadly within the fields of physics, chemistry and applied science. Soon after this discovery, in 1987, Wu *et al* [14] observed superconductivity in the $\text{YBa}_2\text{Cu}_3\text{O}_{7-\delta}$ (YBCO or Y-123) system with $T_c \sim 92$ K, which formed a very important step forward, since, significantly, this material was the first to exhibit superconductivity above 77 K, the boiling point of liquid nitrogen. Hg-1223 with a T_c as high as 153 K (and 163 K under pressure), H_2S with a T_c approaching 200 K (under a pressure of 150 GPa) and LaH_{10} with T_c as high as 250 K (again, under a pressure of 170 GPa) have emerged subsequently with even higher superconducting temperatures [15, 16]. In parallel, new superconducting systems, described as intermediate superconductors with T_c in the range 30 K–60 K, including MgB_2 [17] and several Fe-based materials (LaFeAs , SmFeAs , FeSe and more) [18–20], have emerged over the last two decades that are fascinating from physics point of view and are being researched further to explore their suitability for applications. Detailed reviews on these topics can be found elsewhere [21, 22]. To date (2020) as many as seven Nobel Prizes have been awarded for different aspects of superconductivity, from the discovery of superconductivity to their application (including Josephson junctions [23]), which is unprecedented in field of applied science. In the present review, we will present mainly the various processing, characterisation and applied properties of rare-earth based bulk, HTS cuprate materials. Of particular focus will be the processing of these materials into large, single grains by techniques based on melt-growth and infiltration-growth, which will be described in detail. Recent

Table 1. Characteristic parameters of some type-I and type-II superconducting materials.

Category	Material	Critical temperature T_c (K)	Critical field H_c (T)	Coherence length ξ_0 (nm)	Penetration depth λ_0 (nm)	
Type-I superconductors	Al	1.2	0.01	1600	16	
	In	3.4	0.03	400	25	
	Sn	3.7	0.03	300	28	
	Pb	7.2	0.08	110	37	
	Nb	9.3	0.2	38	85	
Type-II conventional superconductors	NbTi	10	11	6	300	
	V ₃ Ga	15	23	3	90	
	NbN	15.7	15	6.5	200	
	V ₃ Si	16	20	3	60	
	Nb ₃ Sn	18	26	4	50	
	Nb ₃ Al	17.5	32.4	4		
	Nb ₃ Ge	23.2	38	3	90	
	LaBCO	30	65	1.5		
Type-II non-conventional high-temperature superconductors	YBa ₂ Cu ₃ O _{7-x} (Y-123)	92	120	ξ_{a-b} : 2 ξ_c : 0.4	150 800	
	Bi ₂ Sr ₂ Ca ₂ Cu ₃ O ₁₀ (Bi-2223)	110	100	1.4	200	
	TlBCCO	125	33	ξ_{a-b} : 8 ξ_c : 280	220	
	MgB ₂	39	40	ξ_{a-b} : 4–12 ξ_c : 1.6–3.6	85–180	
	H ₂ S	T_c : 200 K (under a pressure of 150 GPa)				
	LaH ₁₀	T_c : 250 K (under a pressure of 170 GPa)				

**Figure 2.** Discovery of superconductors with increasing T_c as a function of time (inspired from [10]). The cuprate-based HTS that are the prime focus in this review are indicated by the squares (red, online).

developments in these fabrication methodologies will be summarised with the important results highlighted on a (RE)BCO material-by-material basis. Finally, the superconducting and mechanical properties of bulk (RE)BCO superconductors fabricated by these techniques and the potential pathways for their practical application will be presented.

1.2. Phase diagram, peritectic temperature and flux pinning

The rich information contained within the relevant phase diagram provides an easy path, not only to understanding the

phase kinetics of the relatively complex (RE)BCO system, but also for formulating a compositional route for the growth of individual single grains by a variety of available melt-growth processing techniques. Details of the complex ternary phase diagrams for different (RE)BCO compositions have been described previously in several reports [24–27]. Here, we provide only a broad and general overview of the use of phase diagrams for materials processing purposes for readers new to this field in order to aid understanding of the (RE)BCO system and to inform subsequent discussion. Further details and understanding of the (RE)BCO phase diagrams can be found in the above references.

The thermodynamic behaviour of YBCO has been studied extensively from equilibrium phase diagrams for the Y₂O₃–BaO–CuO_x system over a broad temperature range. In particular, a pseudo-binary phase diagram has been developed based on the solidification of different phases in the system (YBa₂Cu₃O_{7- δ} (Y-123), Y₂BaCuO₅ (Y-211) and BaCuO₂–CuO) at different temperatures, which has provided an insight into, and appreciation of, fine-tuning of the parameters that then enable the single grain growth of YBCO via different melt-growth techniques. The oxygen partial pressure is known to influence strongly the phase diagram of oxide, with particular emphasis on the SmBCO and NdBCO systems, within which LRE/Ba solid solutions can form easily due to the comparability of the sizes of the RE and Ba ions. The pseudo-binary phase diagram for YBCO is shown in figure 3(a), which indicates the temperature window for liquid phase formation and provides information on the peritectic temperature in the phase region where Y-123 melts incongruently to form Y-211 and a liquid phase. This reversible reaction also provides valuable information of when to seed the system

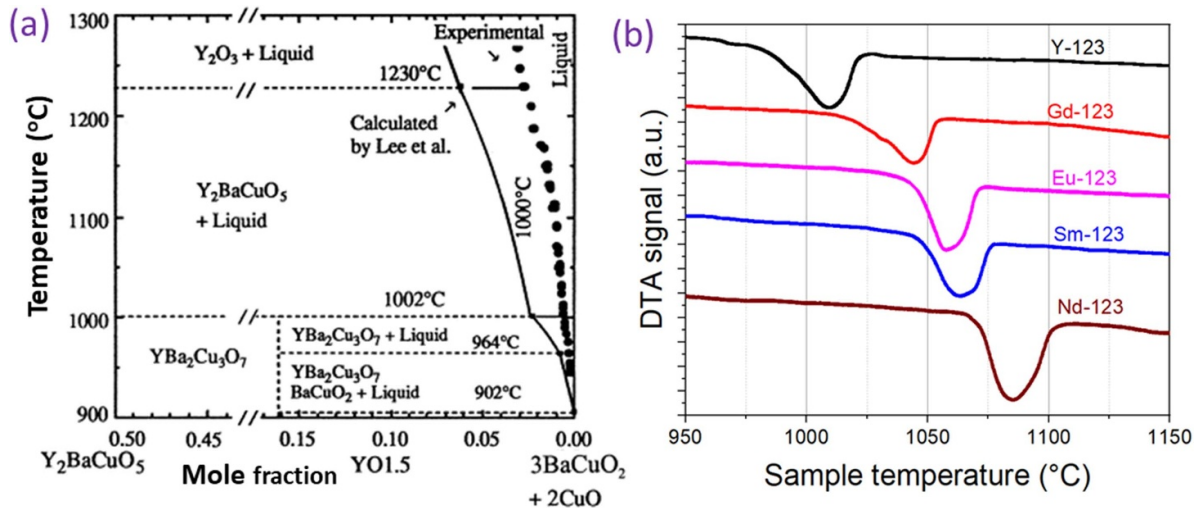


Figure 3. Pseudo-binary phase diagram of the YBCO system providing information on the peritectic temperature of the compound and on fine-tuning the heat treatment parameters to obtain a single grain of YBCO, by a controlled seeding process. The isothermal line, reaction zone and the liquidus line can also be seen in the figure. Reprinted from [29], with the permission of Elsevier. (b) DTA scans of some of the cuprate-based high temperature superconducting materials exhibiting a peritectic temperature.

Table 2. Peritectic temperatures of various rare-earth based (RE)BCO superconductors, measured in air.

RE in (REBa ₂ Cu ₃ O _{7-δ)}	Peritectic temperature T_p (°C) (error: ± 5 °C)
Nd	1068
Sm	1054
Eu	1046
Gd	1030
Dy	1010
Y	1005
Dy	1005
Er	990
Yb	960

(as in the so-called hot-seeding approach) to enable heterogeneous nucleation and to fine-tune the heat treatment conditions to enable the growth of a single grain. Lee and Lee [28], carried out experiments and studied liquidus line formation in the Y₂O₃–BaO–CuO_x system at 1223 K and 1273 K at 0.21 atm oxygen pressure. DTA thermal scans showing the decomposition temperatures of some of the cuprate-based materials are shown in figure 3(b). Finally, the T_p , for (RE)BCO compounds are summarised in table 2.

2. Practical and economic processing of (RE)BCO for engineering applications

The ability of a bulk superconductor to trap a large magnetic field is determined generally by the product of the critical current density, J_c , and the length-scale over which the current flows (usually the sample grain size ' d '), $J_c d$ [1, 2]. It is essential, therefore, that (RE)BCO is processed in the form a large, single grain with a uniform, high J_c if it to be used in practical

applications, with state of the art (RE)BCO materials exhibiting current densities in excess of 10 000 A cm⁻² at 77 K and single grain sizes of up to 6 cm. Extensive work was carried out between 1987 and 2003 to fabricate (RE)BCO bulk superconductors as individual single grains. As a result, a variety of successful melt processing techniques had been developed by 2003, with the thermal profiles for the different systems almost fully optimised, albeit under a reduced-oxygen atmosphere, and particularly for Sm and Gd based (RE)BCO compositions. A detailed account of the processing of (RE)BCO bulk, single grain superconductors prior to 2003 can be found in several publications, including review articles and handbook chapters [30–33]. This review article addresses primarily the development of the processing of (RE)BCO single grains since 2003, during which substantial progress has been made towards the reliable growth of bulk (RE)BCO superconductors with increased trapped field and processed, more practically, under an air atmosphere.

2.1. Fabrication techniques based on MG: TSMG

Bulk (RE)BCO HTS tend to be granular in nature, with their current carrying capacity limited severely by the weak-link nature of any grain boundaries and the presence of pores and other macro-defects present in the sample microstructure. To overcome the grain boundary problem, concerted attempts have been made to develop a number of effective melt processing routes, including QMG [34], MPMG [35], OCMG [36] and TSMG [37] to transform the entire sample into one large, single grain. TSMG has emerged over the past two decades as the most practical and successful process for the fabrication of (RE)BCO single grains that can support current densities in excess of 10 000 A cm⁻² at 77 K (note this current-carrying ability is enhanced further at lower temperatures).

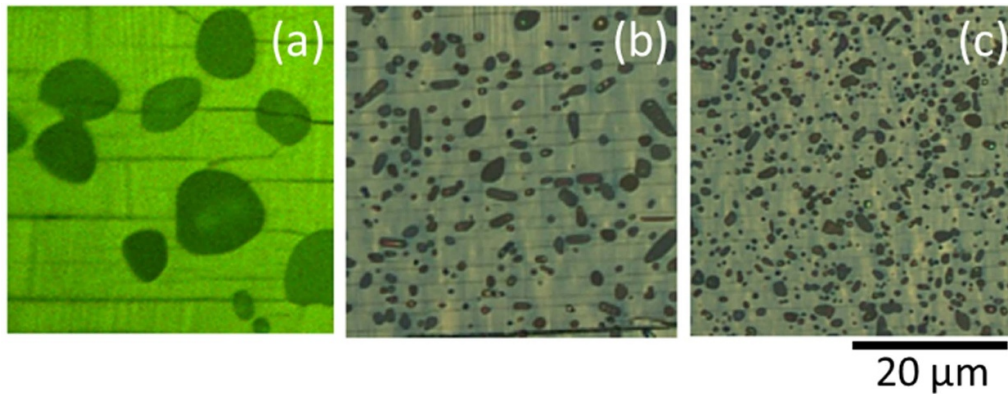
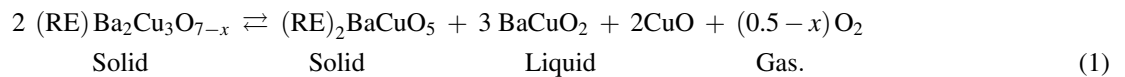


Figure 4. The influence of grain-refining agents on the bulk (RE)BCO single grain microstructure. (a) Standard SmBCO with no added grain-refiner, (b) SmBCO containing added Pt and (c) SmBCO containing added CeO₂. The micrographs show the presence of Sm-211 inclusions in a superconducting Sm-123 phase matrix. CeO₂ has emerged as a more effective Sm-211 grain-refining agent than Pt for the SmBCO system. Images in this figure are reprinted from [44], with necessary permissions.



The use of a seed crystal to control heterogeneous grain nucleation and growth can be used further to reduce substantially the number of grain boundaries formed during the MG process. The pre-form compact for the TSMG fabrication route, or green body, is prepared using precursor powder comprised mainly of RE-123 enriched with added RE-211 to constitute a mixture corresponding typically to RE-123: RE-211 ~ 75: 25 by weight. A seed crystal (of higher melting temperature, such as NdBCO or SmBCO for YBCO) is used to nucleate and grow a single grain of (RE)BCO. The addition of RE-211 to the RE-123 precursor powder prior to melt processing serves three purposes:

- To provide a greater concentration of RE-flux at the growth-front to propagate growth more rapidly;
- To minimise the out-flow of liquid phase during the precursor melting stage and;
- To provide extra RE-211 phase in the final, as-grown sample, which generates flux pinning centres and enhances the current density of the single grain (to be discussed later).

Various grain-refiners are also used in the TSMG process to refine the size and distribution of RE-211 inclusions within the final sample microstructure in order to optimise its superconducting properties and to increase microstructural

homogeneity. Pt and CeO₂ have emerged as successful grain-refining agents for YBCO, in particular. Of these, CeO₂ is significantly more cost-effective than Pt, which is important for the development of a large-scale production process. Microstructures of a typical single grain of SmBCO sample fabricated by TSMG are shown in figure 4. This figure illustrates the influence of grain refining agents on the size of RE-211 phase inclusions embedded within the superconducting RE-123 phase matrix (CeO₂ refines the Sm-211 phase efficiently compared to Pt in the case of SmBCO [44]).

2.2. Seeding

Seeding is a critical step for heterogeneous nucleation and single grain growth of (RE)BCO bulk superconductors via a melt process. The following three important characteristics qualify a material to function as an effective seed crystal, at least in the so-called cold seeding process:

- A higher melting temperature than the (RE)BCO system being grown into a single grain;
- A similar crystal structure to the material being fabricated and;
- Phase-stability with the melt.

Cleaved seed crystals either of the same system (as used in so-called hot seeding) or of systems with higher peritectic temperature (as used in so-called cold seeding) form the site where the single grain nucleation process occurs in the

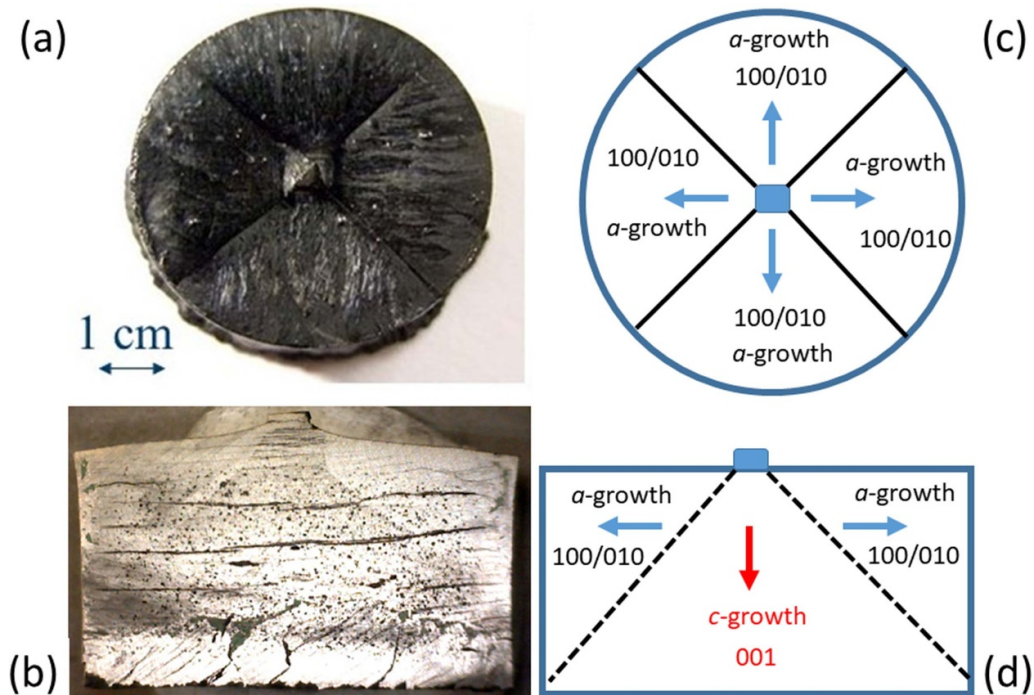


Figure 5. (a) The top surface of an YBCO single grain from which faceted growth can be seen clearly. Growth facet lines as observed experimentally in YBCO sample along the a - b plane and along the c -axis are shown in (a) and (b). These features are represented schematically in (c) and (d), respectively. Cross-sectional image in (b) is reprinted from [46], with necessary permission.

semi-molten, or peritectically-decomposed, (RE)BCO material. Cleaved seed crystals with perfect a - b crystallographic plane alignment are therefore employed to fabricate (RE)BCO bulk superconductors in the form of single grains. Both MG and IG techniques employ seed crystals to grow large, single grain, as will be discussed later. The influence of morphology and size of seed crystal on single grain growth via the TSMG process has been studied by Sudhakar Reddy *et al* [45]. It was observed that the use of small, square-shaped seed crystals to nucleate MG results characteristically in point nucleation with the usual habitual growth symmetry, whereas circular- and triangular-shaped seeds modify the initial growth sector geometry of the (RE)BCO single grain. The use of a large seed decreases significantly the processing time associated with single grain fabrication, although, on a microscopic scale, large-sized seeds are susceptible to containing numerous defects, which can cause the nucleation of unwanted sub-grains. Practical melt processes, therefore, use small, perfectly aligned seed crystals (with higher melting temperature) to obtain single grains of (RE)BCO. An example of a YBCO single grain fabricated using such a seed, with the growth directions marked schematically, is shown in figure 5.

2.3. Isothermal vs undercooling—growth rate studies and misorientation studies

TSMG processing usually involves two distinct heat-treatment techniques:

- (a) Isothermal decomposition and nucleation, and
- (b) Controlled undercooling.

The isothermal process involves cooling the system from the maximum temperature of the melt (T_{\max} , as illustrated schematically in figure 6(a)) to a temperature typically of $6\text{ }^{\circ}\text{C}$ – $10\text{ }^{\circ}\text{C}$ below the T_p of the target RE-123 phase. The system is then held at this temperature, T_{iso} , for between 100 and 150 h to enable the nucleated growth front to propagate and transform the entire sample into one single grain. In the undercooling process, on the other hand, the sample assembly is cooled slowly through the T_p of the compound (i.e. from the growth temperature T_{g1} to the growth temperature T_{g2}) until single grain growth is complete. Undercooling involves slow cooling the entire sample assembly at a rate typically between $0.2\text{ }^{\circ}\text{C h}^{-1}$ and $0.5\text{ }^{\circ}\text{C h}^{-1}$ from T_p to a temperature of about $25\text{ }^{\circ}\text{C}$ – $30\text{ }^{\circ}\text{C}$ below T_p . The combination of the various steps in the respective processes enables the growth of a single grain, although each has a unique influence on the microstructure and associated superconducting properties of the fully processed single grain. For example, the effects of crystallographic misorientation (small angle mis-alignments within an individual single grain) are typically more severe in samples processed using the undercooling approach. However, the number and density of pores and cracks generated by the undercooling technique is generally lower than that of the isothermal method. The undercooling technique also yields a finer and well distributed RE-211 phase within the superconducting RE-123 phase matrix, which is desirable for enhanced flux pinning, and is a particular strength of this approach. Hlášek *et al* [47] recently carried out a further comparison of these fabrication techniques; the characteristics of the two processes are illustrated in figure 6. TSMG based on the undercooling approach is now accepted generally as the preferred

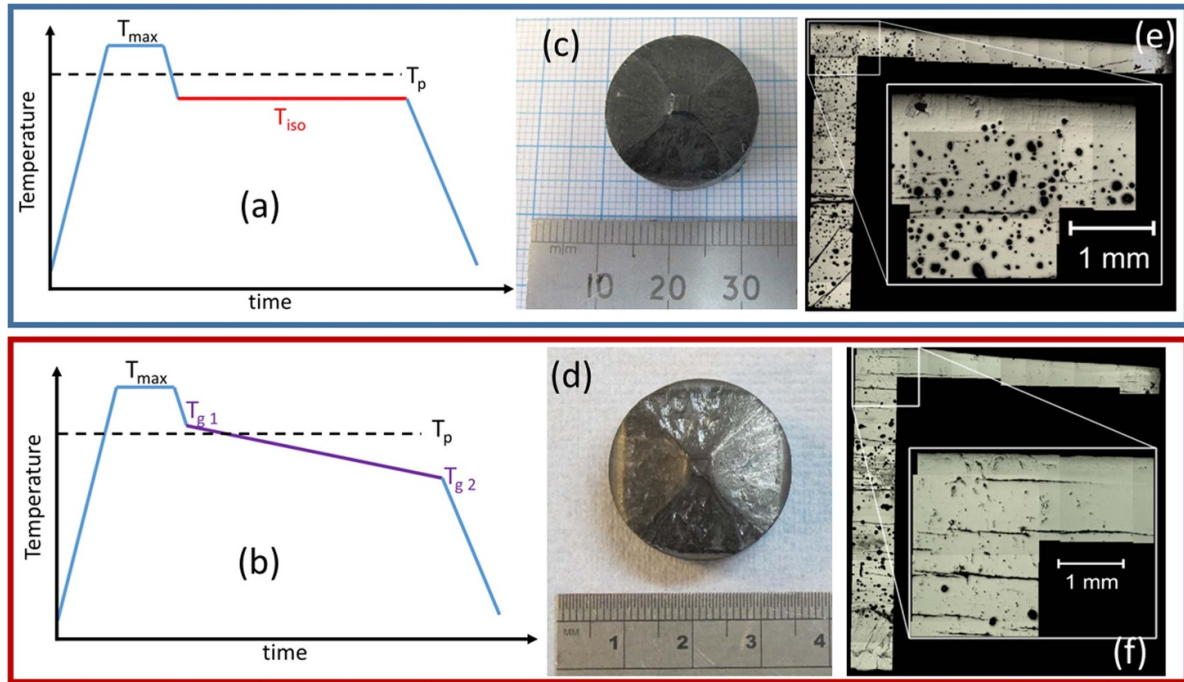


Figure 6. Schematic illustration of the heat profiles used to grow single grains of (RE)BCO via (a) isothermal and (b) undercooling approaches via TSMG. YBCO samples grown by these techniques are shown in (c) and (d), respectively. Optical micrographs obtained from the cross-sections of the samples in (c) and (d) are shown in (e) and (f). Images shown in (e) and (f) are reprinted from [47], with necessary permissions.

fabrication methodology for obtaining large, single-grain bulk superconductors with the best properties for practical applications.

2.4. Growth rate studies

Isothermal processing of bulk samples carried out at several temperatures with different dwell times provides a pathway to measuring the growth rate of the various (RE)BCO and (RE)BCO + Ag single grain systems. This information is fundamental to the formulation of appropriate and effective heat treatment profiles, both to enable single grain growth whilst, simultaneously, retaining the liquid phase component within the sample during undercooling via both TSMG and TSIG techniques. The growth rate ‘ R ’ is usually modelled by the expression $R = \alpha (\Delta T)^\beta$, where ΔT is the undercooling temperature and α , β are constants (i.e. fitting parameters). The growth rates along the a - b and a - c planes are very different due to the fact that the RE-123 phase is anisotropic. Experiments performed to date indicate that the growth rate along the ac -plane (referred to as R_a) and along the ab -plane (referred to as R_c) have produced values for R_a and R_c of $4.5 \times 10^{-7} (\Delta T)^{1.9} \text{ mm s}^{-1}$ and $2.8 \times 10^{-6} (\Delta T)^{1.3} \text{ mm s}^{-1}$ [29, 48]. Significantly, the growth rate of YBCO when additional Y-211 is added to the precursor powder increases from about 0.1 mm h^{-1} to $\sim 0.3 \text{ mm h}^{-1}$ at an undercooling temperature of 10°C [49]

(this rate is increased further at higher undercooling), as shown in figure 7.

Similar growth studies carried out for YBCO with specific phase additives to enhance flux pinning, such as Y_2O_3 and $\text{Y}_2\text{Ba}_4\text{Cu}_1\text{M}_1\text{O}_y$ (Y-2411) [50], also indicate an increase in the growth rate by ~ 0.1 – 0.2 mm h^{-1} at an undercooling temperature of 12°C , associated with the additional supply of Y-ions to the growth front, which aids the growth of the Y-123 phase. Determination of the growth rate is more complex for the YBCO + Ag system and resulted in the development of the CCIH approach adopted by Congreve *et al* [51] to measure growth rates for this system. In this, the growth length ‘ L ’ is determined from the following equation (equation (2)):

$$L = \int_{t_s}^{t_e} R_{cc} dt + R_{ih} t_{ih} \quad (2)$$

where t_s and t_e are the times associated with the start and end of the continuous cooling period, R_{cc} is the growth rate during continuous cooling and R_{ih} is the growth rate during the isothermal hold period. As a result, the growth rates for the YBCO + Ag system have been reported as:

$$R_a = 1.4 \times 10^{-3} (\Delta T)^{1.76} + 0.035 \text{ mm h}^{-1}$$

and

$$R_c = 4.5 \times 10^{-3} (\Delta T)^{1.42} + 0.035 \text{ mm h}^{-1}.$$

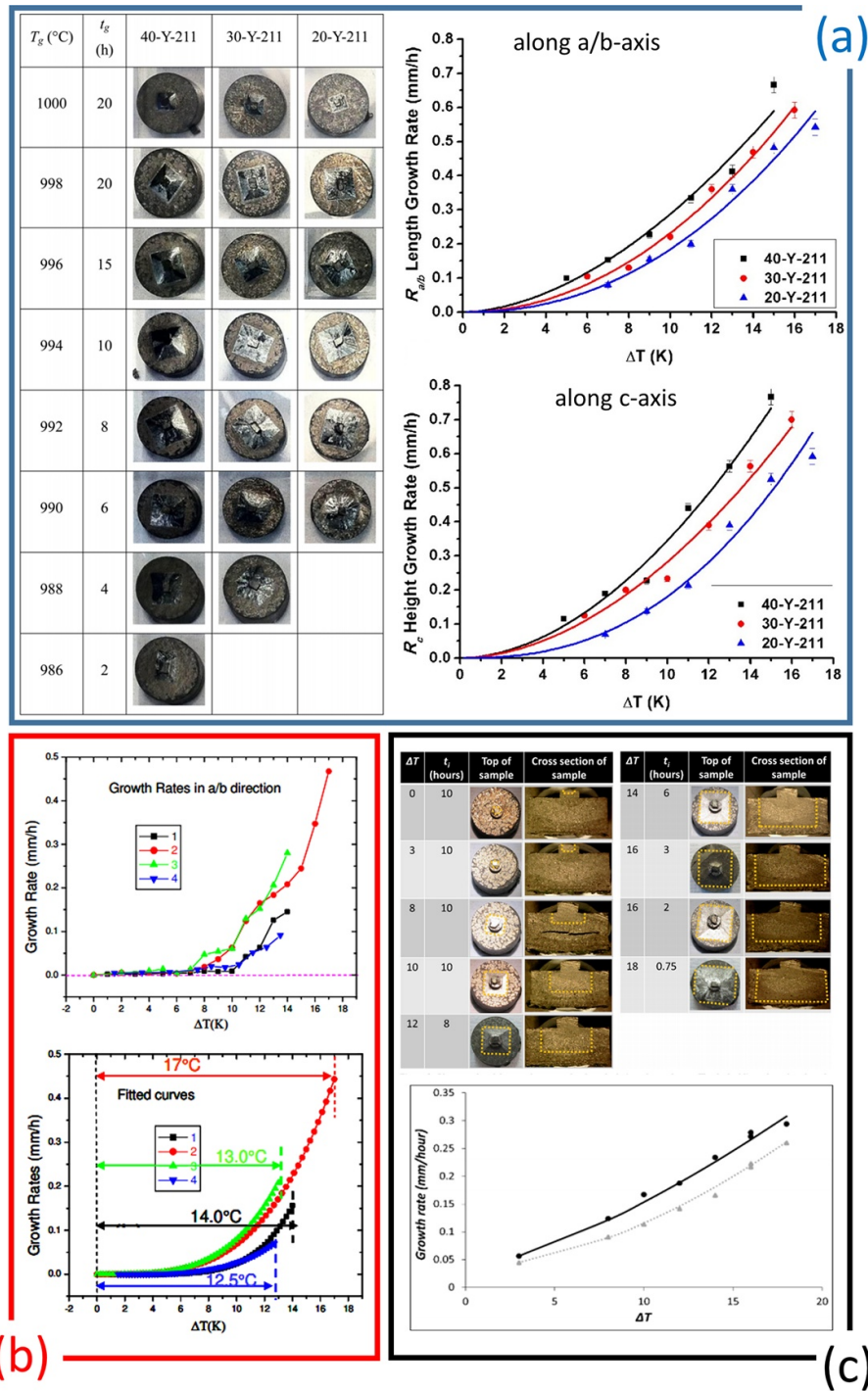


Figure 7. Growth rate studies of (a) YBCO with varying Y-211 (20%, 30% and 40%) content, (b) YBCO with different additives (Y_2O_3 and Y-2411) and (c) YBCO + Ag. Growth rates both along *a/b*- and *c*-axes are also shown. The nomenclature is as follows. In figure (a), T_g and t_g represent isothermal growth temperature and growth time (in hours). The corresponding growth lengths are measured and the growth rates plotted as a function of undercooling temperature (ΔT). In figure (b), the growth rates measured in the *a/b*-direction (both the experimental data and theoretical predictions) in YBCO bulk superconductors containing different phases namely Y-211, Y_2O_3 and Y-2411(M) are shown.

In this figure:

1 represents the composition: 1 mole Y-123 + 0.25 mole Y-211 + 0.1 wt% Pt,

2 represents the composition: 1 mole Y-123 + 0.25 mole Y_2O_3 + 0.1 wt% Pt,

3 represents the composition: 1 mole Y-123 + 0.25 mole Y_2O_3 + 0.1 wt% Pt + 4 wt% Y-2411 (M = Bi),

4 represents the composition: 1 mole Y-123 + 0.25 mole Y-211 + 0.1 wt% Pt + 4 wt% Y-2411 (M = Bi).

Images in this figures are reprinted from [49–51], with necessary permissions.

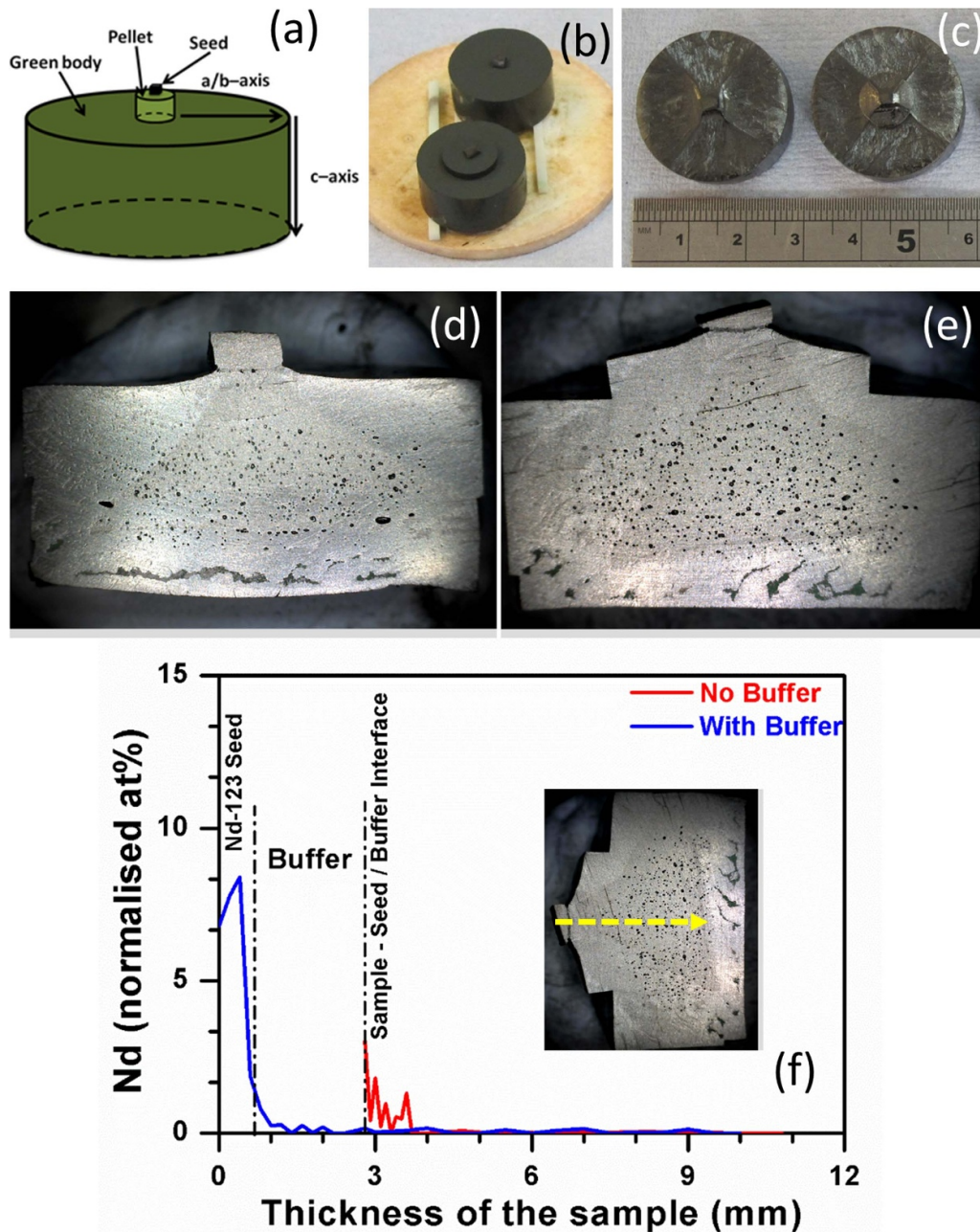


Figure 8. The sample-buffer arrangement for TSMG: (a) schematic illustration of the sample assembly, (b) sample assemblies with and without a buffer pellet and (c) the samples in (b) after TSMG growth. Figures (d) and (e) show the cross-sections of the samples processed by TSMG and BA-TSMG. Figure (f) shows EDX data confirming that the diffusion of the Nd-element from the seed crystal is limited to within the buffer pellet region. The direction, indicated with an arrow (yellow in colour), along the thickness of the sample where the EDX data is obtained and plotted are represented in the inset of (f). Images in this figure are reprinted from [57], with necessary permissions.

Based on the results of these growth studies, it was concluded that the growth rate is higher but often exhibits undesirable steps at the growth front if the sample assembly is subjected to large undercooling (i.e. greater ΔT). Hence, the processing temperatures are usually selected to produce a moderate growth rate and improved crystallinity at the propagating growth front. Any residual un-solidified component of the sample during melt processing transforms

typically into a solid via a spheroidal growth process [52]. The growth rates were also used to inform the configuration of the sample assembly. For example, as observed in the interior seeding approach [53], the growth rate along the c -direction was found to be higher than that along the a -direction during the initial growth step. However, these growth rates reversed as the sample grew larger. It should also be emphasised that the presence of impurities or unwanted defects in the precursor

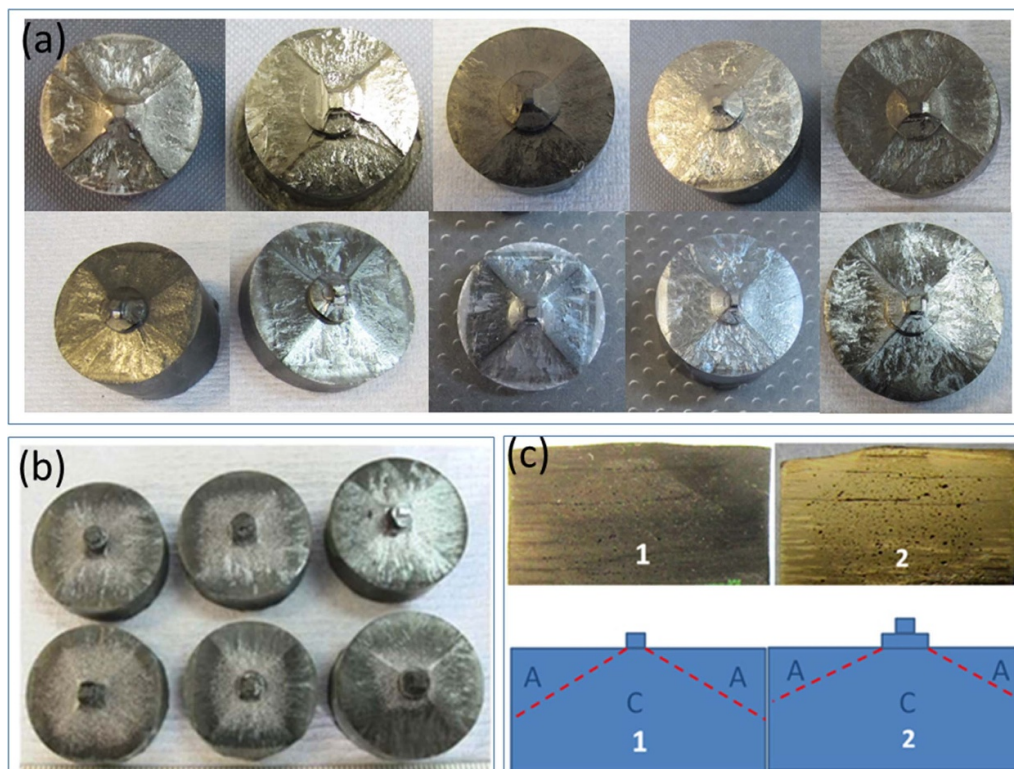


Figure 9. (RE)BCO single-grain bulk superconductors obtained via the BA-TSMG process. (a) YBCO and (b) GdBCO + Ag, (c) optical micrographs of the GdBCO + Ag sample cross-sections taken within the extended c -growth regions are shown schematically in (c). Images in this figure are reprinted from [57, 58], with necessary permissions.

mixture can affect significantly the growth of the RE-123 phase, which eventually leads to the formation of unwanted sub-grains in the bulk (RE)BCO microstructure.

2.5. BA-TSMG

The TSMG technique enables the fabrication of high-quality, single grains of (RE)BCO with improved applied superconducting properties, although, historically, the reliability of the process has been poor. In particular, the success rate for producing single grains by TSMG was limited initially to $\sim 30\%$ – 40% [54], resulting in several, fairly recent, attempts to improve the process significantly. Integrating TSMG with the so-called buffer technique [55, 56], for example, has emerged as a successful modification to the process, for the reliable fabrication of both (RE)BCO and the more technically challenging (RE)BCO + Ag bulk superconductors in single grain form (Ag is usually added to the precursor powder to improve the mechanical strength of the single grain). The buffer technique involves placing a small buffer pellet between the seed crystal and the (RE)BCO precursor pre-form to be grown into a single grain prior to melt processing. The buffer pellet works in two ways: (a) It minimises or eliminates any diffusion of the seed crystal elements into the bulk (RE)BCO sample being melt processed, thereby reducing the formation of any low T_c phase material beneath the position of the seed

crystal and; (b) it inhibits infiltration of the seed crystal by Ag within the (RE)BCO pre-form to avoid the partial/complete melting of seed crystal element [the presence of Ag reduces the (RE)BCO peritectic temperature significantly]. Various features of TSMG and buffer-assisted TSMG (BA-TSMG) are shown in figure 8. Detailed research [55–60] has been performed more generally to optimise the composition and aspect ratio of the buffer pellet to aid specifically the growth of (RE)BCO single grains.

The buffer pellet provides sufficient volume to contain elements diffusing from the seed crystal (diffusion is unavoidable at elevated temperature), thereby providing an effective barrier and preserving the composition of the bulk (RE)BCO sample during the growth process. The buffer acts effectively as a one-way channel that allows the propagation of crystallographic texture through its thickness, a shield for the diffusion of elements from the seed crystal and minimises simultaneously the transport of Ag to the seed crystal for (RE)BCO + Ag systems. The BA-TSMG process has improved dramatically the reliability of the TSMG process over recent years, and has increased the success rate for the growth of large, (RE)BCO and (RE)BCO + Ag single grains to greater than 90%, which is particularly significant for the commercial production of bulk superconductors. BA-TSMG is now an established process for batch processing, with a selection of single grains fabricated by this technique shown in figure 9.

2.6. Generic seed crystals and the suppression of solid solution formation

The compounds Nd-123 and Sm-123 have a higher T_p than Y-123 and are therefore suitable for use as seed crystals for the YBCO system. However, the availability of seed crystals is a major issue for the growth of single grains of other (RE)BCO systems, including GdBCO, SmBCO, and NdBCO [i.e. the so-called light rare element (LRE) in (RE)BCO compounds]. Initial attempts using MgO as a seed crystal were only partially successful, however, due to the significant mismatch (of around 11%) between the MgO crystal structure and that of the RE-123 phase compounds, chemical incompatibility, resulting in Mg contamination/diffusion into the (RE)BCO bulk sample and the formation of low T_c phases during the MG process. In 2005, it was observed that the addition of up to 1% Mg to the NdBCO system enhanced the T_p of the doped Nd-123 phase by 20 °C [61, 62] (as can be seen in figure 10), which was an important step towards developing an effective TSMG process for the fabrication of (LRE)BCO single grain, bulk superconductors. The new Mg-doped NdBCO seed crystals were termed ‘generic seeds’ since they were used successfully to seed every known superconducting (RE)BCO system. The development of generic seeds opened pathways for exploring the fabrication of single grain (LRE)BCO on a large scale, which is significant due to their higher T_c and higher H_{irr} , which leads directly to greater potential for enhanced engineering performance. On a parallel track, a second important contribution to improving the reliability of the general melt process was the development of a NdBCO thin-film seed by Yao *et al* [63, 64], which, due to super-heating phenomenon, exhibited a higher melting temperature and hence could also be used successfully to seed every (RE)BCO system. Both these important seed-related developments enabled single grain (LRE)BCO systems to be fabricated reliably and developed specifically for practical applications.

Light rare-earth (LRE)BCO systems have a higher T_c , and hence higher $J_c(H)$ and associated higher trapped field at a given temperature (and at LNT, in particular) when compared to YBCO, as shown in figure 11(a). However, solid solutions of the type of $\text{LRE}_{1+x}\text{Ba}_{2-x}\text{Cu}_3\text{O}_y$ can form easily in these systems, due to the comparable ionic radii of LRE and Ba, and because the T_p of (LRE)BCO systems is highly sensitive to the oxygen partial pressure during melt processing (a small change in the composition of the furnace atmosphere during growth process can disturb the growth kinetics significantly). The effects of substitution result generally in the formation of superconducting phase regions of low T_c within the bulk microstructure, thereby reducing significantly the values of T_c and $J_c(H)$. The solid solution formation problem in different (RE)BCO systems, and particularly those based on Gd, Eu, Sm and Nd, has been addressed since 2000 primarily by adding extra BaO_2 (1–4 wt.%) to the precursor powder, which, desirably, enables bulk samples to be processed in an air atmosphere. The influence of the addition of BaO_2 to the

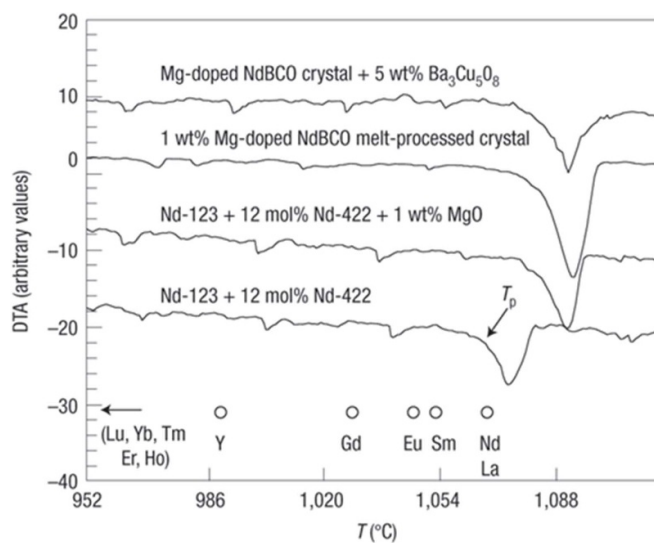


Figure 10. DTA scans with respect to temperature for the NdBCO system, with and without added MgO. Data for Mg-doped NdBCO crystal + 5 wt.% $\text{Ba}_3\text{Cu}_5\text{O}_8$ are shown for purposes of comparison. The melting temperatures of RE-123 compounds based on Y, Gd, Eu, Sm and Nd are shown as individual points (circles). Figure reprinted from [62], with necessary permission.

GdBCO system, as reported by Shi *et al* [65], can be seen in figure 11(b). Similarly, the influence of the addition of BaO_2 on trapped field in SmBCO is shown in figure 11(c). It can be concluded from these studies that 1–2 wt. % of BaO_2 addition to the GdBCO system and 3–4 wt. % of BaO_2 addition to SmBCO is effective in minimising the formation of solid solutions in these systems, thereby defining a processing route for the fabrication of bulk samples with significantly improved superconducting properties. Subsequent work on Ba-rich precursor powders has yielded high-quality (LRE)BCO bulk superconductors [66–68] with self-field current densities of up to $\sim 50\,000\text{ A cm}^{-2}$ at 77 K. More recently, cost-effective attempts have been made to produce YBCO and (LRE)BCO bulk superconductors directly from the raw oxide powders (RE_2O_3 , BaO_2 and CuO) [69]. This enables the characteristics of the precursor powder to be tuned and optimised to yield a reliable melt process and consistent superconducting properties in the fully processed bulk single grains. Further information on the powder preparation process and the influence of the composition, morphology and properties of the precursor can be found in the review by Pathak *et al* describing several synthesis processes to obtain Y–Ba–Cu–oxide powder precursor powders [70].

2.7. Growth of mixed binary and ternary RE-systems (YGd, NSG, NEG, YSN)

Attempts to fabricate binary ‘ $(\text{RE}_1, \text{RE}_2)\text{BCO}$ ’ and ternary ‘ $(\text{RE}_1, \text{RE}_2, \text{RE}_3)\text{BCO}$ ’ bulk superconductors comprising of a mixture of multi RE-elements have been made with the objective of introducing additional flux pinning centres to the

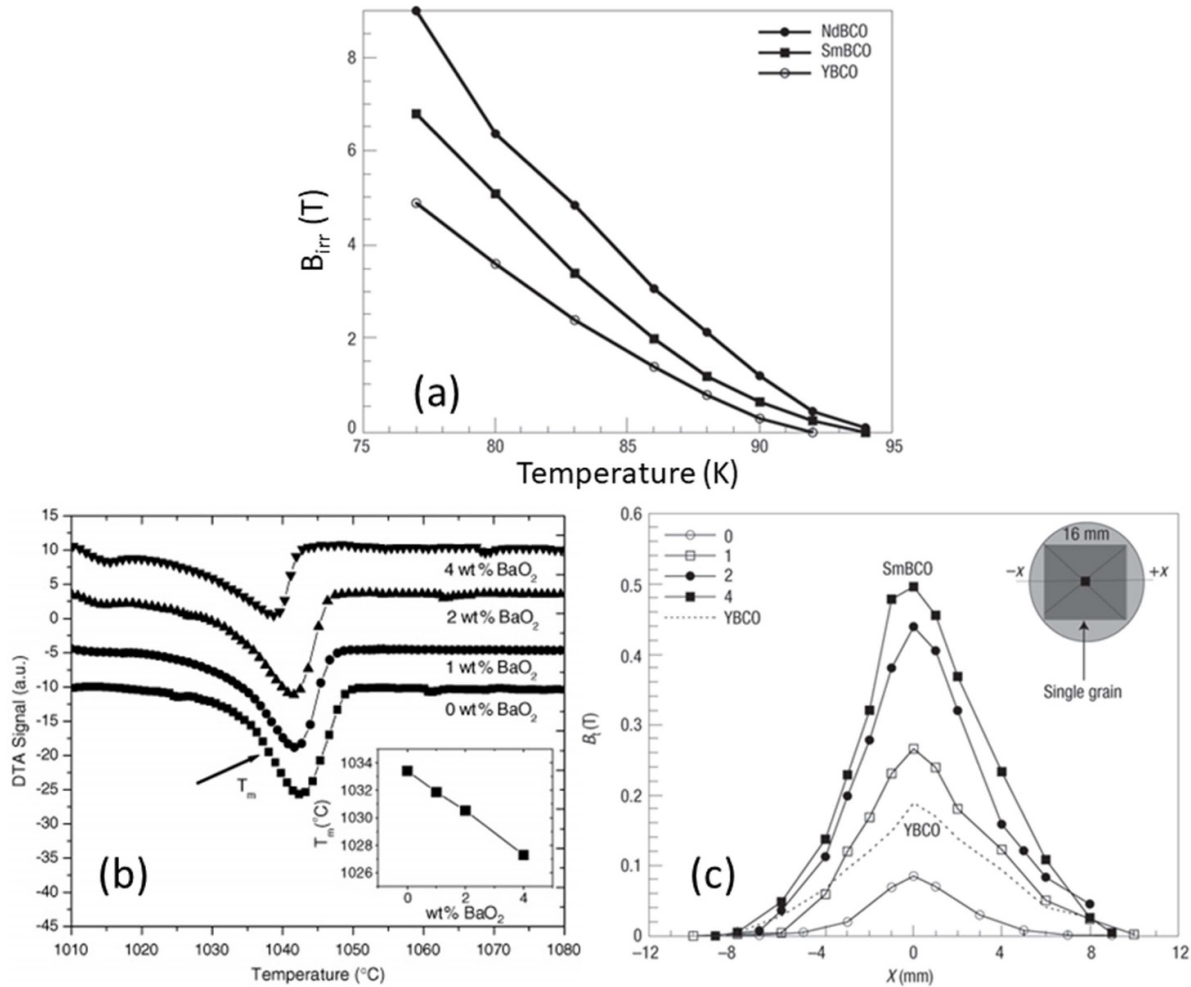


Figure 11. (a) Increased potential of NdBCO and SmBCO (LRE)BCO bulk superconductors compared to YBCO for the field-dependent generation of trapped field. (b) Temperature dependence of DTA signals in GdBCO with added BaO₂ (0–4 wt.%). The reduction in melting temperature with increased BaO₂ content of the precursor powder in the GdBCO system is shown in the inset. (c) Enhancement of trapped field for SmBCO system with added BaO₂ (2 and 4 wt.%). Images in this figure are reprinted from [62, 65], with necessary permissions.

(RE)BCO matrix in the form of discrete regions of lattice mismatch. As a result, several systems, including (YGd)BCO [71] (NSG)BCO [72], (NEG)BCO [73], (SEG)BCO [74] (YSN)BCO [75], have been reported to exhibit record values of various superconducting properties. In each of these systems, the ratio RE₁:RE₂:RE₃ was maintained as 1:1:1. (NEG)BCO bulk superconductors containing 40 mol% NEG-211 inclusions, for example, exhibit values of J_c in excess of 68 kA cm⁻² at 77 K and record values, in general, in applied magnetic field of up to 2.5 T [73]. It has been observed that RE-211 secondary-phase particles are distributed homogeneously in the (Nd,Eu,Gd)Ba₂Cu₃O₇ phase matrix during melt processing, which is desirable for effective flux pinning, with a particle size of ~ 0.8 μ m and a typical volume content of between 16% and 18%. Large, single grain (SmEuGd)BCO bulk superconductors, in particular, have been prepared successfully by the OCMG process [74] and a T_c of 93 K has been reported for a (YSN)BCO single grain with (001) texture [75]. TEM studies carried out on ternary (RE)BCO systems have indicated the presence of dislocations and stacking faults within the superconducting matrix, resulting in an enhancement of $J_c(H)$, as shown in figure 12.

2.8. Infiltration growth strategy

The IG melt process has emerged as an alternative and viable approach to conventional MG processing since it addresses many of the limitations inherent to the general MG technique [76–78], including near-net shape processing and the formation of a dense single grain microstructure. The fabrication of (RE)BCO single grains via the TSIG approach is shown in figures 13(a) and (c). Here, the RE-211 pre-form is capped with a seed crystal and is placed in intimate contact with the liquid phase reservoir pellet. A copper-rich liquid phase comprising BaCuO₂ and CuO forms in the liquid phase reservoir during the heat treatment in the TSIG approach, which infiltrates subsequently into the porous RE-211 pre-form at a temperature below T_p of the compound, ultimately reacts with RE-211 to form the RE-123 phase, as described by equation (3). Heterogeneous nucleation occurs at the seed crystal as the sample assembly is cooled slowly back through T_p and the single grain growth front propagates throughout the entire bulk material as the sample is cooled further. Unlike other MG techniques, no oxygen gas is evolved during the heat treatment, resulting in the formation of fewer pores in single

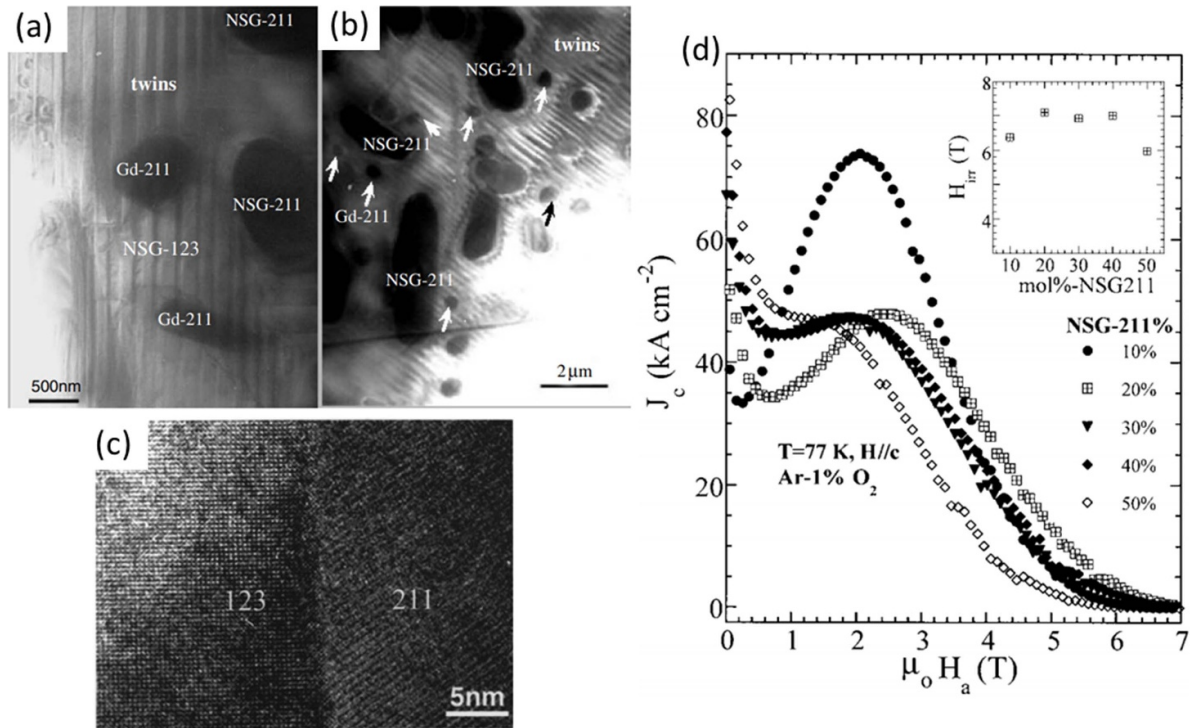
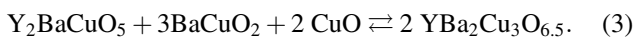


Figure 12. (a) and (b) The presence of fine Gd-211 and NEG-211 inclusions in the size range $\sim 500\text{--}800$ nm in the matrix of NEG-123. The twinned structure can also be seen in these figures. (c) High-resolution TEM image obtained at the RE-123/RE-211 interface. (d) Field dependence of J_c , including the peak/fishtail effect, for (NEG)BCO single grains prepared with different mol% NSG-211 content. Images in this figure are reprinted from [72], with necessary permissions.

grains processed by TSIG compared to samples fabricated by conventional melt-growth (thereby producing a much denser microstructure). A schematic comparison between the TSMG and TSIG processes is shown in figure 13(d). Cross-sections of YBCO single grains fabricated via these two processing techniques are shown in figure 13(e). The fabrication of (RE)BCO bulk superconductors via the IG process is now established, and there are many reports of the successful application of this technique to fabricate bulk, single grain samples [76, 79–83].



The fabrication of single-grain (RE)BCO bulk superconductors via TSIG is significantly more challenging than other MG-based techniques for two main reasons: (a) the liquid phase infiltration and seeding processes progress simultaneously, which can easily cause single grain growth failure and; (b) sub-grains can form readily, including at sites within the liquid phase reservoir pellet if its composition is not tuned and optimised appropriately. Furthermore, given that (RE)BCO processed by TSIG tended historically to exhibit inferior superconducting properties than samples fabricated by TSIG, only limited effort had been made until recently to fabricate (RE)BCO bulk superconductors via IG processing. As a result, the focus of IG research prior to 2015 was on the fabrication of near-net shapes and on scoping the processing domain of Y, Sm, Gd and Dy-based systems [82–86]. Significant improvements were made to the TSIG fabrication approach between 2015 and 2017, however, by tuning and optimising a number

of processing parameters, which enabled the reliable production of (RE)BCO single grains with superior microstructural and superconducting properties required for practical applications, and typical (RE)BCO bulk superconductors fabricated by TSIG now exhibit current densities of $\sim 20\text{--}50$ kA cm $^{-2}$ and trapped fields of $\sim 0.5\text{--}0.9$ T at 77 K. Three particularly important contributions made to the development of the TSIG technique are:

- The introduction of the buffer technique;
- Control of RE-211 content and;
- The use of a two-step BA-TSIG process.

The use of a buffer pellet to increase the reliability of the single grain growth process has been observed to be more critical to TSIG than TSMG, due primarily to the presence of a relatively large quantity of aggressive, Cu-rich liquid phase that forms during the melt process in the former. The liquid phase, which initiates in the reservoir pellet and infiltrates subsequently into the RE-211 pre-form, can reach and react with the seed crystal relatively easily, thereby compromising its ability to act effectively as a seed, resulting in multiple grain nucleation sites and, as a result, severe sub-grain formation. Failed and successful attempts to grow a single grain sample by the TSIG process without and with a buffer are shown in figure 14(a). The effect of a suitable buffer pellet positioned between the sample and the seed crystal is to minimise the diffusion of seed crystal element (such as Nd or Sm) into the bulk sample and, more importantly,

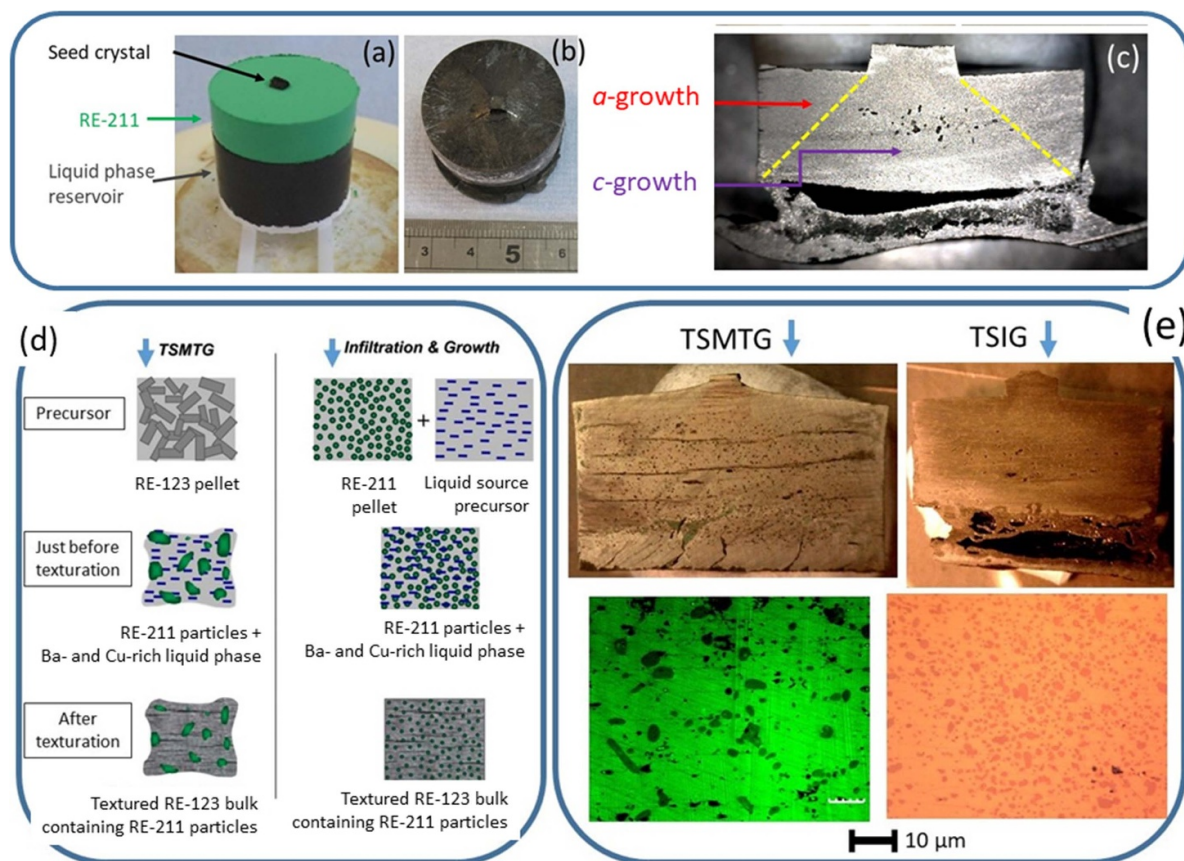


Figure 13. Single grain (RE)BCO bulk superconductors fabricated via the TSIG technique. (a) Assembly comprising of a Y-211 pre-form (green in colour, on-line version) placed in contact with the liquid phase reservoir pellet (comprising of BaCuO_2 and CuO), which is supported by a thin plate of Yb_2O_3 . (b) Single grain YBCO fabricated by the TSIG process. (c) Typical cross-section of the sample, including the formation of a -growth and c -growth regions (separated by the yellow dashed lines). (d) Schematic comparison of the TSMG and TSIG processes at several stages: Precursor, just before texturing and in the final product [81]. (e) Cross-sectional optical micrographs and RE-211 particle size distribution in the matrix of RE-123 for both TSMTG and TSIG fabrication processes.

to limit the extent of liquid phase component reaching the seed crystal, which is essential to achieve single grain nucleation and growth. Systematic studies have been performed to identify the most appropriate liquid phase composition for the reservoir pellet that avoids any sub-grain formation, whilst, at the same time, enabling the appropriate growth kinetics (i.e. at an appropriate temperature) for faster RE-123 growth. A Yb-based liquid phase (corresponding to a composition of $\text{Yb}_2\text{O}_3:\text{CuO}:\text{BaCuO}_2 = 1:6:10$ [87]) works well for most (RE)BCO systems, although a Y-based liquid phase is effective for the single grain growth of higher T_p materials, such as SmBCO and NdBCO. More detailed studies on the optimisation of the buffer pellet and composition of the liquid phase can be found elsewhere [57, 60, 86].

Attention turned to understanding the underlying reasons for the inferior superconducting properties of (RE)BCO bulk superconductors fabricated by TSIG following the development of a successful, single grain melt process. It was observed, in a series of careful and detailed microstructural studies, that the presence of a significant excess amount of RE-211 in the RE-123 phase matrix (i.e. greater than 40%) was the primary reason for this poor performance. A typical optical micrograph showing excess Y-211 content and

its distribution within a single grain processed by TSIG is shown in the bottom half of figure 14(a). Unlike TSMG (where the size and distribution of RE-211 inclusions is relatively easy to engineer), the control of RE-211 phase formation is much more difficult in TSIG given the nature of the liquid phase infiltration process and the subsequent reaction of liquid with RE-211 to form RE-123, which determines critically the residual content of RE-211 in the final sample. As a result, it is extremely challenging to tune the processing parameters in TSIG, since several processes such as liquid infiltration, the peritectic reaction, heterogeneous nucleation and single grain growth all occur either simultaneously or within a small temperature-time window during the heat treatment. As a result, two primary approaches to enable control the RE-211 content in IG processed material have been investigated: (a) The provision of additional liquid phase component within the RE-211 pre-form (optical micrographs from these samples containing 10 wt% and 20 wt% liquid phase added to Y-211 pre-form are shown in figure 14(b)) and; (b) varying the infiltration temperature and time to enable prolonged and suitable infiltration of liquid phase to yield optimum RE-211 content in the fully grown single grain (see figure 14(c)). Although both approaches have enabled improved control of RE-211

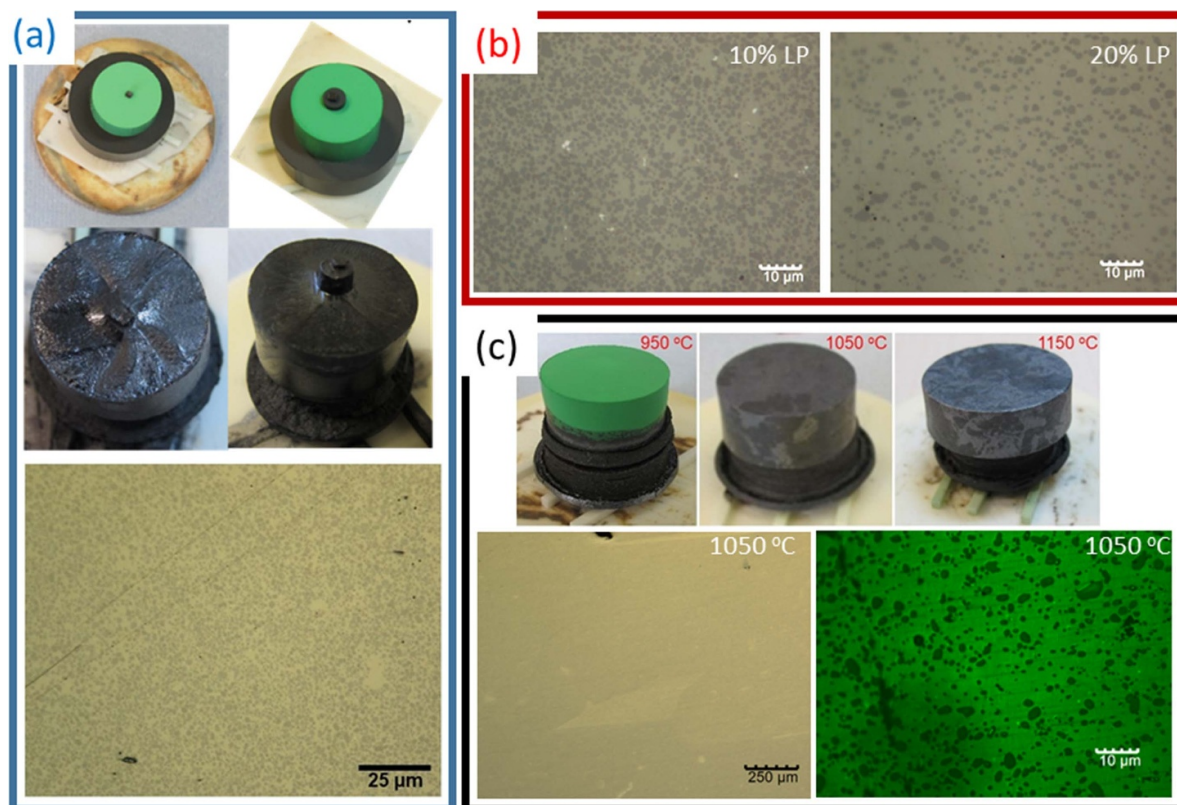


Figure 14. (a) YBCO samples processed without, unsuccessfully, and with, successfully, a buffer via TSIG. Optical micrograph illustrating excess Y-211 present in YBCO processed by TSIG. (b) Control of Y-211 content is possible by the addition of the liquid phase component to the Y-211 pre-form prior to processing. (c) The effect of infiltration temperature within the range 950 °C–1150 °C. An optimum infiltration temperature/time of 1050 °C/1 h was identified for obtaining good superconducting properties at 77 K by considering RE-211 size and distribution in the fully processed single grain. Images in this figure are reprinted from [88–90], with necessary permissions.

content in the sample microstructure, the second approach optimising infiltration temperature and time has proved to be the most successful, yielding a dense microstructure containing relatively few pores and cracks, as shown in figure 14(c). This figure demonstrates the novelty and inherent advantages of the IG process, whilst controlling simultaneously the Y-211 content in the single grain. The long-standing issue of inferior superconducting properties of samples fabricated by IG has therefore been addressed successfully and hence now both MG and IG processes are able to yield single grain samples that are comparable in terms of both their microstructure and superconducting properties. The reliability of the TSIG process for the fabrication of (RE)BCO single grains with enhanced superconducting properties has been improved further by the development of a two-step BA-TSIG process [90], as shown in figure 15. In this advanced version of the TSIG process, the two critical steps of infiltration and single grain growth have been separated and performed sequentially to make the process more effective, easy to control and more reliable. As a result, a success rate in excess of 95% has been observed in the processing of single grains of (RE)BCO bulk superconductors by this relatively novel two-step BA-TSIG fabrication technique. More recently, the process has been extended to (RE)BCO + Ag systems, which are currently under investigation and have already produced some

promising initial results. GdBCO [91–93], SmBCO [94] and even binary systems such as (Y,Gd)BCO [95] bulk superconductors have been fabricated by TSIG-based techniques. In addition, the TSIG approach is suitable for the fabrication of dense generic seeds [96], which has enabled directly the manufacture of Mg-doped NdBCO seed crystals that are characterised by both a higher melting temperature and by reduced porosity in their microstructure, therefore limiting dramatically the possibility of liquid phase segregation within the seed crystal and hence avoiding possible melting of the seed. The availability of these dense generic seed crystals now enables the reliable single grain growth of (RE)BCO and (LRE)BCO systems, including those containing Ag, which provides a potential pathway for the commercial production of bulk, single grain superconductors for practical applications.

Significantly, the individual merits of TSMG and TSIG advanced processing techniques have motivated additional effort to bridge these two approaches and to optimise the processing and performance of (RE)BCO single grains. In this hybrid approach, which is referred to as the LA-TSMG process [97], liquid phase enrichment is provided by supporting the TSMG sample assembly with a small layer of liquid phase compact, which leads to the formation of a higher concentration of RE-species at the growth front and speeds-up significantly the single grain growth process. This, in turn,

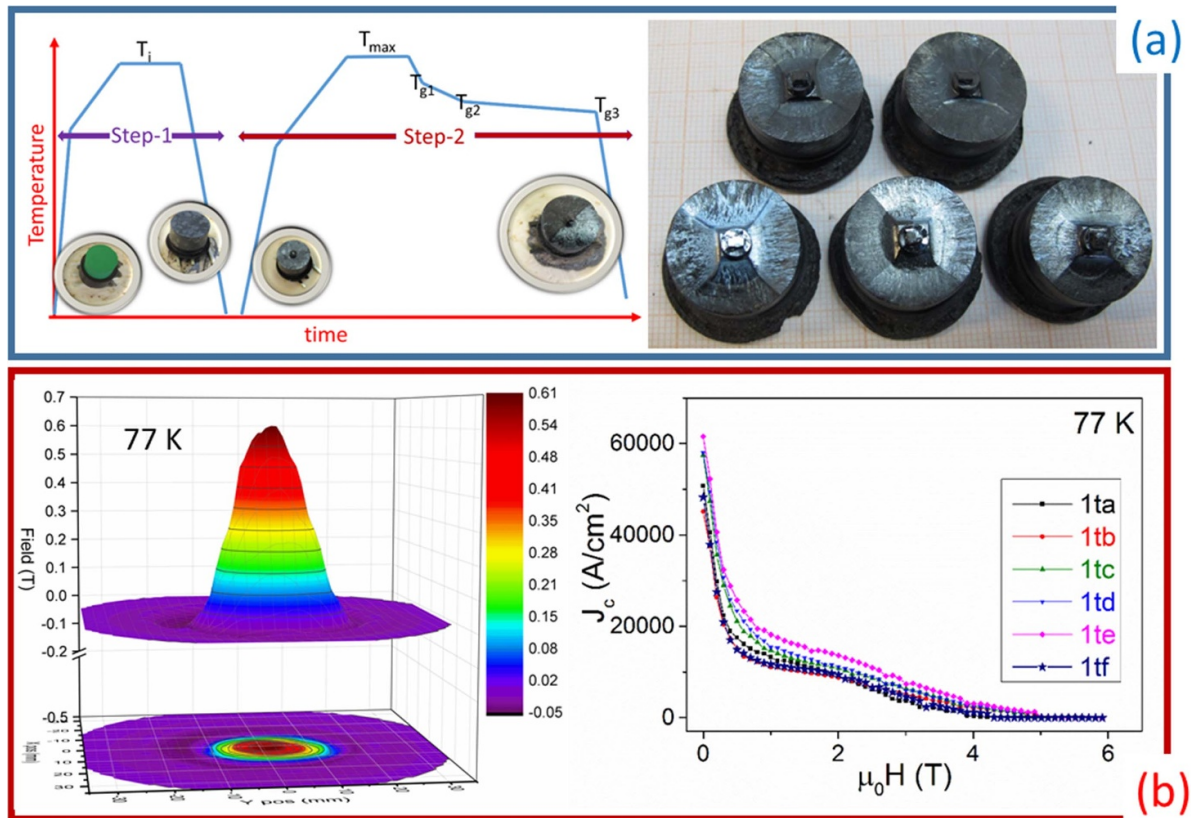


Figure 15. (a) Schematic illustration of the two-step BA-TSIG process. Batch-processing of GdBCO samples establishing the reliability of single grain growth by the two-step BA-TSIG process can be seen. (b) An observed trapped field of 0.6 T and relatively high $J_c(H)$ over a wide field range at 77 K, further with uniformity in superconducting properties can be observed in YBCO samples fabricated by the two-step BA-TSIG. Images in this figure are reprinted from [90], with necessary permissions.

leads to a homogenous distribution of RE-211 particles within the RE-123 superconducting phase matrix, thereby increasing the uniformity of superconducting properties, the reliability of single grain growth and reducing porosity in the as-processed bulk sample. Congreve *et al* [97] recently fabricated YBCO and YBCO + Ag bulk superconductors successfully by the LA-TSMG process to combine the merits of both MG and IG techniques.

2.9. Flux pinning in (RE)BCO—peak effect

The theoretical depairing current density in (RE)BCO superconductors, at which currents circulating in the material cause the Cooper pair charge carriers to break, resulting in the disappearance of the superconducting state (I_c varies as $\frac{H_c}{\lambda}$, where H_c is the thermodynamic critical field), is $\sim 10^8$ A cm⁻² at 77 K, which is nearly 3–4 orders of magnitude higher than the critical current densities observed experimentally. The primary reason for the difference in observed and predicted performance is associated primarily with the movement of magnetic flux within the interior of the superconductor. For type-II superconducting materials, when the magnetic field is applied and the system is in the so-called mixed state, quantised magnetic flux lines in the form of individual flux vortices enter the body of the superconductor (the interfacial energy between superconducting and non-superconducting regions of the sample is minimised in type-II superconductors in the

mixed state). In this case, one quantum of magnetic flux, Φ_0 , is equivalent to 2.1×10^{-15} T m². Flux vortices, as predicted by Abrikosov [98], are known to form a triangular lattice when no pinning centres are present within the superconducting material. These flux lines can move easily under the influence of the Lorentz force (which is directly proportional to magnetic field), resulting in flux-flow and, therefore, the dissipation of energy. This, in turn, reduces significantly the current carrying ability of these materials. The presence of flux pinning sites, associated generally with defects in the superconducting matrix, can reduce locally the energy of a flux line and, therefore, further minimise its energy, effectively pinning the fluxon to the pinning site and limiting the extent of flux flow. Magnetic flux pinning, therefore is both a critical and fundamental phenomenon for generating enhanced current densities in type-II superconductors, even in the presence of applied magnetic field. Effective flux pinning is achieved typically when the size of the defect is of the order of the superconducting coherence length. Specific defects that constitute effective flux pinning sites include oxygen defects, stacking faults, dislocations, twins, twin boundaries and columnar defects (such as those created by irradiation) [99–102]. The influence of APC on, and their presence in, the RE-123 phase creates a variety of defects within the superconducting matrix, as shown in figure 16. The enhancement in $J_c(H)$ due to the presence of pinning centres is also illustrated in this figure.

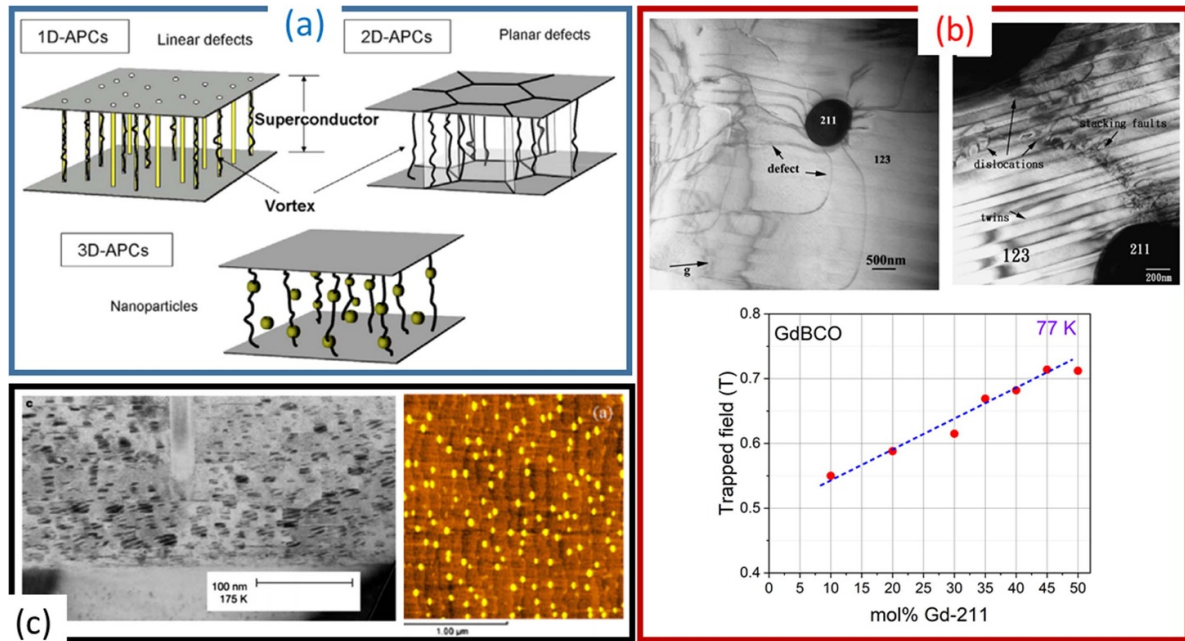


Figure 16. (a) Schematic representation of magnetic flux pinning (with 1D, 2D and 3D APC). (b) TEM micrographs showing the presence of dislocations and stacking faults at the RE-211/RE-123 interface in (RE)BCO single grain. Effect of Gd-211 on the trapped field performance (at 77 K) of GdBCO single grain is shown. (c) Nano-sized pinning centres that are known to enhance current carrying capacity in (RE)BCO thin-films. Images in these figures are reprinted from [101, 102], with necessary permissions.

Ideally, the size of a pinning centre should be of the order of the superconducting coherence length, i.e. $2\xi_{ab}$ of the material (for YBCO, for example, $\xi(0\text{ K}) \sim 1.5\text{ nm}$ and $\xi(77\text{ K}) \sim 4.5\text{ nm}$) [103, 104]. The presence of RE-211 phase inclusions within the RE-123 matrix naturally forms a source of flux pinning in (RE)BCO bulk superconductors. In reality, stacking faults and dislocations formed at the RE-211/RE-123 interface (shown in figure 16(b)), enhance the current carrying ability of these materials significantly. As a result, considerable effort has been made to refine and control the size of the RE-211 particles in order to improve the flux pinning density and therefore to enhance $J_c(H)$. For example, the refinement of Y-211 in YBCO was achieved by employing different Y-211 synthesis routes, including the fabrication of nano-whiskers via electrospinning [105], the milling of coarse Y-211 particles and by ultrasonication [106]. All these approaches have enabled enhancement in $J_c(H)$ in single grain YBCO bulk superconductors. Hari Babu *et al* synthesised a new type of nano-scale flux pinning centre based on the $\text{Y}_2\text{Ba}_4\text{Cu}_1\text{M}_1\text{O}_y$ (Y-2411) phase (with M as Bi, Mo, Nb, Ta, Ti, W and Zr) and subsequently added this phase to various (RE)BCO systems, which enabled a significant improvement in flux pinning strength [107]. Gd-211 particles of size in the range $\sim 20\text{--}50\text{ nm}$ produced by ball-milling with Zr_2O_3 were introduced into the superconducting matrix of (NEG)BCO to create numerous point-like flux pinning centres to generate current densities of up to 80 kA cm^{-2} at 77 K and up to $\sim 10\text{ kA cm}^{-2}$ at 90 K [108]. Engineering the flux pinning within the bulk microstructure by these techniques has enhanced significantly the superconducting properties of these technologically important materials at temperatures as high as

90 K, both in the low and intermediate magnetic field ranges, which effectively extends their application to temperatures that may be achieved using liquid oxygen [109, 110]. TEM studies of (SEG)BCO have revealed the presence of nano-scale precipitates of size $\sim 100\text{ nm}$ that produce J_c in excess of 150 kA cm^{-2} at 77 K and up to 10^4 A cm^{-2} to 86 K [111]. Furthermore to the addition of RE-211, efforts have been made to introduce other chemical pinning centres into the superconducting matrix in the form of dopants. Doping (RE)BCO with Mo (from a MoO_3 source) and Nb (from NbO_3), for example, yields a significant enhancement in J_c via a striking peak effect at 77 K at around 4.5 T and improving the H_{irr} significantly [112, 113]. Samples irradiated in an attempt to create columnar nano-defects in order to improve (directional) flux pinning strength have also produced a significant enhancement in B_t and associated $J_c(H)$. Other approaches to introduce suitable micro- and nano-scale inclusions to the bulk RE-123 phase matrix have yielded an improvement in the overall flux pinning strength in (RE)BCO bulk superconductors and hence the field dependence of J_c . A recent review by Bartunek *et al* [114] on flux pinning in bulk materials describes other approaches for enhancing the pinning strength in these materials not addressed here in this more general overview.

The thermodynamic nature of flux pinning causes critical current density to reduce with increasing magnetic field, with the rate of decay depending on the strength of pinning present in the system. This mechanism of reduction in J_c , which is observed typically in undoped YBCO, is termed as ‘ δI -pinning’ [115]. The pinning mechanism, however, is very different in other RE-based systems, including (LRE)BCO and YBCO containing specific dopants, and results in an

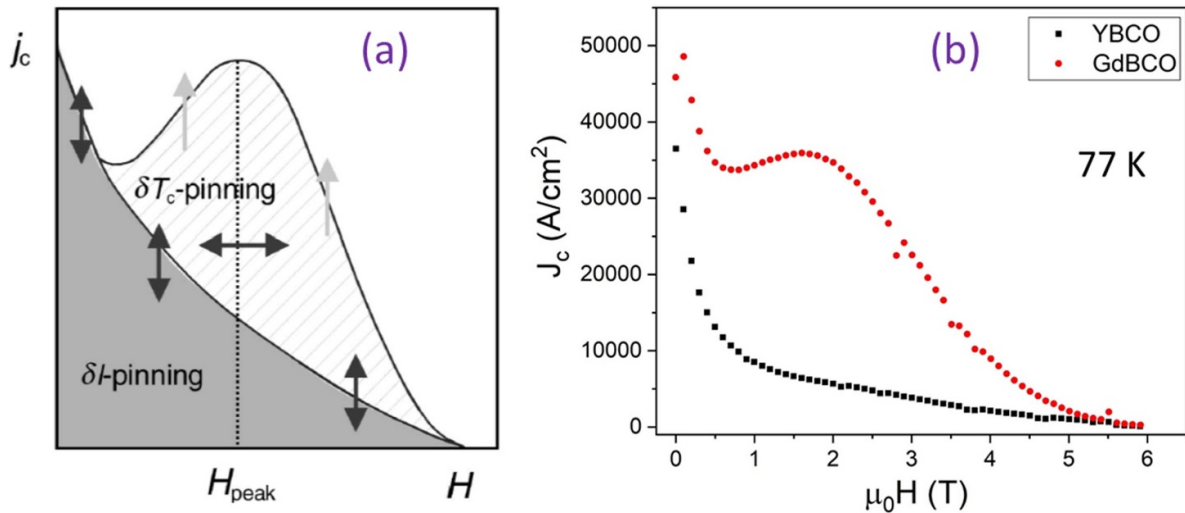


Figure 17. (a) Schematic representation of the variation of J_c with increasing magnetic field, illustrating the influence of ‘ δl -pinning’ and ‘ δT_c pinning’. (b) Experimental $J_c(H)$ for YBCO and GdBCO at 77 K. Image shown in (a) is reprinted from [117], with necessary permission.

enhancement in critical current density at intermediate fields within the range 1–4 T. This re-entrant behaviour in J_c is known as the peak, or fish-tail, effect and this type of flux pinning is known as ‘ δT_c pinning’. The presence of oxygen deficient phases and/or solid solutions in the RE-123 phase matrix are also known to enhance J_c further at intermediate fields, as illustrated by the $J_c(H)$ data shown in figure 17(a) (schematic version) and figure 17(b) (experimental data at 77 K). Furthermore, defects within various ranges of size and the vortex lattice spacing, a_f , are also known to influence the peak field, H_p , at the peak in J_c , with the latter given by the relation [116]:

$$H_p = \frac{2\Phi_0}{\sqrt{3}a_f^2} \quad (4)$$

where Φ_0 is the flux quantum ($=h/2e$).

2.10. Multi-seeding (0–0, 45–45) and interior seeding

The relatively small growth rate of the superconducting RE-123 phase compound has motivated research towards a multi-seeding approach, in which two or more seeds are employed in a controlled heterogeneous nucleation process, and particularly for the fabrication of large samples. In multi-seeding, the alignment of the seeds and their positioning on the pre-form compact is critical for obtaining a quasi-single grain of (RE)BCO. Shi *et al* [118] employed NdBCO seed crystals arranged in different configurations, including the size of seed, distance between seed and, more significantly, their *ab*-plane alignment (either with 0°–0° or 45°–45°) to grow successfully quasi-single grains with good superconducting and microstructural properties in the fully processed samples. It was observed in these studies that regions containing non-superconducting phases form generally at grain boundaries and that this undesirable build-up of impurity phase could be minimised by adjusting the configuration of the seed crystals.

The use of a buffer layer enabled further control of the orientation of the seed crystals in a multi-seeding process, thereby enabling a route for the successful production of high quality, large quasi-single grains. Some of the key results from the multi-seeding research are shown in figure 18. Many further successful attempts have been made subsequently to develop the multi-seeding process based on the potential of this approach [119–126].

Shi *et al* [127] reported a study that compared the properties of a single-seeded and multi-seeded YBCO bar-shaped bulk samples of dimensions $\sim 60 \times 20 \times 12 \text{ mm}^3$. In addition, three square-shaped samples packed together closely in an array to constitute a similar geometry to that of the single and multiple seeded samples was studied to provide a reference. Magnetic levitation measurements carried out at 77 K using different sample and that assembled from individual, single-seeded samples exhibited better performance than that of the single-seeded, bar-shaped sample. This is encouraging for the development of levitation devices, in particular, given the challenge associated with growing large single grains due to the relatively low growth rates of the RE-123 phase. The trapped field distribution and levitation force measurements for these samples are shown in figure 19(a).

Kim *et al* [128] developed a novel ‘interior seeding’ approach in which two (RE)BCO samples can be grown simultaneously from a single seed placed at their interface, as shown in figure 19(b). In this study, an open channel was created in the compacted pre-form to enable simultaneously air/oxygen to reach the seed crystal during growth whilst minimising the contact area between the seed and the liquid phase. A $\text{Y}_{1.5}\text{Ba}_2\text{Cu}_3\text{O}_y$ bulk single grain (42 mm in diameter) produced by this approach trapped a magnetic field of 0.64 T at 77 K [53]. Lee *et al* [129] further proposed a buffer-bridge process for the growth of multiple YBCO single grains from a single seed. Significantly, each of the individual blocks constituted a single grain, as shown in figure 19(c).

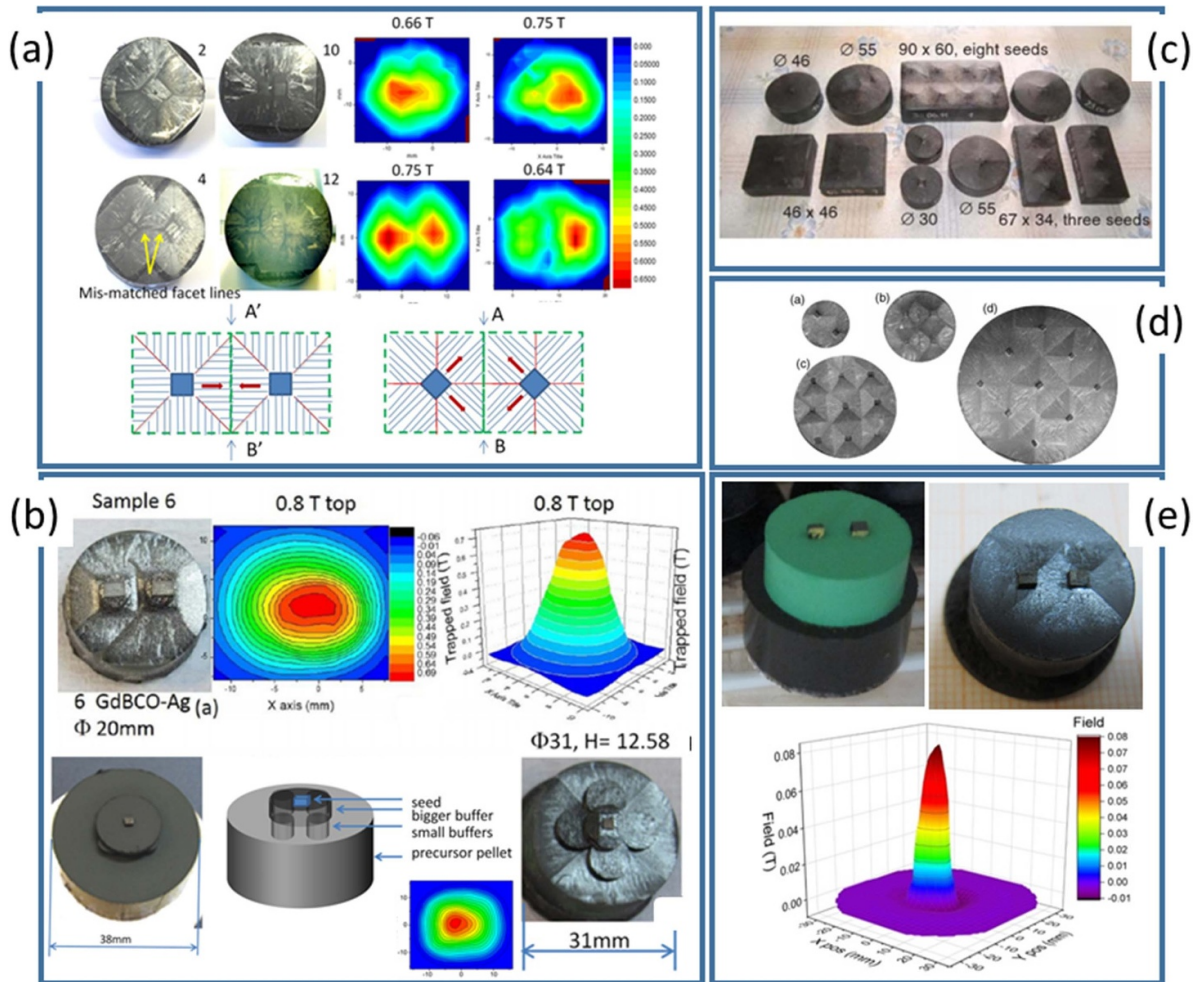


Figure 18. (a) Multi-seeded YBCO with the ab -planes of seeds oriented at 0° – 0° and 45° – 45° to one another. (b) Quasi GdBCO bulk superconductors fabricated via a multi-seeding process integrated with the buffer technique. (c) Multi-seeded YBCO fabricated by ATZ GmbH. (d) Multi-Seeded bulk YBCO superconductors (28 mm, 46 mm, 65 mm and 100 mm diameter) and (e) Multi-seeded YBCO fabricated by the infiltration growth technique. Images in this figure are reprinted from [118, 122–126], with necessary permissions.

2.11. Reliability in growth, batch processing, commercial production and recycling techniques

The development of buffer-aided TSMG and TSIG approaches has enabled bulk, single grains of (RE)BCO to be fabricated reliably with a success rate in excess of 90%. Batch processing has been used successfully to produce several single-grain (RE)BCO bulk superconductors in conventional box furnaces at both at the research laboratory scale and at industrial level. The batch-processing of YBCO, GdBCO, GdBCO + Ag and (NEG)BCO and bulk sample by various laboratories around the world, are shown in figure 20 [130–135].

Failure in the (RE)BCO single grain growth process has been an unavoidable due to the complexity of the processing. Many critical processing parameters, such as the selection of an appropriate composition, mixing and homogenisation of the precursor powders, choice of the seed crystal with appropriate texture and orientation, heat treatment profiles and temperature distribution within the furnace, are fundamental to determining the success or failure of the single grain growth process. Every step of processing is equally important and critical to the

fabrication of a single grain, and, if not selected appropriately, can lead to either partial or complete failure of single grain growth, as illustrated in figure 21(a). The success rate of single grain growth in (RE)BCO to date has been limited historically to 30%–40%, although this has increased significantly to around 90% following the more recent incorporation of a buffer strategy within MG processes. However, there remain tonnes of failed (RE)BCO bulk superconductors in both industrial and academic research laboratories around the world.

The recycling approach developed to transform failed, multi-grain bulk samples into single grains is particularly significant within this context. Broadly speaking, two techniques have been developed for this purpose. The first version of the recycling method [136] developed almost a decade ago involved initially crushing mechanically failed bulk samples for several hours using a high energy mill and repeating this process 2 or 3 times to obtain fine-sized powders. The crushed powders were further subjected to homogenisation and mixing, compacted into cylindrical preforms and melt processed. This approach transformed the failed samples into individual, recycled single grains that were observed to exhibit

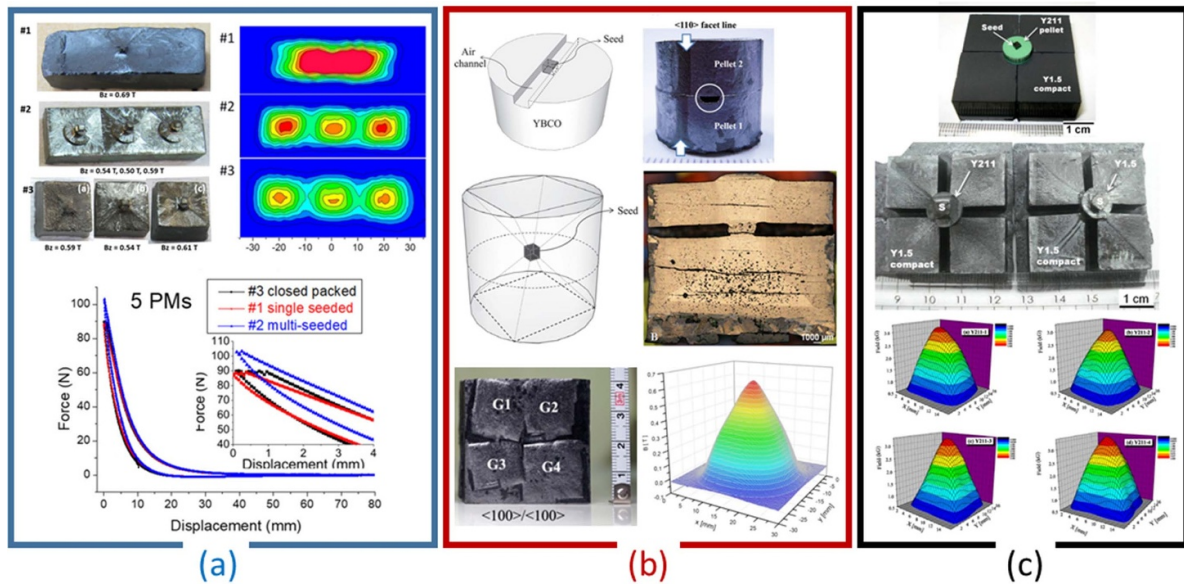


Figure 19. (a) Single and multi-seeding in bar-shaped YBCO samples showing the influence of one or three grains on trapped field and levitation force. (b) Interior seeding approach with one seed crystal enabling the simultaneous growth of two single grains (one growing downwards and the other upwards to the top pre-form). (c) A single seed crystal supported by a buffer pellet for the simultaneous growth of four YBCO blocks. Each block constitutes a single grain. Images in this figure are reprinted from [53, 127, 129], with necessary permissions.

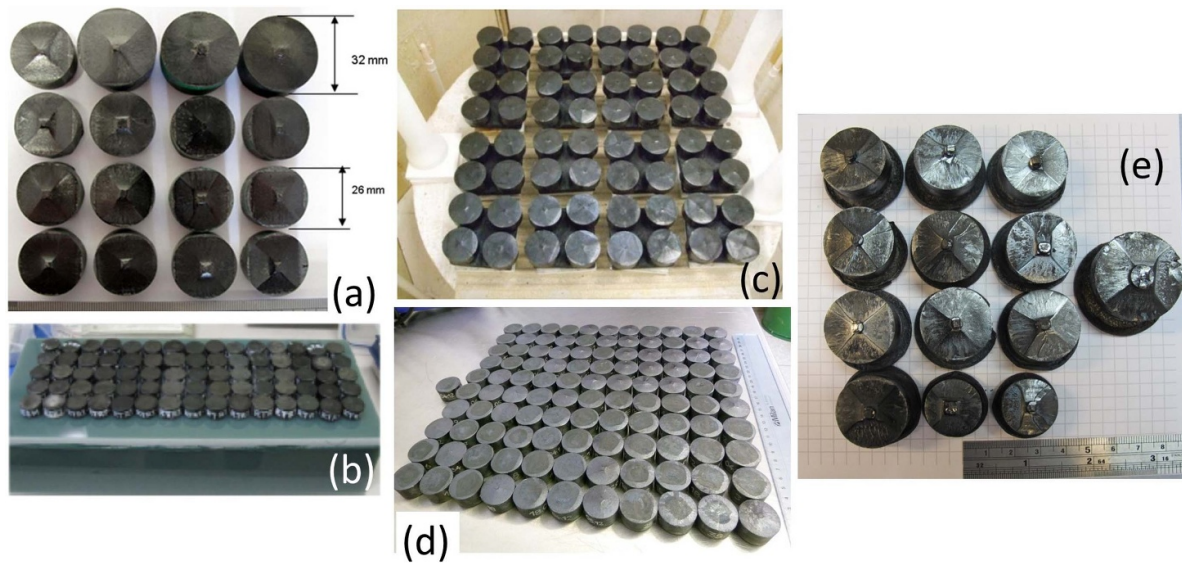


Figure 20. Batch-processed (RE)BCO single grains by different research groups. (a) Shi *et al.*, (b) Muralidhar *et al.*, (c) Plechacek *et al.* (CAN Superconductors), (d) Adelwitz Technologiezentrum GmbH (ATZ), and (e) Namburi *et al.* Images in this figure are reprinted from [88, 90, 130–135] with necessary permissions and also with courtesy of CAN Superconductors and ATZ GmbH.

superconducting properties (including values of trapped field) of $\sim 80\%$ – 90% compared to those observed in primary grown (RE)BCO. However, this recycling approach is time consuming and requires access to specialised equipment, such as high energy mills/auto mixers, with appropriate calibration and optimisation of the crushing parameters and homogenisation processes, which further complicate the single grain growth process. The second approach to recycling, which has been investigated by several research groups, is more straightforward and is applicable to a wider range of (RE)BCO sample compositions [137–141]. In this approach, the top surface of

the failed sample is simply polished, supported on a liquid-phase reservoir pellet and heat treated using the buffer-aided TSMG heating profile. This approach has already addressed the relatively low yield rate in the production of single grain (RE)BCO bulk superconductors.

The recycled single grain samples, as shown in figure 21, obtained by this second approach typically exhibit trapped fields of $\sim 70\%$ – 80% of those observed in primary-grown samples. Furthermore, as with those processed by infiltration growth, the recycled samples exhibit a moderate improvement in their mechanical properties, which makes them potentially

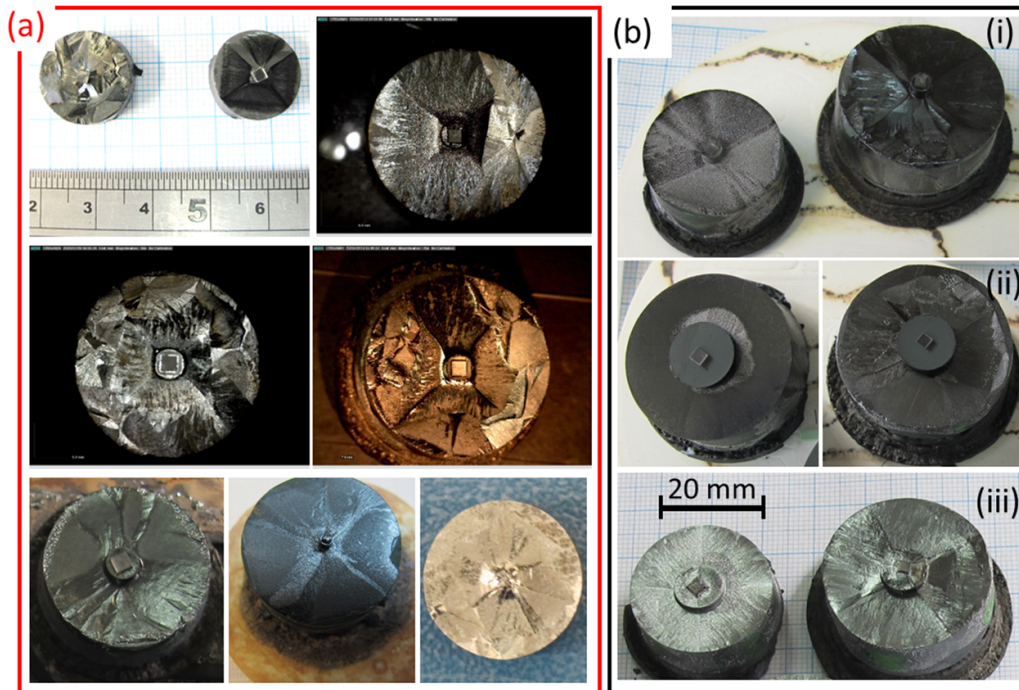


Figure 21. (a) Partial/complete failure of single grain growth as observed in several (RE)BCO systems. (b) Two failed GdBCO + Ag samples (shown in b(i)) that were subsequently recycled by polishing their top surfaces (shown in b(ii)) and performing secondary MG processing to yield a single grain, as evidenced by the four-faceted growth characteristic observed on the top surface of the sample (shown in b(iii)).

suitable for application in levitation-based vehicles, levitation demonstration kits and in applications where mechanical properties may limit the overall performance of the device. These developments in recycling further increase the cost-effectiveness of the production technology and decrease the overall environmental impact of the melt process.

3. Microstructure and properties

Microstructure plays a fundamental role both in the processing of single grain bulk (RE)BCO superconductors and in determining their superconducting and mechanical properties. The key microstructural features of these materials are presented in this section, including anisotropy, the a - and c -growth regions, growth facets, sector boundaries, misorientation, crystal structure, the role of oxygen in the crystallographic lattice and inclusions and other microscopic features in the superconducting phase matrix.

3.1. Influence of microstructure on the properties of (RE)BCO

Type-II HTS are generally extremely anisotropic, and have very different ξ , in the a - b plane and along the c -axis (for YBCO, for example, $\xi_{a-b} \sim 1$ – 4 nm and $\xi_c \sim 0.1$ – 0.5 nm in the temperature range 0 K–77 K [142, 143]), and this anisotropy is further pronounced in the Bi-based and Tl-based systems. Typical a -growth and c -growth regions observed in single-grain (RE)BCO have been discussed previously (see figure 5). The RE-123 phase nucleates from the seed crystal and then

grows within the a - b plane and along the c -axis at different rates. The RE-211 phase (shown as green particles in the figure 22(a)) reacts with liquid phase at the solid/liquid interface zone (referred as reaction zone in the figure) ahead of the growth front, forming a continuous RE-123 phase with embedded RE-211 inclusions. The distribution of RE-211 within both the a - and c -growth regions is shown in figures 22(c) and (d), respectively.

It has been observed that the macro-segregation and distribution of RE-211 particles in the RE-123 phase matrix depend on the growth rate and growth direction for both a - and c -growth sectors. The number of RE-211 particles that are either trapped or pushed with the growth front depends largely on two parameters: (a) The growth rate of the RE-123 phase and; (b) the size of the RE-211 inclusions. The growth kinetics largely determine the final microstructure, including the RE-211 particle density and any crystallographic misorientation, and these observations are in reasonable agreement with the relatively well-known particle pushing/trapping theory [144]. Two major forces act broadly on the RE-211 particle in the reaction zone; the drag force ' F_d ' (acting due to the viscous flow around the particle) and the interfacial force ' F_i ' (occurring due to the interfacial energy at the solid/liquid interface, which, in turn, depends on a number of factors such as pressure and thermal conductivity). The reaction zone is indicated by a uniform solid/liquid interface in the schematic illustration shown in figure 22(a). In reality, however, this is not generally the case. Very often, this interfacial solid/liquid interface is complex due to the influence of many other forces (such as gravity and van der Waals forces) that act on the system, making it considerably more complex. In this simplified model,

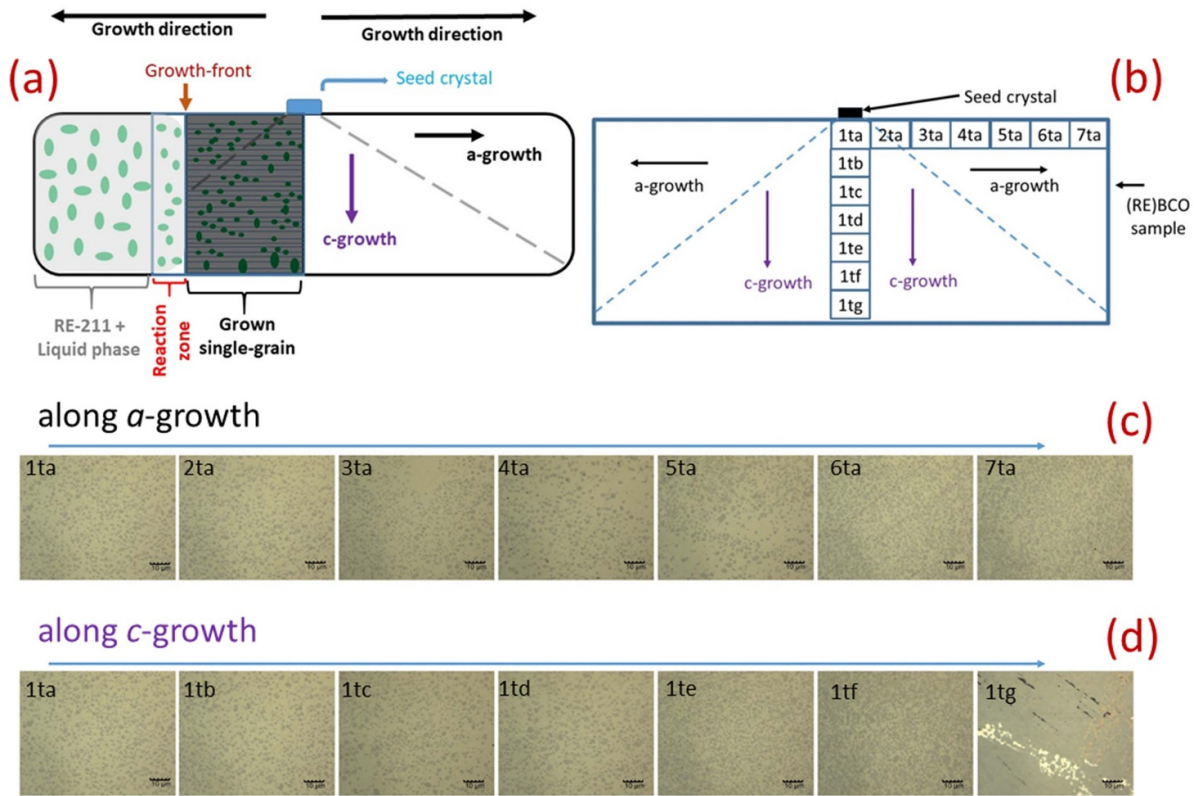


Figure 22. (a) Schematic illustration of the growth of the RE-123 phase with inclusions of fine-sized RE-211 particles (indicated by circles/ellipses in green) within the continuous RE-123 phase matrix. Reaction of RE-211 with the liquid phase occurs in the reaction zone (left-hand half of the sample). The RE-123 matrix entraps unreacted, fine-sized RE-211 particles as growth propagates. The *a*-growth and *c*-growth regions present in the fully processed sample are shown schematically (right-hand half of the sample). (b) Locations of the regions within the (RE)BCO single grain where the optical micrographs were recorded. Typical RE-211 distributions along the *a*-growth and *c*-growth regions are shown in (c) and (d), respectively. The scale bar in (c) and (d) represents 10 μm .

however, the interface energy ' $\Delta\sigma_0$ ' for the RE-123/RE-211 system may be defined as:

$$\Delta\sigma_0 = \Delta\sigma_{\text{SP}} - \Delta\sigma_{\text{LP}} - \Delta\sigma_{\text{SL}} \quad (5)$$

where $\Delta\sigma_{\text{SP}}$, $\Delta\sigma_{\text{LP}}$ and $\Delta\sigma_{\text{SL}}$ represent the surface energies involved at the solid/particle, liquid/particle and solid/liquid interfaces, respectively. The influence of interfacial and drag forces on a particle at the solid/liquid interface and the size and distribution of RE-211 inclusions in the matrix of RE-123 are shown schematically in figures 23(a) and (b). The area fraction of Y-211, denoted as $A_f^{\text{Y-211}}$, calculated from optical micrographs for a typical TSMG-processed YBCO sample along both the *c*-growth and *a*-growth regions are shown in figures 22(c) and (d), respectively. It can be observed that the Y-211 content varies from $\sim 8\%$ (in the vicinity of the seed crystal) to $\sim 30\%$ (at the edge/bottom location of the grain) along both growth regions in the TSMG processed samples. Systematic studies carried out by varying the Y-211 content in YBCO single grains showed a corresponding spatial variation in the critical current density [54, 71, 73, 145].

According to particle pushing/trapping theory, the critical size (r^*) of a RE-211 particle that becomes trapped in the solid RE-123 phase matrix depends on three critical parameters: (a) the growth rate, R^* , in the reaction zone, (b) the interfacial

energy, $\Delta\sigma_0$, and (c) the viscosity, η , of the melt. This dependence is given as follows:

$$R^* \propto \frac{\Delta\sigma_0}{\eta \cdot (r^*)^n} \quad (6)$$

where n is in the range 1–2.

The seed crystal, with (001) texture, provides a centre for the RE-123 grain to nucleate and subsequently to grow and transform the entire material into a textured, single grain. A typical x-ray diffractogram recorded for a textured YBCO single grain sample is shown in figure 24. Several microstructural features observed typically in single grain (RE)BCO, including texture, misorientation, sub-grains, growth sector-grain boundaries, mechanisms for sub-grain formation and the influence of macro cracks and their orientation on superconducting properties, are discussed in detail by Diko [145].

The microstructure of an as-grown (RE)BCO single grain sample fabricated by melt-growth (shown in figure 25(a)) exhibits a relatively large fraction of porosity, and typically in the range 15%–20% [54, 88–90]. Careful examination of the sample reveals that the pores are found to be distributed within two distinct size ranges: 1–10 μm and 50–250 μm . The reason for the occurrence of porosity in these materials is two-fold. The first is due to compaction porosity and the other to

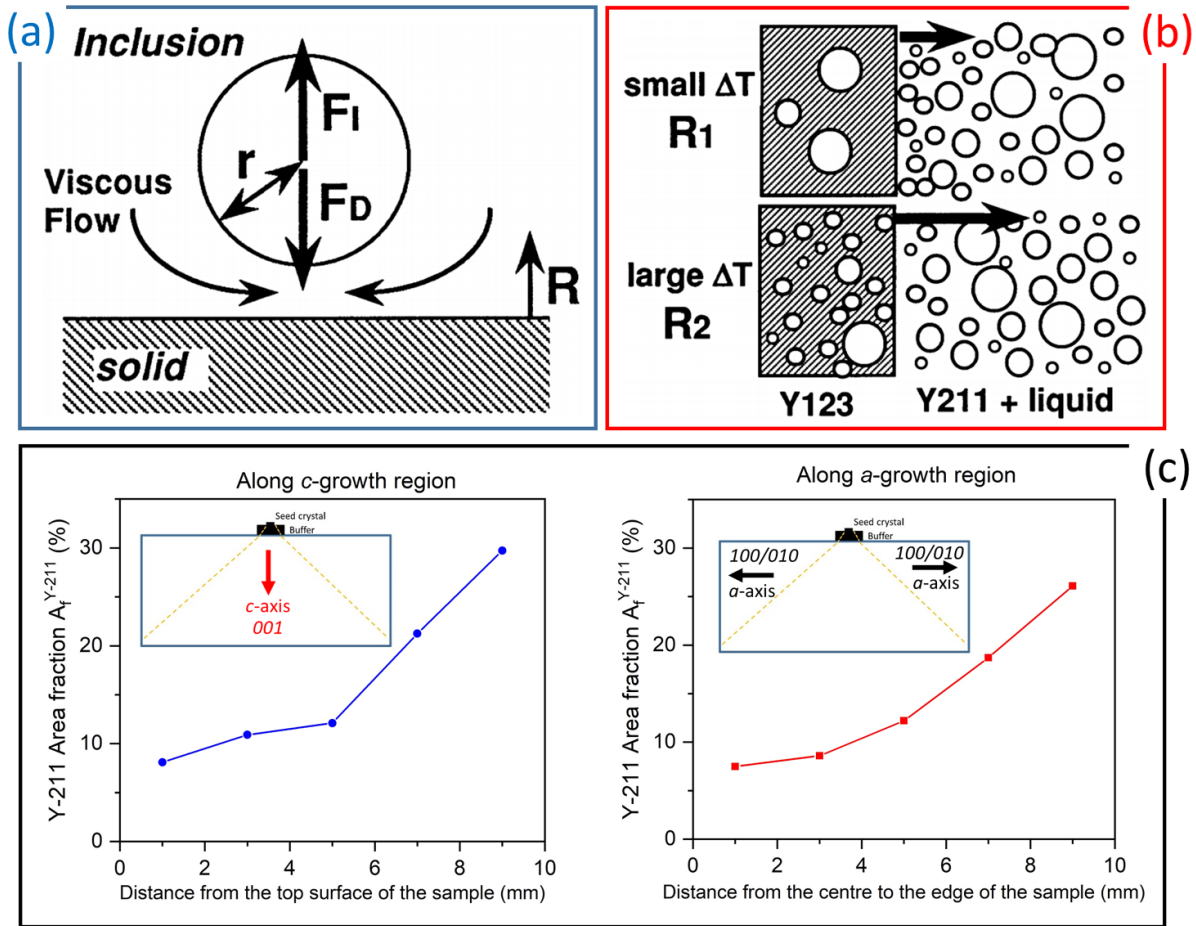


Figure 23. Schematic illustrations showing (a) the interfacial and drag forces acting at the solid/liquid/particle interfaces and (b) the size and distribution of trapped RE-211 inclusions in the RE-123 phase matrix under conditions of small and large undercooling (ΔT). The figures in (a) and (b) are reprinted [144] with necessary permission. (c) Variation of Y-211 content referred as A_f^{Y-211} (in %) along both the *c*-growth and *a*-growth regions of a melt-processed YBCO single grain sample.

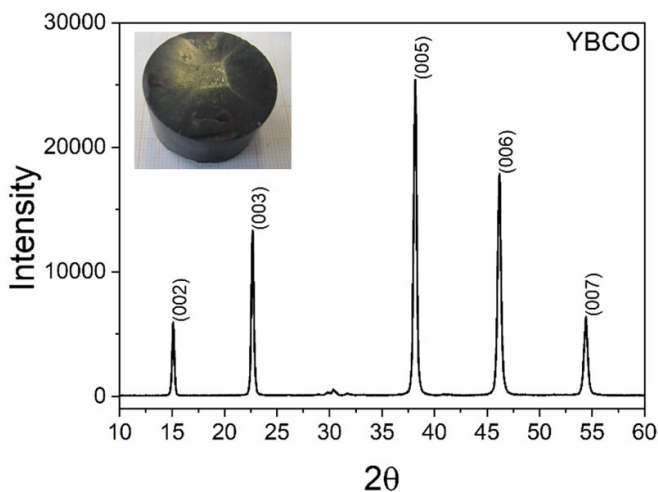
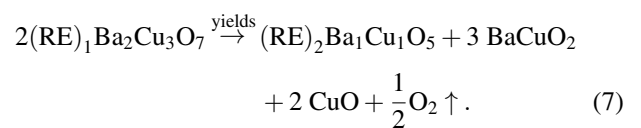


Figure 24. X-ray diffractogram obtained for textured YBCO single grain (sample shown in the inset).

the evolution of oxygen gas during processing at elevated temperature. The primary RE-123 phase melts during TSMG at a temperature above the peritectic temperature of the (RE)BCO

compound, forming RE-211 (solid) and liquid phase, with the associated evolution of oxygen gas, as described by the following equation:



The evolution of oxygen gas within the interior of the sample during melt processing results directly in the formation of pores within the bulk microstructure. Gas produced at the circumference and edges of the sample, however, can diffuse out of the single grain during growth, resulting in a reduction in the volumetric fraction of pores in regions around exposed edges of the sample, whereas gas evolved in the body of the sample remains trapped within the bulk microstructure, as can be seen in figure 25(a). The pores become filled subsequently with the liquid phase that eventually reacts completely with RE-211 to form the RE-123 phase, resulting in the formation of RE-123 regions that are free of RE-211 inclusions, as can be seen in figure 25(b). The inhomogeneous microstructure that forms as part of the pore-filling and reaction process can

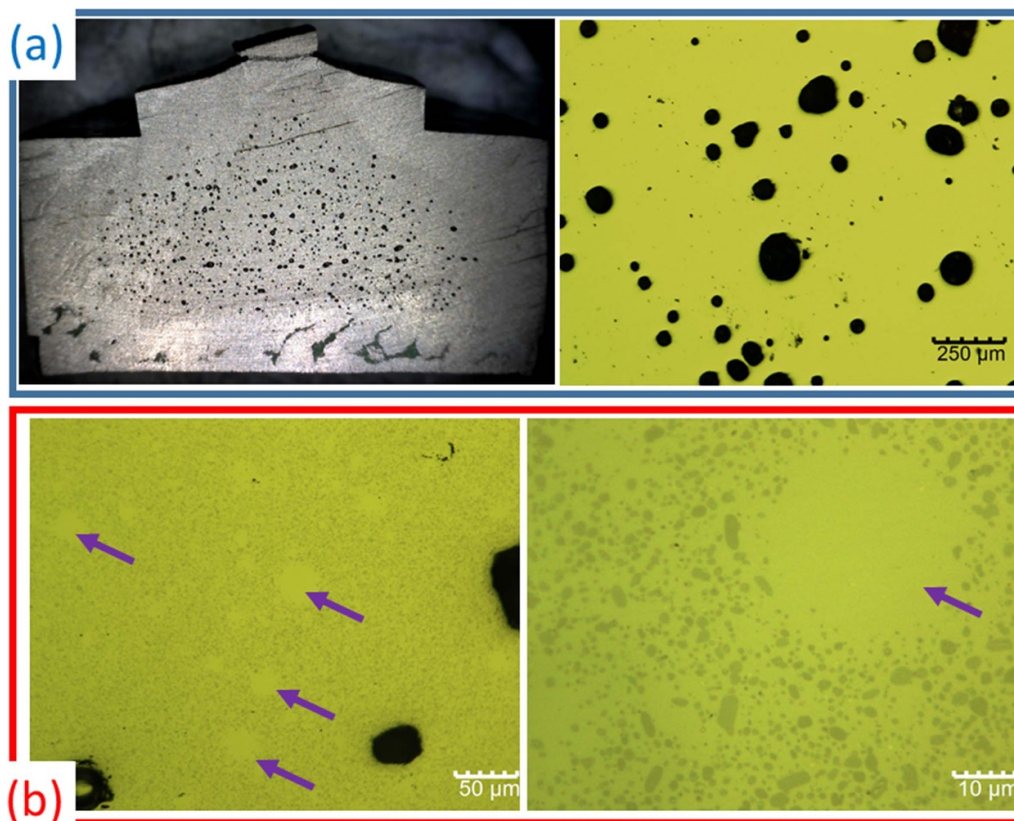


Figure 25. (a) Cross-section of an YBCO sample fabricated by the top seeded melt-growth technique and an optical micrograph obtained at a magnification of $50\times$ of the same sample indicating the presence of pores (visibly in two size ranges). (b) The presence of RE-211-free regions (indicated by the arrows) in the microstructure of melt-grown YBCO. The presence of very fine RE-211 phase inclusions in the vicinity of free edges of the sample indicates that the liquid phase has reacted with, and consumed, the majority of RE-211 at these locations. Images in this figure are reprinted from [88, 89] with necessary permission.

lead directly to non-uniform superconducting properties in the fully processed single grain, as has been observed by several researchers [78, 146, 147].

It is worth noting that the bulk microstructure of single grains fabricated by the IG technique is generally considerably more dense than that obtained by TSMG, as discussed in section 2.8 and illustrated in figures 13(c) and (e). No RE-123 phase is present in the primary RE-211 pre-form compact in TSIG, so no melting and no associated gas evolution occurs during the IG process. As a result, pores of similar size (generated during compaction of the green body) tend to form during TSIG, as shown in figure 26.

Oxygenation is an important and critical post-melt processing step for transforming the crystallographic structure of the as-processed RE-123 tetragonal phase to the superconducting orthorhombic phase. $\text{YBa}_2\text{Cu}_3\text{O}_{7-\delta}$ is named according to the 1:2:3 stoichiometry of its constituent cations as Y-123, with the oxygen content of the unit cell varying between 6 and 7. An oxygen content between 6 and 6.4 generally characterises the non-superconducting tetragonal Y-123 phase, whereas values of oxygen between 6.4 and 7 define the orthorhombic superconducting phase, with the highest value of T_c being observed for an oxygen content of about 6.95 [148–150]. The crystal structures of the tetragonal and orthorhombic forms of Y-123 are shown in figure 27.

3.2. Other microstructure-related studies

The temperature distribution within the interior of the furnace is critical to the nucleation and growth of a (RE)BCO single grain. Small fluctuations in local temperature during the crystallisation process have been observed to cause Y-211 particles to concentrate in the form of bands oriented parallel to the Y-123 growth front [151], as shown in figure 28(a). As a result, a number of studies have been performed to understand the growth of Y-123 under different compositional and thermal conditions. For example, the growth rate of Y-123 bulk crystals in the $\text{Y}_{1.5}\text{Ba}_2\text{Cu}_3\text{O}_x$ system with added CeO_2 was investigated by Volochová *et al* [52]. This study indicated that single grains of YBCO can be grown in an isothermal growth window of $988\text{ }^\circ\text{C}$ – $1003\text{ }^\circ\text{C}$. Too large an undercooling, however, is known to result in spheroidal growth, as shown in figure 28(b). CeO_2 present in the peritectically decomposed state also is known to react partially with the liquid phase forming BaCeO_3 , as can be seen in figure 28(c).

Macro- and micro-cracks occur in the RE-123 superconducting matrix during oxygenation post-melt processing, as shown in figure 29(a). Micro-cracks within the a - b plane of the single grain, in particular, are known to form around RE-211 particles during the cooling process within the tetragonal phase of RE-123 and provide effective channels for

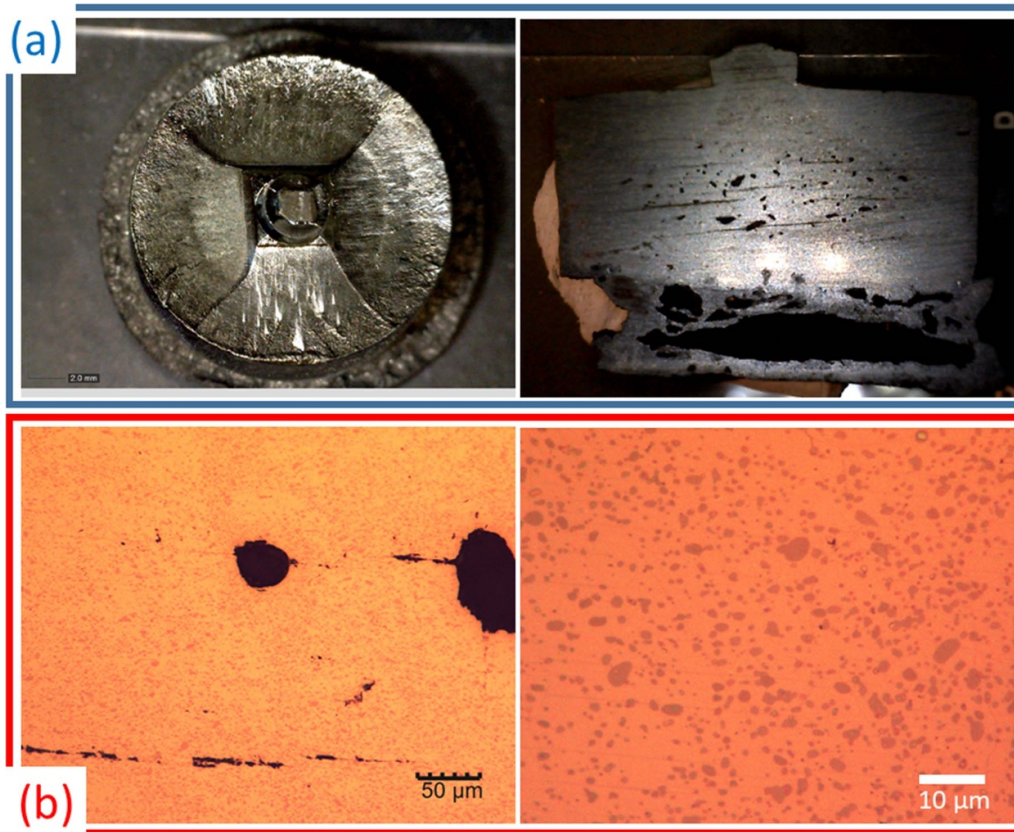


Figure 26. (a) Top surface and cross-section of a GdBCO single grain sample processed by TSIG that exhibits uniform porosity. (b) Homogenous distribution of RE-211 inclusions in the RE-123 phase matrix, which is characteristic of the TSIG technique. No traces of RE-211-free regions are present in the microstructure of IG-processed materials.

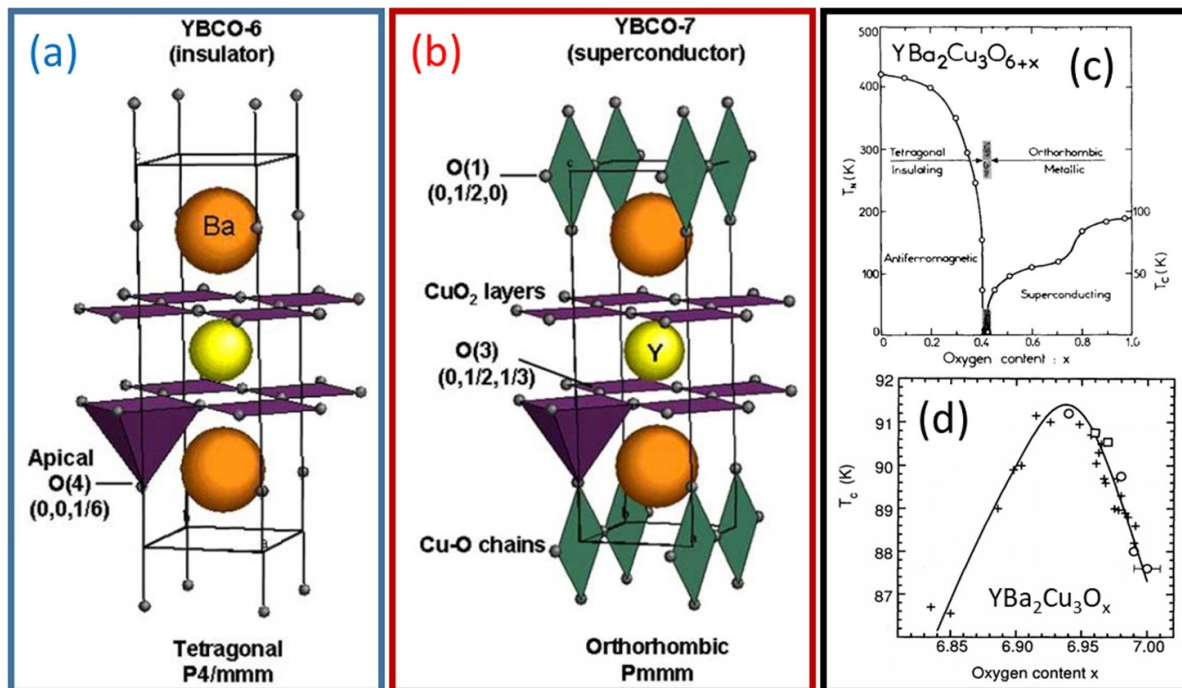


Figure 27. Crystal structure of Y-123: (a) $YBa_2Cu_3O_{6+\delta}$ (tetragonal) and (b) $YBa_2Cu_3O_{7-x}$ (orthorhombic). The transformation from tetragonal to orthorhombic with varying oxygen content can be seen in (c). Further refinement on the total oxygen content to generate the highest T_c is shown in (d). Images shown in this figure are reprinted from [148–150] with necessary permissions.

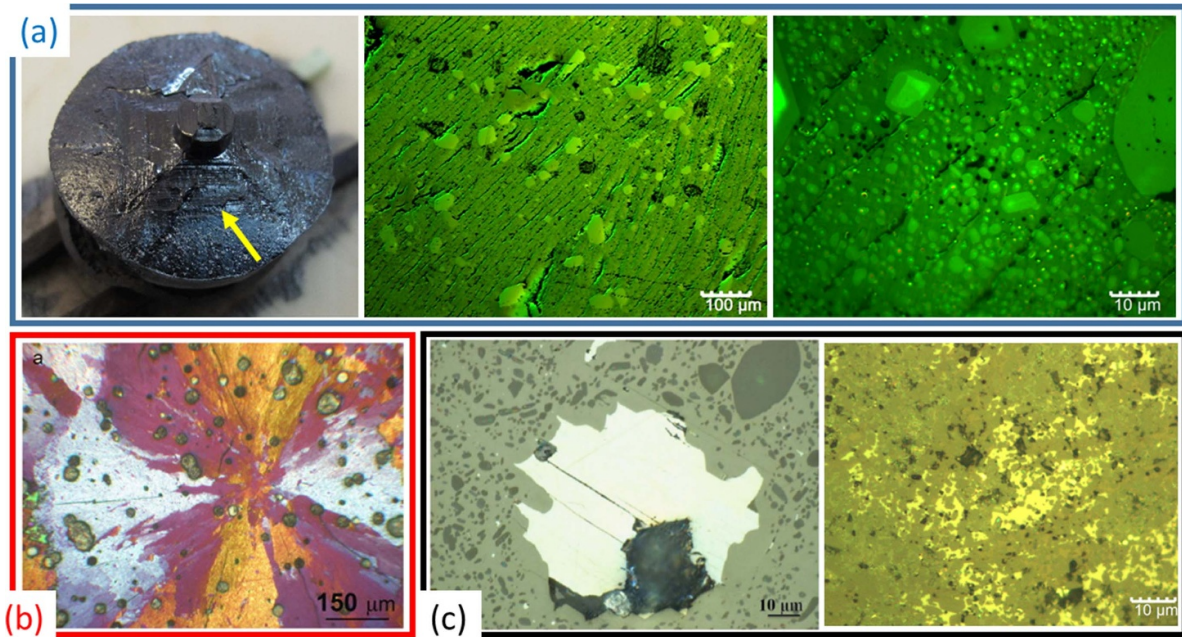


Figure 28. (a) Macroscopic band-structure observed on the surface of an as-grown YBCO sample. Optical micrographs obtained under a magnification of 100 \times and 1000 \times are also shown. (b) Spheroidal growth observed in a (RE)BCO sample and (c) BaCeO₃ formation in the RE-123 phase matrix. Image in (b) is reprinted from [152] with necessary permission.

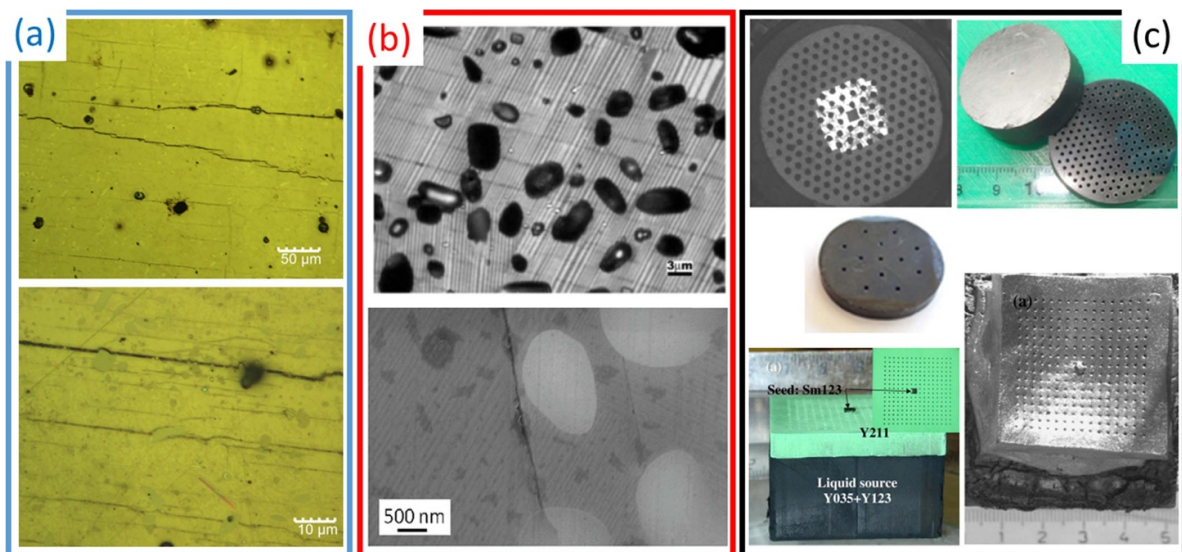


Figure 29. (a) Micro-cracks and (b) twins observed in single grain YBCO fabricated by TSMG. (c) Bulk YBCO fabricated from samples with pre-formed, artificial holes (the holes are drilled in the pre-forms prior to heat treatment) obtained by MG and infiltration growth techniques. Images in (b) and (c) are reprinted from [99, 155–157] with necessary permissions.

oxygen to permeate through the material [153]. The transformation of the tetragonal to the orthorhombic phase, on the other hand, leads to the formation of twins and twin boundaries, which form effective sites for flux pinning [154]. These features are shown in figure 29(b). YBCO with holes pre-drilled in the green body, as shown in figure 29(c), has emerged as another interesting geometrical approach that facilitates faster oxygenation and more rapid cooling. Additionally, this approach opens-up pathways to improving the mechanical strength of the bulk superconductor when the artificial holes

are back-filled with suitable metals and or resins post heat treatment.

3.3. Electrical properties

The electrical properties of bulk superconductors are interesting and fundamental to their practical application, although they are generally challenging to measure accurately. For example, it is necessary to employ relatively sophisticated instruments for the measurement of dc electrical resistance,

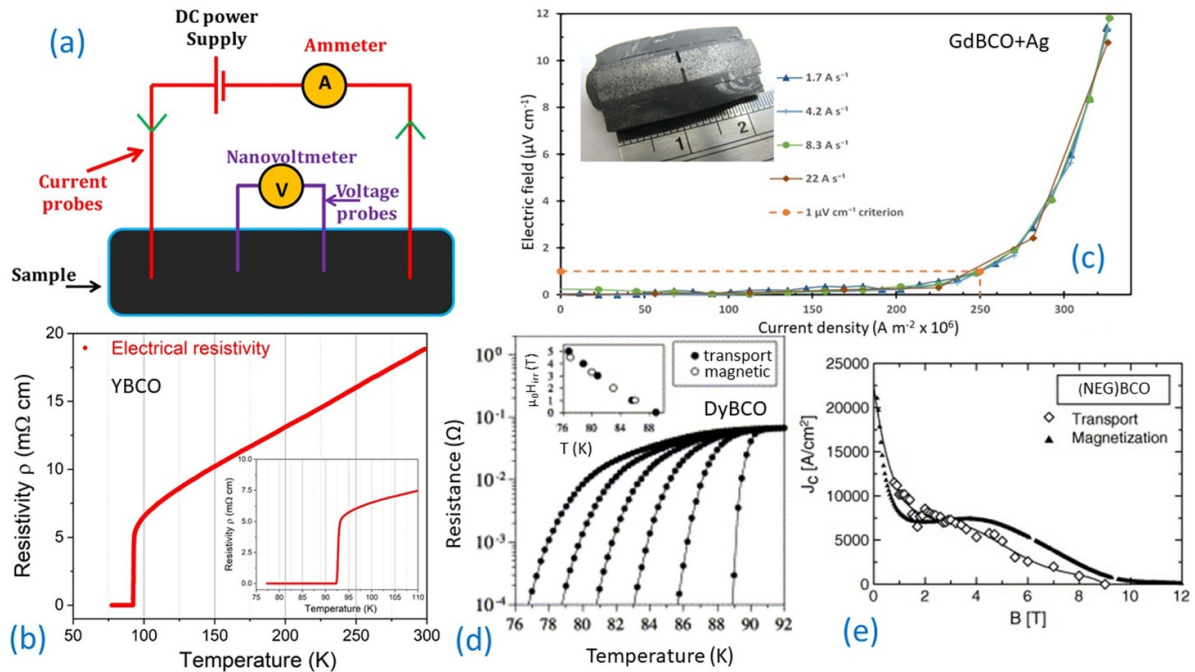


Figure 30. (a) Schematic illustration of the four-point probe technique used for measuring electrical resistance in a superconductor. (b) Temperature dependence of electrical resistivity obtained for a narrowed bulk YBCO block. The inset shows a magnified version of (b) showing the T_c and sharp transition width. (c) Electric field as a function of critical current density measured for a GdBCO + Ag bulk sample. (d) Temperature dependence of electrical resistance measured in different applied magnetic field for a DyBCO bulk sample. The so-called irreversibility lines obtained for both transport and magnetic measurements are shown in the inset to (b), and (e) Field dependence of critical current density $J_c(H)$ for a (NEG)BCO mixed rare-earth based bulk superconductor. Images in (c)–(e) are reprinted from [161–163] with necessary permissions.

which is very small in superconductors, including a precise current source, cryogenic temperature controller and a nanovoltmeter with high sensitivity. The temperature dependence of electrical resistivity (ρ defined as RA/l , where R is resistance, A is cross-sectional area and l is the distance between the voltage tapping points) measured in the superconducting material provides information on both the T_c and the width of the transition from the normal to the superconducting state, ΔT_c . A four-point probe technique is used commonly to measure electrical resistance in superconductors. A schematic illustration of the four-probe technique and a typical ρ vs T plot obtained for YBCO is shown in figures 30(a) and (b), respectively, and from which the high T_c at ~ 92 K with an associated sharp transition width ($\Delta T_c < 1$ K) indicates the high quality of the material. Bespoke specimens have to be prepared with a very thin cross-section to enable transport J_c measurements to be made using commercially available current sources (i.e. with a measurement capability in the range 100–200 A). The technical difficulty in performing high current transport measurements means that magnetic measurements are used generally to estimate current densities in bulk samples, even though they require relatively complex calculations and rely on a number of assumptions regarding the distribution of current within the sample, as described typically by the Bean model [158] and its various extensions [159, 160]. Furthermore, in magnetic measurements, the properties under investigation are typically normalised to the particular sample and do not, therefore, entirely represent actual current densities. Rush *et al* [161] recently reported an efficient sample preparation methodology

by obtaining I-shaped bulk specimens to enable transport current density measurements to be performed directly. The results obtained for a GdBCO + Ag bulk specimen with a small cross-sectional area of 0.44 mm 2 are shown in figure 30(c). Similar studies carried out on DyBCO [162] and (NEG)BCO [163] bulk superconductors in the presence of an applied magnetic field are shown in figures 30(d) and (e), respectively.

3.4. Magnetic properties

The ability of a bulk (RE)BCO superconductor to trap magnetic field is a true figure of merit for practical purposes, since this represents the macroscopic performance of the sample and its suitability for practical applications. Trapped field B_t depends on the product of J_c and the size of the single grain (d);

$$B_t \propto J_c \times d. \quad (8)$$

Magnetisation of the sample is an important step in the magnetic field trapping process in bulk superconductors, and can be performed broadly in one of three ways:

- (a) FC;
- (b) ZFC and;
- (c) PFC.

In the case of field-cooling, the superconductor is cooled to the target temperature in the presence of an applied magnetic

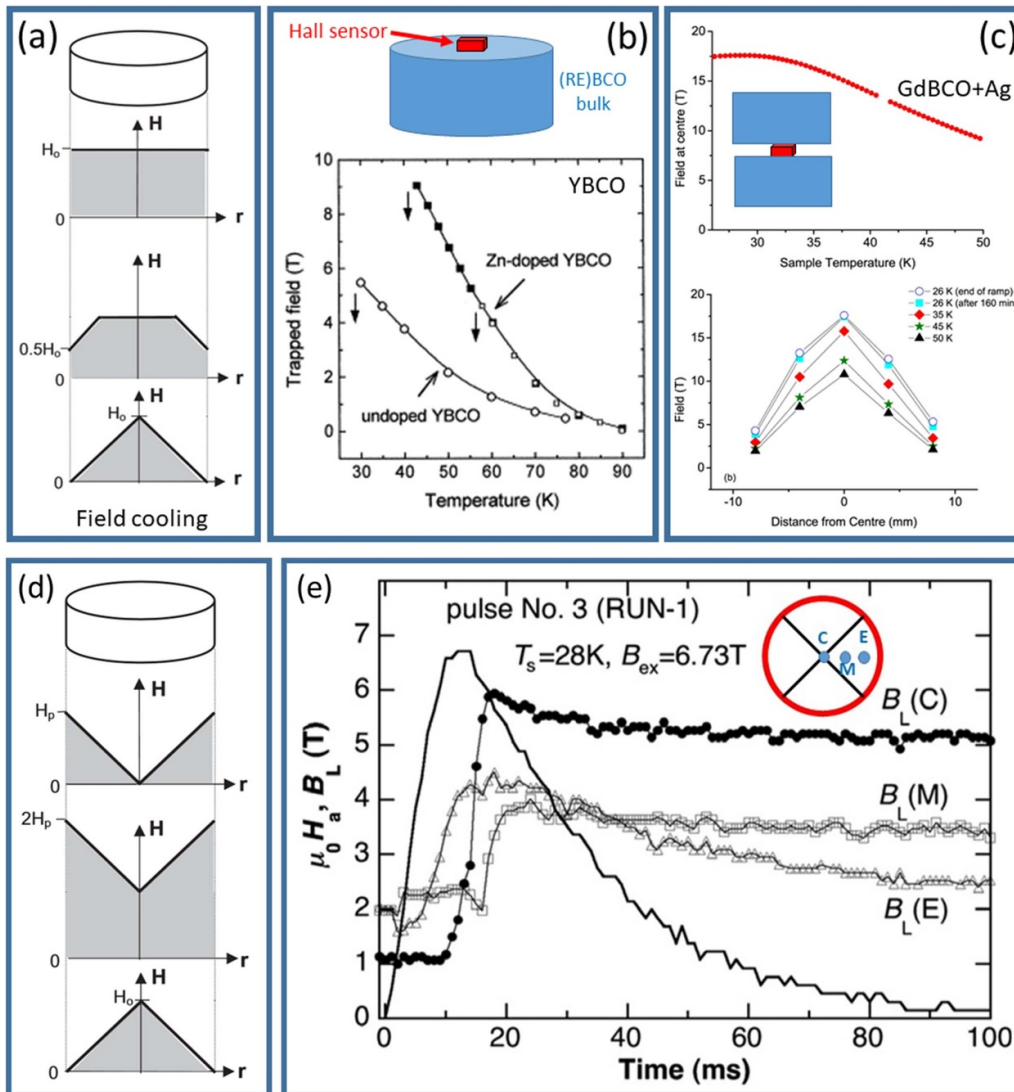


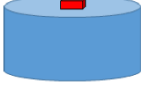
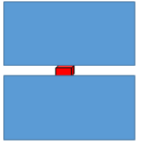

Figure 31. (a) Schematic illustration of the steps used to magnetise a bulk superconductor by the field-cooling technique. The trapped field achieved (b) at the surface and (c) at the centre of a stack of two (RE)BCO samples. (d) The penetration of field into the bulk sample by a ZFC technique based on the Bean model and (e) a trapped field of >5 T achieved at 30 K for a GdBCO bulk single grain of diameter 45 mm via the PFM technique. Images are reprinted from [143, 165–168] with necessary permission.

field. In the FC process, an applied field of similar strength to that of the trapped field ability of the sample is sufficient to magnetise the sample fully and, as a result, is used routinely to trap magnetic field in (RE)BCO bulk superconductors. The FC magnetisation process is illustrated in figure 31(a). Once the sample has been magnetised, a Hall sensor with a small active area is used to measure the trapped field at different points close to the surface of the sample. Trapped field data reported by several research groups for a variety of (RE)BCO HTS bulk superconductors are given in table 3. As discussed earlier, doping the RE-123 superconducting phase with selected elements improves its flux pinning strength, and hence the trapped field, significantly. This is evident from figure 31(b), where Zn-doped YBCO exhibits improved trapped field performance compared to undoped YBCO [164]. A similar field cooled approach was used to magnetise a stack of two GdBCO-Ag,

single grain samples, which trapped a then world record magnetic field of 17.6 T at 26 K [165], as shown in figure 31(c). The trapped field observed in bulk discs of YBCO at 77 K is typically within the range 0.7–1.1 T [88–90, 166], and the observed value of peak trapped field can be as high as 1.3 T at 77 K for (LRE)BCO bulk superconductors [72]. A record peak trapped field of ~ 3 T has been achieved in a 65 mm diameter GdBCO-Ag bulk superconductor [167].

In the case of ZFC, the superconductor is first cooled to the target temperature (usually in liquid nitrogen) below its critical temperature and then magnetic field is applied and removed. In this case, up to twice the field strength is required typically to magnetise the sample completely, as shown schematically in figure 31(d). PFM, which is based on the ZFC technique, is a relatively novel approach for trapping magnetic field in bulk (RE)BCO materials. The PFM technique

Table 3. Trapped fields obtained in (RE)BCO via the different magnetisation techniques.

Magnetisation	Sample configuration	System	Trapped field	Remarks	Ref.
FCM	 <p>Single sample</p>	YBCO	1.1 T at 77 K 11.5 T at 17 K	26 mm diameter sample	[166, 178, 179]
		YBCO	2 T at 77 K	20 mm diameter sample U-irradiated YBCO sample	[180]
		SmBCO + Ag	2.1 T at 77 K 8 T at 40 K	30 mm diameter sample	[181]
		GdBCO	9.1 T at 42 K	46 mm diameter sample	[182]
		GdBCO + Ag	3.05 T at 77 K	65 mm diameter sample	[166]
		YBCO	14.4 T at 22 K	26 mm diameter samples	[164]
		YBCO	14.3 T at 29 K	24 mm diameter, Infiltration growth processed	[46]
		YBCO + Zn	16 T at 24 K	22 mm diameter samples	[178]
		YBCO + Resin impregnation	17.24 T at 29 K	Resin impregnated and wood metal	[183]
		GdBCO + Ag	4.3 T at 77 K	65 mm diameter sample	[166]
PFM	 <p>Two-sample stack</p>	GdBCO + Ag	17.6 T at 26 K	24 mm diameter samples Shrink- fitting with stainless steel	[165]
		GdBCO	5.2 T at 30 K	45 mm diameter sample Modified multi-pulse techni- que combined with stepwise cooling	[168]
		GdBCO-Ag	3 T at 60 K	30 mm diameter sample Flux jump assisted PFM	[177]
		GdBCO	4 T at 20 K	60 mm in diameter	[184]
		YBCO	3 T at 40 K	29.1 mm in diameter	[185]
PFM	 <p>Single sample</p>	GdBCO	5.2 T at 30 K	45 mm diameter sample Modified multi-pulse techni- que combined with stepwise cooling	[168]
		GdBCO-Ag	3 T at 60 K	30 mm diameter sample Flux jump assisted PFM	[177]
		GdBCO	4 T at 20 K	60 mm in diameter	[184]
		YBCO	3 T at 40 K	29.1 mm in diameter	[185]

has considerable potential for use in portable systems where the application of field can be either *in situ* or *ex situ*. In this method of magnetisation, the (RE)BCO sample is cooled to the target temperature and magnetic field is applied in the form of a series of pulses of typical pulse duration of a few milliseconds. This causes magnetic flux to enter the material iteratively, eventually magnetising the sample completely under appropriate conditions. The pulse field nature of the PFM process causes rapid and dynamic movement of magnetic flux, which moves in and out of the bulk superconductor generating heat and increasing the temperature of the sample. This, in turn, reduces flux pinning strength so the bulk sample is less able to trap magnetic field, which is the greatest challenge of the PFM approach. As a result, considerable effort has been made to fine-tune and optimise the PFM parameters to achieve better and more consistent trapped field performance in bulk superconductors [169–172]. A number of notable results have been achieved via the PFM process, including Weinstein *et al*

[173], who reported a trapped field of ~ 2 T at 77 K in irradiated, high J_c YBCO samples and a trapped field of 5.2 T at 30 K in bulk (RE)BCO by Fujishiro *et al* [168] following a modified multi-pulse PFM process with step-wise cooling (MMPSC). Flux jumps or partial flux jumps are known to occur due to experimental conditions during pulse field magnetisation [174–176]. Finally, a portable magnetic field of ~ 3 T at 60 K has been achieved in a GdBCO bulk superconductor of diameter 30 mm by Zhou *et al* [177] via a flux jump assisted PFM approach.

Trapped field can be improved appreciably at lower temperatures, although the considerable Lorentz forces generated during the process can easily damage the relatively brittle (RE)BCO single grains due to their relatively poor mechanical properties. It is necessary, therefore, to contain the maximum tensile stress (σ) that is generated during the application of magnetic field to the bulk sample. In general, the tensile stress σ is given by $\sigma = 0.76 \frac{B_0^2}{2\mu_0}$, where B_0 is the maximum

trapped field of the sample [179]. In order to trap higher fields, therefore, both the superconducting and mechanical properties of the (RE)BCO bulk single grains need optimising. Further details of the mechanical properties of these materials are discussed in the following section.

3.5. Mechanical properties

The peak trapped magnetic field of a bulk superconductor is an indicator of both the general quality of the single grain and, from the field gradient based on the Bean model, the average J_c of the (RE)BCO material. As a result, increasing trapped field is the principle target for applied research and is the main aim of researchers in the field. Trapped field is also one of the most important properties required for practical applications. The high magnetic fields associated with bulk single grain superconductors, such as the current world record of 17.6 T [165, 186], are up to an order of magnitude greater than that the field generated by conventional permanent magnets (and 100 times the energy density). For this reason, bulk superconductors attract considerable research and applied interest across the world. Associated with trapping a large magnetic field, however, is the generation of a large electromagnetic force, which often leads to fracture and materials failure [187]. The world record trapped field for bulk YBCO set in 2003 was held for 10 years before it was eventually broken, which exemplifies the technical difficulty in the fabrication of high performance material [165, 179, 186–188]. The brittle and ceramic nature of bulk (RE)BCO superconductors has been established for a long time. Early experiments showed that the maximum trapped magnetic field of bulk single grains is limited severely by their mechanical properties and the material starts to break, typically, at about 8 T at low temperatures (<50 K) [189]. Therefore, it is the mechanical properties that have effectively hindered the development of (RE)BCO high temperature superconducting materials for practical applications over recent years.

There are a number of defects or features within the single grain microstructure that effectively limit the mechanical properties of the sample, including discrete RE-211 particles, macro- and micro-cracks and pores, all of which occur intrinsically during the single grain fabrication process. The mechanical properties of bulk superconductors have been reported fairly extensively over recent years, although these tend to vary significantly at different positions within a given sample. The tensile strength of sub-specimens cut from a parent bulk (RE)BCO single grain, for example, tend to be scattered widely and differ according to the nature of the test (the strength obtained from three-point bending tests has been observed to be up to three times greater than that obtained from tensile tests [190]). The fracture strength of YBCO has been reported to vary within the range of 40–200 MPa, depending on the quality of the sample. The scatter in the data has been attributed to the variation in the microstructures, including the Y-211 content and porosity density, oxygen content, orientation of the sample and the extent of cracking [191, 192]. Other measurements of the mechanical properties, such as Young's

modulus, compression strength, tensile stress, fracture toughness, hardness and Brazilian test properties have been used to probe the brittle nature of bulk (RE)BCO materials. These are summarised in the following sub-sections.

3.5.1. Effect of RE-211 on mechanical properties. RE-211 particles, which constitute the main second phase embedded within the bulk RE-123 matrix, play a critical role in determining the mechanical properties of the single grain superconductor. It has been established from microstructural analysis that cracks propagating through the sample are deviated by the RE-211 particles. This suggests that the RE-211 inclusions form an effective reinforcing material and contribute significantly to enhancing the resistance of the RE-123 phase matrix to fracture by dissipating energy via interfacial delamination and crack bridging. The mechanical properties of DyBCO, for example, are dependent strongly on the distribution of RE-211 particles within the bulk superconductor, with the homogeneity of their distribution fundamental to achieving good mechanical properties [193]. In general, the mechanical properties of (RE)BCO bulk samples vary significantly with RE-211 or secondary phase content [194–196], and a higher concentration of RE-211 helps generally to improve the mechanical properties of the single grain. For example, the average value of the Young's modulus for the DyBCO system increases with increasing Dy-211 content from 123 GPa to 133 GPa for Dy-211 concentrations of 15 mol% and 25 mol%, respectively. The fracture strength of DyBCO also increases with increasing Dy-211 concentration, with average values of 62 MPa and 87 MPa for concentrations of 15 mol% and 25 mol%. The corresponding Weibull coefficients for DyBCO with these levels of Dy-211 content are 5.1 and 15.0 [197], with a relatively narrow range of data scatter. This trend is very similar to that observed in the SmBCO system, where increasing Sm-211 content was found to enhance the mechanical properties of the sample [198]. The average value of Young's modulus for GdBCO, on the other hand, decreases at high Gd-211 concentrations from 118 GPa to 111 GPa for 33 mol% and 29 mol% Gd-211 [199]. Although increasing RE-211 content improves generally the (RE)BCO mechanical properties, there is a fundamental limitation on the extent of this improvement given the need for connectivity and optimum cross-sectional area of the superconducting RE-123 phase. The optimum RE-211 content, therefore, lies usually in the range of 20–40 wt. % for most (RE)BCO systems depending on the RE element and the particle size within the precursor powder.

3.5.2. Influence of macro- and micro cracks on mechanical properties. The mechanical properties at different orientations in a single (RE)BCO grain, such as within the a/b plane or along the c -direction, differ significantly. For example, the average values of Young's modulus and the tensile strength along the c -axis of GdBCO (37 GPa and 10 MPa, respectively) are significantly lower than those in the perpendicular a/b plane [200] due primarily to the existence of micro-cracks perpendicular to the c -axis. The average Poisson's ratio based on the transverse strain measured parallel to the c -axis (0.15) is

found to be lower than that based on the strain perpendicular to the c -axis (0.30). Three-point bending tests on specimens cut from a single YBCO grain containing 15 wt.% Ag indicate that the bending strength loading along the c -axis is lower than that perpendicular to it [200]. Specimens loaded in the direction perpendicular to the c -axis occasionally fracture catastrophically into pieces along the a/b plane [201]. The reason for the difference in mechanical behaviour for load applied in the a/b plane and the c -direction is associated with three classifications of crack in the single grain microstructure. The most common are a/b -microcracks, which are observed typically as dense lines parallel to the a/b plane, and of length less than that of the RE-211 interparticle separation. a/b -microcracks form at the site of RE-211 particles due to tangential tensile stress developed around each inclusion during cooling from the crystallisation temperature and during the RE-123 lattice uptake of oxygen. The second and the third type of cracks are the so-called a/b - and c -macro-cracks. These typically extend across larger sample areas and are formed under the combined influence of tensile stresses developed during sample oxygenation and stresses induced by the macro inhomogeneity of the RE-211 concentration [202]. It is relatively straightforward to understand these results given that the main micro- and macro-cracks form parallel to the a - b plane during the melt-processing and subsequent oxygenation of the (RE)BCO single grain.

3.5.3. Reducing and filling the pores. It is well-known that high porosity limits severely the mechanical properties of single grain (RE)BCO bulk superconductors [178, 179, 197]. As a result, considerable effort has been made to either reduce the porosity or to add secondary phase material to fill the pores. In particular, it was realised relatively early that the addition of Ag could improve the mechanical properties of the bulk samples significantly [191, 203, 204]. YBCO-Ag and SmBCO-Ag are particularly good examples [189] of samples with improved mechanical properties overall without any deterioration of their field-trapping capability or level of critical current density. Ag particles dispersed in the matrix are able to blunt crack-tips, given their ductility [191], and it is likely that they induce a compressive stress at the crack-tip to resist crack propagation [191]. It has been shown that the addition of Ag improves the mechanical properties to varying extent of all (RE)BCO systems (RE = Nd, Sm, Gd, Dy and Y, and even a combination of RE elements). The effects of Ag content on the mechanical properties of (Nd, Eu, Gd)-Ba-Cu-O [(NEG)BCO] bulk superconductors at RT, for example, have been investigated by various tensile and compressive tests. It has been concluded from these that the addition of an increasing concentration of Ag from 10% to 20% improves the average tensile strength of these samples from 26 MPa to 34 MPa. The Weibull coefficient for (NEG)BCO with 20 wt.% Ag was found to be higher than that of a sample containing 10 wt.% Ag (3.09 and 1.54, respectively). This is attributed presumably to the closure of pre-existing micro-cracks perpendicular to the c -axis in the test specimens [205]. A comparison of the mechanical behaviour of YBCO and GdBCO-15 wt.%

Ag₂O by three-point bend and transversal tensile tests at 77 K and 300 K showed that the GdBCO-Ag samples are less anisotropic and exhibit better and more homogeneous mechanical properties due to the presence of silver particles (filling the pores) in the bulk, superconducting matrix [206].

The addition of a liquid phase of an appropriate composition to the precursor powder, combined with silver, also fills the pores in (RE)BCO single grains and is another technique for improving the mechanical properties of bulk samples. YBCO containing Ag, which has very slow growth rate and is therefore very challenging to process reliably, has been fabricated successfully in the form of large, single grains by a seeded IG technique with reduced porosity [207] by adding additional liquid phase to the bottom of the pre-form pellet [208] in a relatively large scale melt process. The combined effect of providing both additional liquid and Ag during the growth process improves significantly the mechanical strength of YBCO bulk superconductors. As a result, small beams of YBCO-Ag fabricated by the IG technique were able to withstand stresses over 170 MPa before failure. This increase in failure stress is due to the combined effects of a reduction in the area occupied by pores and a reduction in the average pore size. Microstructural studies revealed that the added silver partially filled most of the pores within the sample, therefore reducing significantly both the area occupied by and the average size of the pores.

The use of a Gd₂BaO₄ (Gd210)-BaCuO₂-CuO precursor has also enabled the synthesis of very large GdBaCuO bulk single grains of up to 140 mm in diameter [71, 194, 209] that, from their observed ability to trap fields as high as 2.3 T at 77 K, appear to contain no serious cracks or flaws. In this case, the formation of a liquid phase similar to that described above enhances densification of the precursor by liquid phase sintering. As a result, the mechanical strength of the sintered precursor is increased compared to samples fabricated using a conventional Gd123-Gd211 precursor composition. This technique has significant potential for preventing the formation of cracks and pores during the texturing process of large single-grain samples. IG and TSMG processes can also be modified to reduce single grain porosity by introducing a liquid-rich phase from the bottom of pre-form pellet during MG [89, 90, 97].

Another technique to reduce porosity in the single grain is via melt-processing in pure oxygen. The porosity of DyBCO bulk superconductors melt-processed in pure oxygen is typically below 4%, compared to around 20% in conventional DyBCO single-grain bulk melt-processed in air. The minimum values of fracture toughness measured in low-porosity bulk DyBCO samples is therefore around 15% higher than in bulk samples processed in air [210]. The mechanical properties of these samples, such as Young's modulus and bending strength, are improved significantly by reducing the number of pores. As a result, a maximum value of bending strength in as-grown DyBCO bulk superconductors containing low porosity, melt-processed in 100% O₂, as high as 120 MPa (38% higher than that of DyBCO bulk melt-processed in air) has been reported [211].

Significantly, the presence of pre-drilled holes the bulk microstructure has been observed to limit porosity and reduce

the concentration of macro-cracks, resulting in enhanced mechanical properties of individual, bulk single grains whilst maintaining their ability to trap magnetic field. A maximum trapped field of 0.84 T was recorded 0.2 mm above the top surface of a thin-wall pellet (wall thickness 16 mm) at 77 K [212], which is a relatively high value compared to samples fabricated without holes. The elastic modulus of the perforated bulk samples showed an increase of more than 45% compared to that observed in standard samples. The compressive and tensile strengths are also improved significantly in samples containing artificial holes [213], suggesting there is significant potential for further enhancing the mechanical properties of bulk YBCO by filling the holes with material of appropriate, matched physical properties. Such technology would potentially enable the thermal conductivity to be optimised, which would improve the applications potential and stability of single grain (RE)BCO bulk materials. This technique could lead potentially to an improvement in superconducting properties and in applications utilising PFM, in particular.

3.5.4. Specific mechanical properties. (RE)BCO bulk superconductors are applied inevitably at low temperatures due to their T_c of around 90 K (-183 °C). However, it is considerably more difficult to measure the mechanical properties of these materials at their temperature of operation than it is at RT. Despite the significant challenges associated with low temperature characterisation, a number of effective measurements of the mechanical properties of bulk single grains have been performed at LNTs. For example, the fracture toughness, K_{IC} of YBCO and GdBCO-Ag single-grain samples at 77 K and RT was measured by performing bending tests on V-notched specimens cut from the as-processed bulk single grain. The results show that K_{IC} is scattered from 1.2 to 2.0 MPam^{1/2} at LNT and from 1.4 to 1.7 MPam^{1/2} at RT for YBCO. The measured data for GdBCO-Ag are also scattered from 1.7 to 2.1 MPam^{1/2} at LNT and from 1.3 to 2.1 MPam^{1/2} at RT. The average values of K_{IC} of the YBCO and the GdBCO-Ag bulk samples at LNT of 1.6 and 1.8 MPam^{1/2} were higher than the values observed at RT of 1.5 and 1.6 MPam^{1/2}, respectively [206, 214]. These results suggest that the mechanical properties of (RE)BCO at 77 K are at least as good as those observed at RT. It should be emphasised that the scatter in mechanical properties of (RE)BCO single grains is due to the variation in sample microstructure. The results of three-point bending tests performed under conditions of monotonically increasing and repeated loadings along the c -axis of specimens cut from a single grain SmBCO containing 10 wt.% Ag at LNT showed a scatter in Young's modulus of between 66 and 149 GPa. The maximum value of the Young's modulus in the bulk single grain was observed in the vicinity of the seed crystal. Unsurprisingly, three-point bending tests on specimens cut from a YBCO single-grain containing 15 wt.% Ag at LNT also showed a scatter in the results [200], suggesting this may be associated with pre-existing defects (such as porosity [201]) present in the single grain microstructure. Rather detailed measurements using three-point bend tests to determine the spatial distribution of the flexural strength have been

performed on bar specimens cut from four YBCO single-grain bulk superconductors [192]. A relatively large spread in the flexural strength was measured at RT, with average and standard deviation values of 49.3 MPa and 12.7 MPa, respectively, across the four bulk samples investigated. This was attributed to the systemic variation in microstructure associated with the TSMG process. In particular, the strength of these samples was shown to be related to the distribution of local porosity and Y-211 content in the parent single grain.

3.5.5. Bulk composites. In principle, it is possible to achieve trapped fields of over 20 T in bulk, single-grain HTS. There are, however, a number of barriers to realising such exceptional performance, including the large tensile stresses that develop during the magnetisation of high trapped-field magnets as a result of the Lorentz force, which leads to brittle fracture of these ceramic-like materials at high fields and, secondly, the formation of catastrophic thermal instabilities as a result of flux movement during magnetisation. Moreover, for a batch of samples nominally fabricated identically, the statistical nature of the failure mechanism associated with the intrinsic microstructure of the single grain materials, means that the best performance (i.e. trapped fields of over 17 T) cannot be attained reliably and reproducibly.

As early as 2000, Tomita and Murakami attempted the use of resin impregnation of micro-cracks and micro-pores on the surface of the single grain to improve the mechanical properties of (RE)BCO bulk superconductors [215]. This technique was modified further to include resin with filler [216] to further overcome the plastic nature of the resin, combined with mechanical reinforcement of the exterior of the bulk sample by wrapping it in a fabric of glass or carbon fibre. This combined improved reinforcement process was observed to enhance significantly both the mechanical stability and field-trapping ability of the bulk single grain, even under repeated thermal cycling and trapped field measurements at low temperatures. The combined technique was used to prepare the two sample arrangement for which the first high trapped field record of 17.2 T at 29 K was set for bulk YBCO single grains in 2003 [183, 215, 217]. This extraordinary benchmark was to set a new performance standard for these technologically important materials and to revive interest in their potential for practical applications. A novel composite arrangement consisting of a stack of two superconducting GdBCO-Ag single grains of diameter 24 mm reinforced with pre-stressed, shrink-fitted stainless steel rings was used subsequently to increase the record trapped field in a bulk (RE)BCO single grain to 17.6 T at 26 K in 2014, more than a decade later [165]. The magnetisation process of a bulk superconductor, particularly to higher fields, often damages the sample such that it cannot repeatedly trap high magnetic fields following subsequent magnetisation. An arrangement of a composite stack of two GdBCO-Ag single grain composites reinforced with stainless steel is shown in figure 32, which achieved a trapped field 16.8 T at 26 K and, subsequently a trapped field of 17.6 T at 22.5 K in a separate experiment. This magnitude of trapped

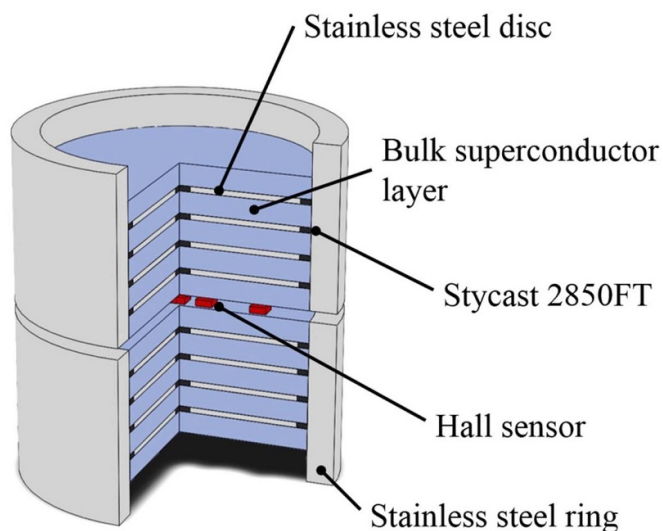


Figure 32. Schematic illustration of a partial sectional view of a bulk superconductor composite structure for trapping large fields on repeated magnetisation. The figure (reprinted from [186] with necessary permission) shows alternating layers of bulk superconductor and reinforcing stainless steel.

field is comparable with the highest trapped field to be reported [165, 186] for bulk superconducting magnets of any mechanical and chemical composition, illustrating the scale of the improvement in overall mechanical properties of superconducting (RE)BCO single grains and their potential for practical applications.

The reinforcing post-melt-processing treatments described above, which are relatively straightforward to implement, can be used to improve both the mechanical properties and the thermal stability of the composite structure, providing a promising route to reliably trapping magnetic fields of over 20 T.

4. Applications of (RE)BCO bulk superconductors

The basic materials requirement for engineering applications of the majority of bulk (RE)BCO superconductors is that the sample should be processed in the form of large, or pseudo, single grains obtained either via single-seeding or multi-seeding techniques. (RE)BCO bulk superconductors also need fundamentally to possess high critical current densities and high irreversibility fields if they are to generate properties that compete with non-superconducting materials at practical operating temperatures. Other important parameters that influence the potential to commercialise bulk superconductors include the ease of manufacturing, yield, cost, mechanical handling strength, long-term life, quality (uniformity) and availability in the appropriate geometrical forms. Potential applications employing bulk superconducting materials can be classified broadly into three categories:

(a) Utilising the force between a bulk superconductor and a permanent magnet in applications that include magnetic bearings for motors and flywheel, systems for energy storage and magnetically levitated vehicles (Maglev);

(b) Utilising the trapped magnetic field for application as quasi-permanent magnets and in portable MRI/NMR;

(c) Utilising the diamagnetic properties of superconductors to realise efficient magnetic shields.

4.1. Static/dynamic applications

HTS materials have a significant potential for MAGLEV-based applications since they self-levitate stably, in contrast to conventional permanent magnets which are intrinsically unstable, when cooled to an appropriate temperature and are exposed to a magnetic field. These applications are particularly relevant for a range of applications from ground rail transport systems to the levitation of conveyor belts in large industries or airports. Low energy consumption and negligible noise emissions are significant enabling features associated with employing HTS materials for Maglev-based applications, the potential for which has been demonstrated practically by many countries, including Japan, China, Russia, Italy and Brazil [218–220]. Particularly significant contributions to date include a HTS Maglev vehicle in 2000 for human passengers that employed YBCO single grains with a levitation capability of 635 kg [221], levitated conveyor belt systems in clean rooms where contactless transportation is a significant advantage [222] and powerful and non-contact mixers for a variety of bio- and pharma-based applications. The ability to mix relatively large charges of chemicals via magnetic coupling and without any mechanical contact has considerable potential for the production of contaminant-free vaccines and medicines. A recent version of a superconducting mixer employing two permanent magnets coupled to a superconductor via flux pinning has been shown to improve both speed of rotation and enable higher load-handling capacities [223].

The reliability and stability of operating Maglev vehicles for systems incorporating bulk (RE)BCO superconductors have achieved competitive technical levels over recent years. The combination of the generation of the opposite pole by the superconductor to that of the permanent magnet to which it is exposed and the flux pinning effect produce stable levitation of a superconductor assembly over an array of permanent magnets. A prototype Maglev was developed by Wang *et al* [224] using a guideway constructed from Nd–Fe–B magnets to levitate a vehicle incorporating 43 YBCO bulk superconductors, each of diameter 30 mm. The resulting Maglev vehicle was able to support a net weight of ~ 11 kN at a levitation height of 10 mm. A recent addition to this work was the development of Maglev-COBRA [225]. A photograph of the Maglev vehicle and its principle of operation are shown in figure 33(a).

A similar application based on the principle of magnetic levitation is used as the basis of a flywheel/magnetic bearing. The bulk superconducting bearings offer negligible rotational losses and hence enable the potential development of energy-efficient flywheels for practical applications. Flywheels employing superconducting bearings are typically up to 1000 times more efficient compared to those incorporating conventional bearings. The speed idling losses achieved via the use of superconducting bearings can be as low as 0.001% per hour [228]. The overall storage efficiency of

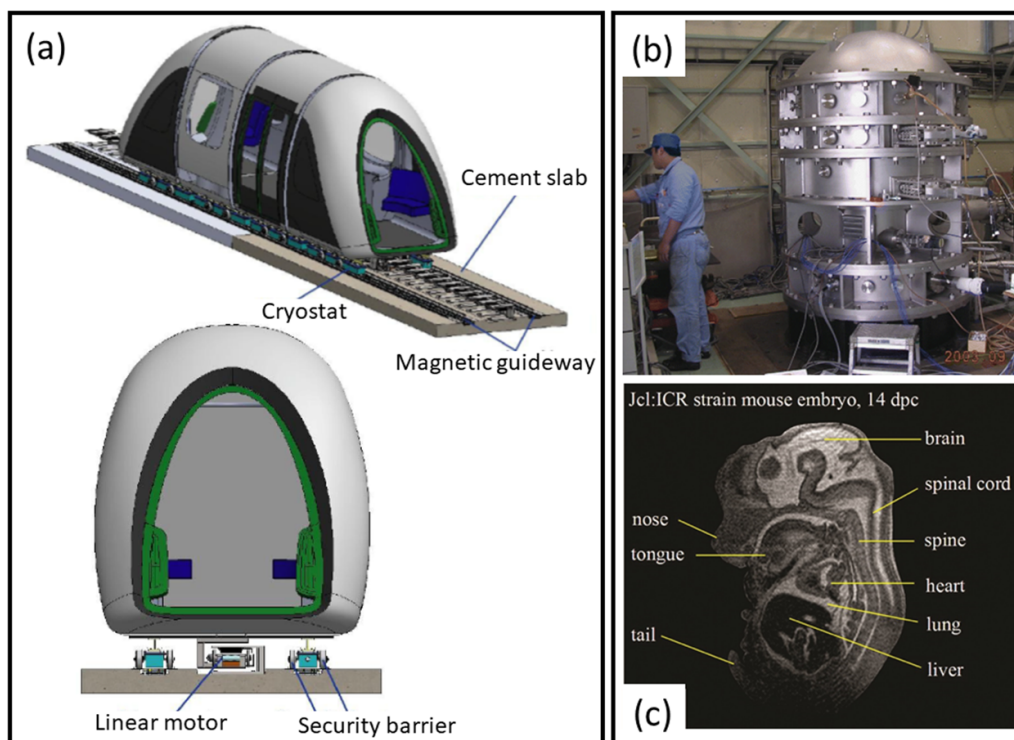


Figure 33. (a) The Maglev-COBRA vehicle and its principle of operation using levitation and guidance coils. (b) A 10 kWh flywheel levitated by bulk superconductors, and (c) a MRI image obtained from a mouse embryo using a primary field generated by stack of six annular EuBCO samples. Images in this figure are reprinted from [217, 225–227] with necessary permissions.

superconductor-based flywheels, taking into account the conduction losses of the cryostat and cooling energy losses of the bulk samples, is $\sim 90\%$, which is very significant from an applications perspective. The inertial part of the flywheel rotates typically with a rim velocity in excess of 1000 m s^{-1} , which is greatly attractive from energy density considerations. A number of examples that exemplify the significant advancements made in this area of application include are the development of 5 kWh flywheel by Strasik *et al* [229] and 10 kWh class flywheel energy storage system by Ichihara *et al* [226], which rotates at 15 000 rpm. Flywheels with rotation speeds of up to 82 000 rpm have also been achieved. A 10 kWh flywheel energy storage facility developed is shown in figure 33(b). A number of power-related applications are emerging currently as a direct result of the significant advancements achieved recently in the production of bulk, thick and thin films of (RE)BCO materials [90, 165, 177–179, 183, 184, 185, 186, 230–232] and due specifically to improved efficiencies and a significant potential reduction (by $\sim 30\%$ – 50%) in the volume and weight of superconducting components. These include, but are not limited to, fault current limiters [233–235], stator systems for wind generators [236], high power and high torque motors for aerospace applications [237], HTS fusion magnets and current leads [238], power generators [239], transformers [240] and many others. The Ampacity project [241] in Essen, Germany connecting two substations that are 1 km apart with superconducting cable (including a cable joint), operating at a core performance of 40 MVA is a good example of the advances in engineering achieved in one particular area of HTS research.

4.2. Medical-based applications

Two significant areas in medical applications where superconducting materials have been playing, and will continue to play, a dominant role are MRI and NMR. Superconductors enable the construction of lightweight, compact and portable systems in both these techniques. The sensitivity of detection depends crucially on the magnitude and stability of the applied magnetic field in MRI and NMR, and the ability of bulk superconductors to trap large magnetic fields forms the key parameter for their deployment in these applications. State of the art versions of both these devices use LTS materials, although substantial effort has been made more recently to develop prototype systems based on HTS. It is preferable to use rings or solenoids to obtain a stable, uniform and flat trapped field profile rather than the characteristic conical trapped fields generated by discs of bulk (RE)BCO. As a result, EuBCO bulk superconductors in the form of rings/solenoids have been investigated and utilised to develop an MRI-based system. Three-dimensional images of a mouse embryo have been obtained subsequently by Ogawa *et al* [227], as shown in figure 33(c). SmBCO-based bulk superconductors have also been used to develop an NMR system [242]. Furthermore, a H^1 (or proton) signal at resolution of 610 Hz has been detected at a resonance field of 2.96 T in silicone rubber. An undulator is another application where bulk superconductors were engineered into periodic structures to replicate an array of alternating dipole magnets. Recently, Calvi *et al* [243] developed a staggered array undulator based on GdBCO bulk superconductors with

alternating fields of ± 1 T at 10 K at a separation of 6 mm.

Magnetic drug delivery systems are a second class of medical-based applications that utilise the unique field-generating properties of bulk superconductors. These techniques can offer significant potential benefit to patients suffering from chronic, localised internal illness, such as tumours or cancers. In current traditional treatment techniques, patients are usually either exposed to repeated, prolonged radiation treatment and/or given oral medicines in relatively large dosages to ensure that at least a reasonable quantity reaches a localised part of the body (i.e. the site of the tumour or cancer). However, this means healthy body cells and tissues are exposed unnecessarily to high doses of medicine, often with unavoidable and excessive side effects. In the magnetic drug delivery system, the drug is attached to a biocompatible magnetic particle and the assembly is guided to the location of the tumour or cancer by an external magnetic field generated by a bulk superconductor. In this case, the magnetic field gradient (dB/dx) forms the key parameter in applying force, F , to the magnetic particle and therefore in its guidance to the location of the tumour [244, 245]. The magnetic force experienced by the particle is given by $F = A \mathbf{B} \frac{dB}{dx}$, where A is a constant and \mathbf{B} is the magnetic induction. The larger the value of field and steeper its gradient, higher the force experienced by the particle (which requires a compact, bulk superconductor and a high trapped field). Once the drug reaches the desired location, the external field is removed by increasing the operating temperature of the superconductor to above its T_c , simultaneously releasing the drug to the tumour location. This technique requires fundamentally a smaller quantity of medicine to treat the body overall, reducing significantly the dose to healthy cells and tissue and simultaneously reducing the cost of treatment and minimising side effects. Such a device based on bulk GdBCO has been developed and tested by Nishijima *et al* [244–246] who reported that the accuracy of drug navigation was better than 80%. The principle of operation of magnetically targeted drug delivery along with a device based on an arrangement of two (RE)BCO bulk superconductors is shown in figure 34(a). Magnetic separation, which is based on the same field-gradient principle, has also been proposed employing bulk superconductors. Polluted water or oil can be effectively and efficiently cleaned in multi-step cleaning processes employing a large-gradient magnetic field generated by bulk (RE)BCO superconductors. Additionally, in conventional purification systems, it is possible to remove debris accumulated in filters by treating the starting liquid with magnetic coagulants, which then cause flocs to form that are easily filtered and removed utilising the high-gradient magnetic field [247]. A prototype magnetic separation unit developed for this purpose has demonstrated efficient filtering in excess of 95%, opening a pathway for the use such mobile units for cleaning contaminated lakes and rivers.

(RE)BCO bulk superconductors are suitable for use in lightweight, compact brushless synchronous motors based on their ability to trap large, surface magnetic fields as high as 8–10 T. Operating the superconductor at a lower temperature increases the field strength significantly to provide an

enhancement in the power density and hence in the overall performance of the motor. An axial gap-type synchronous motor of 500 mm in diameter and 30 mm in length has been developed in which the rotor was composed of eight GdBCO bulk superconductors enabled rotation of 850 rpm with a power output of 10 kW. In this application, the armature coils were fixed to stators and were used to magnetise the bulk superconductors via a PFM approach. In this case, the power factor and efficiency of the reluctance motor was enhanced by the diamagnetic nature of the superconductor.

A non-invasive method of measuring flow-rate or velocity in liquids or fluids is of significant interest in the metal-processing, pharmacological and food industries both for improved performance and also to maintain hygiene standards [250]. Conventional flow-measurement techniques are based on electrical contact, which becomes challenging when the fluid or liquid is hot, non-transparent or chemically aggressive. It is possible to address these problems by employing Lorentz force velocimetry (LFV) where the magnetic field is applied perpendicular to the direction of fluid, thereby measuring the flow rate without any contact with the moving liquid [251]. The force occurring due to the relative motion between the electrically conducting medium (of conductivity σ) as a result of the application of a transverse applied magnetic field (of strength \mathbf{B}), is equivalent to the Lorentz force (\mathbf{F}_L) and is given as: $\mathbf{F}_L = \sigma u V \mathbf{B}^2$, where u is the mean flow velocity of the liquid/fluid and V is the characteristic volume. The fact that the Lorentz force scales as \mathbf{B}^2 , and hence the sensitivity of the technique, has motivated the use of superconductors as the source of magnetic field given their unique potential to generate very large values for \mathbf{B} , even in compact sample volumes. Conventional LFV employing permanent magnets or solenoid coils for liquid metals with high conductivity ($\sim 10^5$ – 10^6 S m $^{-1}$) will still generate a significant force. The only practical option for measuring the flow of slow-moving liquids or fluids with lower values of conductivity, however, is by utilising the dependency on the square of \mathbf{B} and by using single grain, bulk (RE)BCO superconductors, where the trapped field at the surface of the bulk samples can be as high as 8–10 T at 50 K.

4.3. Shielding based applications

Superconductors can function as efficient magnetic shields below certain critical fields based their ability to resist the application of magnetic field due to the Meissner effect. These shields can be of considerable importance in two different technical contexts; (a) to isolate magnetically and protect sensitive devices, such as superconducting quantum interference device magnetometers or cryogenic current comparators, where external stray magnetic field/electromagnetic noise can influence measurements critically, and, (b) to protect the external environment when operating high-field devices such as superconducting magnets. Superconductors have been found to work as efficient passive magnetic shields with performance independent of frequency and over a relatively wide frequency range (80 Hz–100 000 Hz) [252]. Shielding in these applications is provided by macroscopic current loops that

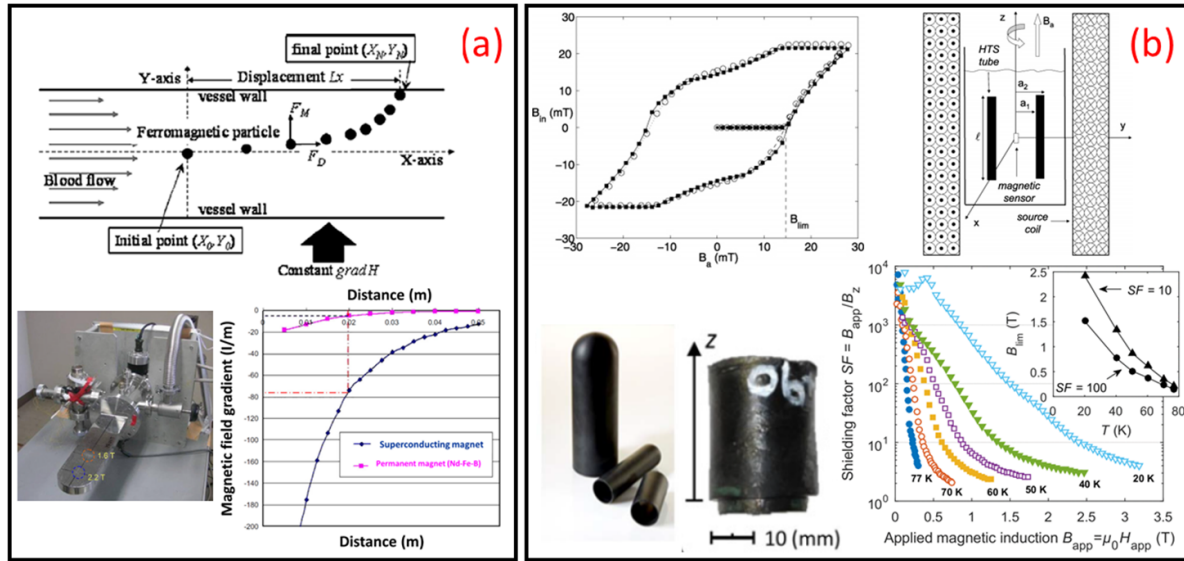


Figure 34. (a) Magnetic drug delivery system: Operating principle of a device employing two different superconductors (YBCO and GdBCO) with trapped fields of 1.6 T and 2.2 T arranged geometrically to obtain a high-gradient magnetic field. (b) Magnetic shielding performance studies carried out in YBCO and Bi-2223 tubes, indicating B_{lim} and a schematic arrangement to measure magnetic shielding performance. The SF as a function of applied magnetic field obtained in an YBCO cavity fabricated by TSMG is also shown. Images in this figure are reprinted from [1, 244, 247–249] with necessary permissions.

circulate along the wall thickness, or outer layer, of the superconducting material, which is usually constructed in the form of tube or cavity for this application. The efficiency of shielding is often measured in terms of two characteristic parameters, namely the SF and the B_{lim} . The SF is defined as the ratio of B_{appl} to the induced field inside the cavity, B_{in} , i.e. $SF \propto \frac{B_{appl}}{B_{in}}$. The limiting field is the field above which the field starts to enter the cavity, as is shown in figure 34(b). In general, the higher the values of SF and B_{lim} , the better the shield. Superconductors in the form of hollow tubes, cavities with bottom sealed, discs and plates have been studied in the context of magnetic shields [248, 253–255], with recent work focussing on (RE)BCO and Bi-2223 HTS materials fabricated in tube geometries. A value of B_{lim} value at 77 K has been observed to be around 14 mT for Bi-2223 [256] and around ~ 51 mT [249] for YBCO tubes.

Compared to the conventional ferromagnetic/mu-metal shields, where shielding performance is limited by the saturation magnetisation of the material, type-II superconductors manufactured in the form of cavities exhibit enhanced performance both at 77 K and at lower temperatures due to enhanced flux pinning strength in these materials. Typically, two aspects that aid shielding performance in superconducting bulk cylinders are: (a) a long cylindrical cavity and (b) higher current density performance. Recently, YBCO and GdBCO cylindrical cavities have been fabricated and tested for this purpose, with shielding of ~ 1.5 T at 20 K being achieved in an YBCO cylinder. A GdBCO cylinder of diameter 32 mm, bore 10 mm and height 13 mm, fabricated employing the TSIG technique, exhibited a shielding performance of 0.4 T at 77 K. Given the challenge of melt processing long cylinders of (RE)BCO material in the form of a single grain, attempts have been made to obtain thick and multiple layers

of YBCO on Ag or Ni substrates [257, 258] using electrophoretic deposition and continuation spray detonation techniques [259, 260]. This approach is useful in two ways; longer cylinders are easier to obtain and both processes typically require relatively small quantities of (RE)BCO powder for deposition as thick film layers (typically accounting to thickness in the range 10–200 μm [249, 257–261]). Of course, continued research is required to achieve good connectivity across multiple grains in thick films of (RE)BCO, although significant progress has been made by employing melt-growth based techniques under reduced atmospheres to improve connectivity. An additional merit in the use of superconductor shields is reduced weight and compactness compared to the conventional shields based on ferromagnets, such as mu-metal, although these benefits are offset to some extent by the need to cool the superconducting samples. These super-efficient magnetic shields fabricated either from bulk materials or from thick film-coated cylinders have considerable potential for application in present and future magnet accelerator projects, in particular.

The quantity, volume and mass of bulk superconductors and/or superconducting components varies from one application to another, depending on the objective, function and range of device. For example, some of the commercial producers of bulk superconductors, such as ATZ (Germany), CAN Superconductors (Czech Republic) and Nippon Steel (Japan), produce more than 1000 single grain superconducting discs annually and tonnes of superconducting powders and other related products for use in a range of applications from demonstration sets to mobile Maglev compact platforms and cryostats, high gradient bearings, sputtering targets, flywheel energy storage and others. There are more than 25 suppliers that produce LTS and HTS wires and tapes commercially,

including thick films, 1G and 2G-HTS wires and coated conductor tapes to facilitate the development of high-field superconducting magnets, fault current limiters, cables, accelerators and MRI and NMR magnets. Associated with the development of robust and continually improving fabrication methodologies for single grain (RE)BCO bulk superconductors is the prospect of new and enabling sustainable engineering technologies, raising the profile of applied superconductivity and opening-up options for a variety of novel technical devices in the short to medium-term.

5. Superconducting wires, magnets and joining techniques

Although this review mainly focusses on bulk (RE)BCO materials, a very short and brief summary on superconducting wires, magnets and associated joining techniques is provided in this section for completeness. The fabrication of long superconducting wires and tapes by economic processes for use in high-field magnets and high power cables has been a principal research and development goal since the discovery of HTS in 1986. Electromagnets with ferromagnetic cores are limited typically to generating fields of 1.6–2 T, since the ferromagnet core saturates completely within this field range and the constituent copper coils cannot support any further increase in current. Resistive magnets (for use in copper tokamaks, for example) with pulsed fields are being utilised in certain plasma physics studies, although continuous field operation is not possible using normal-conductor technology. In addition, the associated costs of maintenance, water cooling and power operations are extremely high and are not economic. As a result, superconducting magnets are the only viable option for generating continuous, dc magnetic fields >2 T over a reasonable accessible sample volume. In addition, the ability of superconducting coils to operate in persistent current mode enables stable magnetic fields to be generated, which is fundamental to a range of applications. Hence, significant effort has been dedicated to developing high quality, low resistance joints between individual superconducting tapes.

5.1. Superconducting wires and tapes

Soon after the discovery of type-II superconductors, which support a mixed/vortex state enabling the superconducting state to be maintained even in the presence of large magnetic fields, effort began worldwide to develop superconducting wires and tapes primarily with the aim of developing high field superconducting magnets and high current cables. Nb wires were used to build the first superconducting magnet that generated a magnetic field of 0.7 T at 4.2 K in 1954 at the University of Illinois [262]. Subsequently, other candidates for superconducting wires, such as MoRe, NbZr and NbTi, were investigated for use in the development of high-field magnets [263]. A Nb-Ti based superconducting magnet was developed in 1961 that generated a field of 8.8 T; this performance has been enhanced over subsequent years primarily by engineering Nb-Ti wires to generate fields of up to 20 T. A recent

record achieved in this direction is the development and successful commissioning of a whole body 11.7 T MRI magnet, using Rutherford cable with Cu/NbTi strands, achieved in 2019 as a part of Iseult project [264, 265]. To date, most superconducting magnets are made predominantly using NbTi LTS wires, which usually require liquid He as a cryogen for their operation.

Work began rapidly to develop wires and tapes for superconducting magnet technology soon after the discovery of HTS in 1986. The first generation (1G) of HTS wire and tape (mainly comprising of Bi–Sr–Ca–Cu–O (BSCCO), primarily $\text{Bi}_2\text{Sr}_2\text{Ca}_1\text{Cu}_2\text{O}_{8+x}$ (Bi-2212) material was developed initially and predominantly in the early 1990s. Bi-2212 wires produced via powder-in-tube (PIT), in particular, exhibited significant potential to generate fields of ~ 20 T at temperatures below 20 K. Ag and Ag-based alloys used to clad these wires, both of which are permeable to oxygen during both the heating and the annealing stages of the PIT process, which is crucial for controlling and optimising the superconducting properties in these materials. Typical cross-sectional micrograph of a 1G-HTS BSCCO wire is shown in figure 35(a) [266]. Superconducting wires employing Bi-2212 of length ~ 1 km were achieved prior to 2011 with engineering current densities (J_e) of 10^6 A mm $^{-2}$. J_e was improved subsequently to 10^7 A mm $^{-2}$ by reducing the porosity present within the wire via high pressure heat treatments. $\text{Bi}_2\text{Sr}_2\text{Ca}_2\text{Cu}_3\text{O}_{10+x}$ (Bi-2223) with higher T_c (108 K) also emerged as a strong candidate for the development of wires, initially in the form of short lengths for coils and current leads. Extensive research in this direction enabled production of Bi-2223 HTS wires/tapes that can now carry current in excess of 160–200 A at LNT with a corresponding J_c of ~ 50 kA cm $^{-2}$ (at 77 K, in self-field). As the value of J_c increases further at lower temperatures, many applications were explored in the temperature range 20 K–40 K.

Second generation (2G) HTS wires and tapes consisting of a sequence of thin layers, referred to generally as coated conductors, and composed mainly of RE–Ba–Cu–O (where RE = Y or Gd) were developed subsequently in the 1990s. These wires and tapes exhibited significantly improved current carrying performance and an ability to overcome the problems of flux creep observed in BSCCO, due to their higher irreversibility fields. The operation of a magnet in persistent current mode requires a very small flux flow resistivity, and this is an advantage of using (RE)BCO as the core material, given its high n -value compared to its LTS counterpart. The weak-link nature of grain boundaries is the primary challenge to the processing of (RE)BCO coated conductors, and is particularly challenging when km-long lengths of wires/tapes have to be produced on a commercial scale. The development of biaxial texture in the conductor substrate; i.e. obtaining rolling-assisted biaxially textured substrates (RABiTSTM, as proposed by Goyal *et al* [267, 268]) was the first significant development that paved the way for achieving 2G-HTS tapes. The current architecture of (RE)BCO HTS tape is rather complicated and involves the IBAD (ion beam assisted deposition) process, in which a buffer layer, the superconducting component and a number of protective layers are plated on to a flexible Hastelloy based substrate via MOCVD. Increasing the

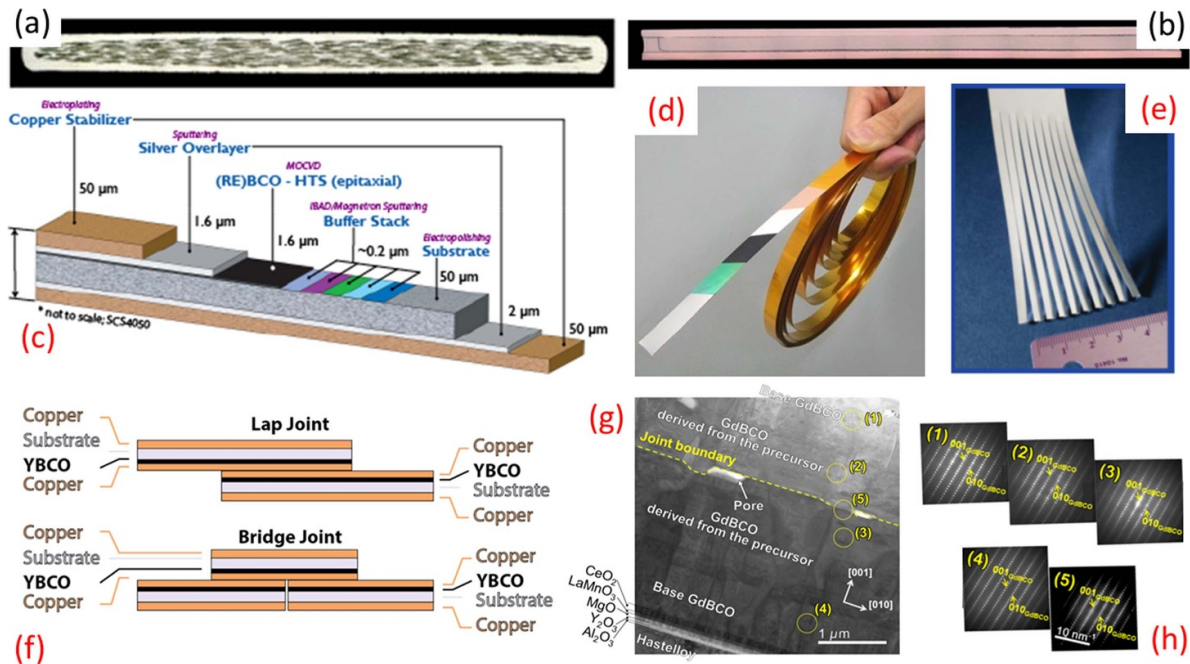


Figure 35. (a) and (b) Cross-sections of a 1st generation (1G) HTS BSCCO wire and 2G-HTS coated conductor tape respectively. (c) The architecture of a typical 2G-HTS (RE)BCO coated conductor adopted by SuperPower Inc. (d) Image of a 2G-YBCO coated conductor of Fujikura Ltd. (e) Illustration of slicing several smaller widths in a 2G-HTS coated conductor as demonstrated by American Superconductor Co. (f) Schematic illustrations of two methods of producing superconducting joints (Lap and Bridge configuration), (g) shows an optical micrograph obtained at a superconducting joint achieved via precursor films between two GdBCO coated conductor tapes (h) the SAEDPs obtained in the marked regions of (g) are shown in (h). Images shown in (a), (b), and (e)–(h) are reprinted from [266, 269, 277, 278] with necessary permissions. Images in (c) and (d) are reprinted with permissions from SuperPower Inc. and Fujikura Ltd respectively.

thickness of the (RE)BCO layer enhances significantly the current carrying ability of the coated conductor tape in the IBAD process. For example, the commercial supplier ‘American Superconductor Corporation’ produced YBCO-coated conductor with a I_c of 275 A per cm width of the tape for one layer of YBCO coating (corresponding to 1 μm thickness), which increased to 560 A per cm width for three layers of coating (corresponding to an YBCO thickness of $\sim 2 \mu\text{m}$) [269]. An example cross-section micrograph of a 2G-HTS YBCO coated conductor is shown in figure 35(b). Other deposition processes such as PLD, thermal and e-beam evaporation and liquid phase chemical deposition are also being explored and investigated as practical techniques to fabricate practical HTS conductors [270, 271]. A typical architecture adopted by SuperPower Inc. is shown in figure 35(c). Lengths of ~ 500 m (RE)BCO coated conductor are now being manufactured by tens of HTS tape producers across the world, but concentrated predominantly in the USA, Europe, China and Japan. These coated conductors can carry currents in the range 100–200 A at 77 K and in self-field for a typical tape of width 4 mm. An actual 2G-HTS coated conductor produced by Fujikura Inc. is shown in figure 35(d). Remarkably, these tapes exhibit current densities in excess of 3 MA cm^{-2} at 77 K and in self-field. It is now possible to fabricate coated conductors with typical thickness in the range 20–100 μm , width in the range 1–40 mm and lengths of up to 1 km [269–272]. Some of the advantages of these 2G-HTS tapes are that they require smaller quantities of silver (only a few micrometres thick), which is useful in terms of cost effectiveness and also facilitates better permeation of

oxygen during the annealing step. A significant advantage of 2G-HTS coated conductors is that they can be produced in a wider configuration and can be sliced subsequently into appropriate widths as required by users, which is simply impossible with 1G-HTS tapes/wires technology. An example of a sliced 2-HTS coated conductor by American Superconductor Co. is shown in figure 35(e). Further reading on HTS wires and coated conductor technology development can be found in [269–276].

5.2. Superconducting magnets

Demand for the development of high-performance superconducting magnets to be used in applications involving nuclear fusion, accelerators, MRI and NMR has grown significantly over the past decade. A number of existing, cutting-edge projects such as the LHC at CERN and evolving projects such as ITER, FCC, large tokamaks in fusion power plants and helical reactors, have a fundamental requirement for high quality and high performance superconducting magnets. This unprecedented demand is due primarily to significant advances both in HTSC wire/tape development and in cryogenic research that have enabled highly efficient coated conductors and economically viable cryostats and refrigerators to be available. The nature of the technology in large-scale applications such as ITER or FCC means that the cost of cryogenics and cooling technology are a relatively small fraction of the total cost of the superconducting magnet (typically $<2\%$ of the total

cost). Operating superconducting magnets at higher temperature, in the range 20 K–50 K for example, will also reduce the cost of operation considerably since this obviates the need for liquid helium, enabling instead the alternative use of relatively cheaper cryogenics, such as liquid hydrogen or liquid neon.

HTS ring magnets [279, 280] have been proposed and developed based on their potential to carry large current densities, with trapped fields of ~ 4.6 T having been achieved using a double-stacked arrangement. Two advantages of this configuration are (a) the size of the HTS ring magnet can be varied by stacking more ring magnets to achieve a longer column (and hence greater length:diameter aspect ratio) and (b) the magnetic field is parallel to the a - b plane, which means the field can be retained under conditions of higher current flow. These ring magnets can be of particular value in applications such as MRI or NMR, which require a more homogeneous magnetic field.

The in-field performance of (RE)BCO coated conductors has improved by orders of magnitude over the past 20 years and through successful incorporation of BaZrO₃ (BZO) or BaHfO₃ (BHO) within the conductor microstructure to form effective flux pinning sites and hence improved superconducting performance [281, 282]. For example, an engineering current density of over 5 kA mm⁻² at 4.2 K and in a field of 14 T field has been achieved in 4 μ m thick (RE)BCO coated conductor tapes and the performance has been observed to be promising up to fields of 31.2 T [231, 283]. 2G-HTS coated conductors were used to develop superconducting solenoids in 2007 that generated fields of 26.8 T [284] (i.e. well above the 23.5 T representing the higher limit possible with NbTi-Nb₃Sn based LTS magnets). In 2017, the National High Magnetic Field Laboratory (NHMFL) at Tallahassee demonstrated a field of 32 T [285], a record that was broken by the same laboratory in 2019 by recording a field of 45.5 T [286]. These results demonstrate clearly the considerable advantages of employing 2G-HTS coated conductors, frequently in combination with LTS and 1G HTS wires. Further reading on the development of high-field superconducting magnets can be found in [277, 283,–293].

Three main parameters require continued development within the context of HTS wires and tapes: (a) the improvement of the mechanical strength of these ceramic-like tapes; (b) reduction in cost and; (c) achieving long-lengths of continuous HTS wire/tape. It is anticipated that both the cost and the continuous length production issues can be addressed to a reasonable extent if economical fabrication techniques such as dip-coating or electrophoretic depositions mature sufficiently to produce coated conductors with the required superconducting properties. The third issue of the production of continuous tapes can be addressed, at least to some extent, by developing effective joining techniques. Some of these joining techniques are summarised in the following section.

5.3. Superconducting joints

The subject of superconducting joints between superconducting wires/tapes is an important topic of research required to facilitate the development of superconducting coils and

magnets, since as the production industry is not yet capable of producing long, continuous lengths of HTS conductors. The development of an effective joining technique, however, requires a combination of good science and experimental skills given that coated conductors are very thin (typically the superconducting layer is in the range of few micrometres) and are damaged easily. A good superconducting joint is required to exhibit good or strong adhesion, exhibit minimal or negligible contact resistance, degradation of critical current being minimal, and, ideally, zero and an ability to withstand both the electrical and mechanical forces present during high field or high current operation. The location of the joint remains critical in determining the overall performance of the combined length of the coated conductor. Broadly speaking, superconducting joints are being developed using four different technologies: (a) soldering, (b) ultrasonic welding, (c) diffusion binding and (d) fusion via partial melting of a superconducting layer.

Soldered joints have been studied reasonably extensively within the context of NbTi and Bi-2223/Ag wires [294–296]. Pressed or soldered joints have also been developed specifically to produce longer lengths of coated conductor for demountable fusion magnets, which involves sandwiching a thin layer of In–Sn or Pb–Sn solder between two HTS coated conductor tapes [297]. A copper/silver shunt at the joint provides an additional parallel path for the flow of current, thereby reducing the effects of heating at the position of the joint. Typical superconducting joints are shown schematically in figure 35(f). Joining via the splicing and soldering approaches has yielded joint resistances of less than 20 n Ω for an overlap of 10 cm across the two conductors being joined. The ultrasonic welding process is essentially a joining technique for metal-coated conductors to fuse together material at the overlap region of the two tapes through frictional heating generated by high frequency ultrasonic vibrations [298]. GdBCO-based, 2G-HTS coated conductors have been fused together successfully via this technique with no measurable decay in the critical current across the fused location under persistent mode operation. This development is a particularly significant step towards realising the long-lengths of HTS coated conductors that are required for coils and magnet applications. A final joining technique explored has been to partially melt the superconducting layers at the overlapping location in coated conductors and to resolidify the superconducting layer to achieve improved connectivity at the fused location [278, 299]. An example precursor layer fused between two GdBCO coated conductor tapes can be appreciated from figure 35(g). The SAED patterns obtained in the marked regions of figure 35(g) are shown in figure 35(h). This technique is generally more complicated to implement, although the results to date are encouraging and bode well from an applications perspective.

6. Summary and conclusions

In this review, we have presented significant advancements that have been made over last two decades in the fabrication of

high performance, high-quality single grain (RE)–Ba–Cu–O bulk superconductors for a variety of sustainable, high field applications. Focus has been generally on the role of several critical processing parameters that have enabled both the performance of (RE)BCO bulk superconductors to be improved and optimised whilst simultaneously improving the reliability of the single grain, bulk fabrication process. A number of important relatively recent advances in processing have been outlined as part of this review, including:

- (a) The development of the buffer technique and its integration with melt-growth based fabrication methodologies, which has been demonstrated to be advantageous in two distinct ways;
 1. the buffer pellet acts as an important gateway for the propagation of texture whilst preventing either the diffusion of the RE seed crystal element into the (RE)BCO sample or the diffusion of Ag from the main sample in the reverse direction (i.e. into the seed crystal), thereby preserving its crystallinity and texture.
 2. the reliability/yield of single grains fabrication both via TSMG and TSIG techniques has improved considerably from ~30%–50% to >90%, therefore enabling batch production of (RE)BCO bulk superconductors.
- (b) Control of RE-211 content in the TSIG approach, with the development of two-step BA-TSIG, is particularly attractive from a processing perspective since it can enable the processing of near-net shaped single grain (RE)BCO and (RE)BCO + Ag bulk superconductors.
- (c) The development of Mg-doped, NdBCO generic seed crystals and NdBCO film seeds, both of which exhibit a higher melting temperature in the range 1090 °C–1110 °C in air has enabled the fabrication of single grains of all (RE)BCO, (LRE)BCO and the equivalent Ag-containing systems. These developments in seed crystal have also enabled careful growth-rate studies to be performed both in the *a*-growth and *c*-growth regions of the anisotropic (RE)BCO, (LRE)BCO systems and Ag-containing systems.
- (d) The development of several mixed, ternary and quaternary (RE)BCO systems has enabled pathways to be established for achieving additional flux-pinning associated with lattice mismatch effects.
- (e) Important correlations of microstructural features to superconducting and mechanical properties have been made over the last two decades to facilitate control of the performance of the optimised single (RE)BCO grains and therefore transition towards practical applications.
- (f) Novel experiments including, but not limited to, interior seeding producing two aligned single grains, multi-seeding producing quasi-single grains, the fabrication of bulk superconductors with artificial holes for quicker oxygenation and rapid cooling in liquid cryogen and the processing of long, effective cavity samples for magnetic shielding applications.
- (g) Internal reinforcement of bulk (RE)BCO superconductors either via the addition of Ag and/or metal or SiC fibres has improved the mechanical strength significantly and in

excess of 40% compared to standard samples. External sample reinforcement, such as shrink-fitting, resin impregnation and composite lamination, have all been found to further improve the mechanical strength of these ceramic-like composite materials.

Trapped fields of between 8 and 10 T are now possible on the surface of individual (RE)BCO bulk single grains in the temperature range of 40 K–50 K, with fields of between 16 and 17.6 T having been achieved at 30 K reliably in a two-sample, stacked configuration. These potentially important technological developments are attributed directly to significant advancements in both processing methodology and in internal and external reinforcement. Indeed, a combination of recent reinforcement techniques, including composite lamination, material is emerging as a promising pathway to realise trapped fields in excess of 20 T, which is consistent with the predictions of theoretical simulations. The development of pulsed-field magnetisation is enabling practical and economical *in situ* magnetisation for high-field applications, in general, and for medical and pharma-related applications, in particular.


Acknowledgments

This research was supported by the projects funded by King Abdulaziz City for Science and Technology (KACST) and the Engineering and Physical Sciences Research Council (EPSRC).

ORCID iDs

Devendra K Namburi  <https://orcid.org/0000-0003-3219-2708>

Yunhua Shi  <https://orcid.org/0000-0003-4240-5543>

David A Cardwell  <https://orcid.org/0000-0002-2020-2131>

References

- [1] Durrell J H, Ainslie M D, Zhou D, Vanderbemden P, Bradshaw T, Speller S, Filipenko M and Cardwell D A 2018 Bulk superconductors: a roadmap to applications *Supercond. Sci. Technol.* **31** 103501
- [2] Cardwell D A 1998 Processing and properties of large grain (RE)BCO *Mat. Sci. Eng. B* **53** 1–10
- [3] Kammerlingh Onnes H 1911 The resistance of pure mercury at liquid helium temperatures. *Leiden Commun.* **120b** 1226
- [4] Easterling K E 1990 *Tomorrow's Materials* 2nd edn (London: Institut of Metals) p 112
- [5] Mathias B T, Geballe T H, Geller S and Corenzwit E 1954 Superconductivity of Nb₃Sn *Phys. Rev.* **95** 1435
- [6] Kunzler J E 1961 Superconductivity in high magnetic fields at high current densities *Rev. Mod. Phys.* **33** 501
- [7] Kittel C 2005 Chapter-10: superconductivity *Introduction to Solid State Physics* 8th edn (Hoboken, NJ: John Wiley)
- [8] Burns G 1992 *High Temperature Superconductivity: An Introduction* (New York: Academic Press)
- [9] Rose-Innes A C and Rhoderick E H 1994 *Introduction to Superconductivity* 2nd edn (Oxford: Elsevier Science)

- [10] Einaga M *et al* 2016 Unraveling the crystal structure of a record high-temperature superconductor (available at: <https://phys.org/news/2016-08-unraveling-crystal-high-temperature-superconductor.html>)
- [11] Testardi L R, Wernik J H and Reyer W A 1974 Superconductivity with onset above 23 K in Nb-Ge sputtered films *Solid State Commun.* **15** 1–4
- [12] Bardeen J, Cooper L N and Schrieffer J R 1957 Microscopic theory of superconductivity *Phys. Rev.* **106** 162–4
- [13] Bednorz J G and Muller K A 1986 Possible high T_c superconductivity in the Ba-La-Cu-O system *Z. Phys. B* **64** 189–93
- [14] Wu M K, Ashburn J R, Torng C J, Hor P H, Meng R L, Gao L, Huang Z J, Wang Y Q and Chu C W 1987 Superconductivity at 93 K in a new mixed-phase Y-Ba-Cu-O compound system at ambient pressure *Phys. Rev. Lett.* **58** 908
- [15] Drozdov P, Erements M I, Troyan I A, Ksenofontov V and Shylin S I 2015 Conventional superconductivity at 203 kelvin at high pressures in the sulfur hydride system *Nature* **525** 73–6
- [16] Drozdov P *et al* 2019 Superconductivity at 250 K in lanthanum hydride under high pressures *Nature* **569** 528–31
- [17] Nagamatsu J, Nakagawa N, Muranaka T, Zenitani Y and Akimitsu J 2001 Superconductivity at 39 K in magnesium diboride *Nature* **410** 63
- [18] Kamihara Y, Hiramatsu H, Hirano M, Kawamura R, Yanagi H, Kamiya T and Hosono H 2006 Iron-based layered superconductor: LaOFeP *J. Am. Chem. Soc.* **128** 10012–3
- [19] Nomura T, Kim S W, Kamihara Y, Hirano M, Sushko P V, Kato K, Takata M, Shluger A L and Hosono H 2008 Crystallographic phase transition and high- T_c superconductivity in LaFeAsO:F *Supercond. Sci. Technol.* **21** 125028
- [20] Cui Y J, Chen Y L, Cheng C H, Yang Y, Wang Y Z, Li Y C and Zhao Y 2011 Preparation of REFeAsO $_{1-x}$ F $_x$ (RE=Sm and Gd) superconductors at a relatively low temperature *J. Phys. Chem. Solids* **72** 449–52
- [21] Buzea C and Yamashita T 2001 Review of the superconducting properties of MgB $_2$ *Supercond. Sci. Technol.* **14** R115
- [22] Hänisch J, Iida K, Hühne R and Tarantini C 2019 Fe-based superconducting thin films—preparation and tuning of superconducting properties *Supercond. Sci. Technol.* **32** 093001
- [23] Josephson B D 1974 The discovery of tunnelling supercurrents *Rev. Mod. Phys.* **46** 251–4
- [24] Krabbes G, Bieger W, Schätzle P and Wiesner U 1998 Improved HTSC bulk materials: a thermodynamic approach to processing *Supercond. Sci. Technol.* **11** 144–8
- [25] Riches J D, Alarco J A, Yamashita T and Barry J C 1998 Phase evolution of the quenched melt of YBa $_2$ Cu $_3$ O $_{7-y}$ with 20 mol% Y $_2$ BaCuO $_5$ additions *Supercond. Sci. Technol.* **11** 830–6
- [26] Klemenz C and Scheel H J 1993 Liquid phase epitaxy of high T_c superconductors *J. Crystal Growth* **129** 421–8
- [27] Scheel H J and Licci F 1991 Phase diagrams and crystal growth of oxide superconductors *Thermochim. Acta* **174** 115–30
- [28] Lee B-J and Lee D N 1991 Thermodynamic evaluation for the Y $_2$ O $_3$ -BaO-CuO $_x$ system *J. Am. Ceram. Soc.* **74** 78–84
- [29] Shiohara Y and Endo A 1997 Crystal growth of bulk high T_c superconducting oxide materials *Mater. Sci. Eng.* **R19** 1–86
- [30] Murakami M 1999 *Melt Processed High Temperature Superconductors* (Singapore: World Scientific Publishing)
- [31] Lo W 2000 Recent progress in large-grain REBCO melt texturing *J. Miner. Met. Mater. Soc.* **52** 18–21
- [32] Salama K and Lee D F 1994 Progress in melt texturing of YBa $_2$ Cu $_3$ O $_x$ superconductor *Supercond. Sci. Technol.* **7** 177–93
- [33] Cardwell D A and Ginley D S (eds) 2003 *Handbook of Superconducting Materials Volume I: Superconductivity, Materials and Processes* (Cornwall: IOP Publishing Ltd)
- [34] Morita M, Takebayashi S, Tanaka M, Kimura K, Miyamoto K and Sawano K 1991 Quench and melt growth (QMG) process for large bulk superconductor fabrication *Advances in Superconductivity III* eds K Kajimura and H Hayakawa (Tokyo: Springer-Verlag) pp 733–6
- [35] Yanmaz E, Drake A, Harris I R and Abell J S 1993 Melt processing of powdered arc-cast YBa $_2$ Cu $_3$ O $_y$ materials *J. Alloys Compd.* **195** 23–6
- [36] Murakami M, Yoo S-I, Higuchi T, Sakai N, Weltz J, Koshizuka N and Tanaka S 1994 Flux pinning in melt-grown NdBa $_2$ Cu $_3$ O $_y$ and SmBa $_2$ Cu $_3$ O $_y$ superconductors *Japan. J. Appl. Phys.* **33** L715
- [37] Murakami M 1990 Melt processing of YBaCuO superconductors and critical currents *Mod. Phys. Lett. B* **4** 163–79
- [38] Jin S, Tiefel T H, Sherwood R C, Van Dover R B, Davis M E, Kammlott G W and Fastnacht R A 1988 Melt-textured growth of polycrystalline YBa $_2$ Cu $_3$ O $_{7-\delta}$ with high transport J_c at 77 K *Phys. Rev. B* **37** 7850
- [39] Murakami M, Morita M, Doi K and Miyamoto K 1989 A new process with the promise of high J_c in oxide superconductors *Japan. J. Appl. Phys.* **28** 1189
- [40] Lee D F, Selvamanickam V and Salama K 1992 Influences of Y $_2$ BaCuO $_5$ particle size and content on the transport critical current density of YBa $_2$ Cu $_3$ O $_x$ superconductor *Physica C* **202** 83–96
- [41] Dewhurst C D, Lo W, Shi Y H and Cardwell D A 1998 Homogeneity of superconducting properties in SmBa $_2$ Cu $_3$ O $_{7-\delta}$ -seeded melt processed YBCO *Mater. Sci. Eng. B* **53** 169–73
- [42] Izumi T, Nakamura Y and Shiohara Y 1993 Crystal growth mechanism of YBa $_2$ Cu $_3$ O $_y$ superconductors with peritectic reaction *J. Cryst. Growth* **128** 757–61
- [43] Lo W, Cardwell D A, Dewhurst C D and Dung S-L 1996 Fabrication of large grain YBCO by seeded peritectic solidification *J. Mater. Res.* **11** 786–94
- [44] Zhao W, Shi Y-H, Radušovská M, Dennis A R, Durrell J H, Diko P and Cardwell D A 2016 Comparison of the effects of platinum and CeO $_2$ on the properties of single grain, Sm-Ba-Cu-O bulk superconductors *Supercond. Sci. Technol.* **29** 125002
- [45] Sudhakar Reddy E, Hari Babu N, Iida K, Withnell T D, Shi Y and Cardwell D A 2005 Effect of size, morphology and crystallinity of seed crystal on the nucleation and growth of single grain of Y-Ba-Cu-O *J. Eur. Ceram. Soc.* **25** 2935–8
- [46] Namburi D K, Durrell J H, Jaroszynski J, Shi Y, Ainslie M, Huang K, Dennis A R, Hellstrom E E and Cardwell D A 2018 A trapped field of 14.3 T in Y-Ba-Cu-O bulk superconductors fabricated by buffer assisted seeded infiltration and growth *Supercond. Sci. Technol.* **31** 125004
- [47] Hlášek T, Shi Y H, Durrell J H, Dennis A R, Namburi D K, Plecháček V, Rubešová K, Cardwell D A and Jankovský O 2019 Cost-effective isothermal top-seeded melt-growth of single-domain YBCO superconducting ceramics *Solid State Sci.* **88** 74–80
- [48] Shiohara Y and Izumi T 2015 Chapter-30: crystallisation mechanisms of high critical temperature superconductors

- Handbook of Crystal Growth* 2nd edn, ed D T J Hurler (Amsterdam: Elsevier) pp 1229–75
- [49] Zhai W, Shi Y H, Durrell J H, Dennis A R and Cardwell D A 2014 The influence of Y-211 content on the growth rate and Y-211 distribution in Y–Ba–Cu–O single grains fabricated by top seeded melt growth *Cryst. Growth Des.* **14** 6367–75
- [50] Shi Y-H, Yeoh W, Dennis A R, Hari Babu N, Pathak S, Xu Z and Cardwell D A 2010 Growth rate of YBCO single grains containing Y-2411(M) *J. Phys. Conf. Ser.* **234** 012039
- [51] Congreve J V J, Shi Y H, Dennis A R and Cardwell D A 2017 Growth rate of YBCO-Ag superconducting single grains *IOP Conf. Ser.* **279** 012027
- [52] Volochová D, Diko P, Radušovská M, Antal V, Piovarči S, Zmorayová K and Šefčíková M 2012 Growth of Y123 bulk crystals in $Y_{1.5}Ba_2Cu_3O_x$ system with CeO_2 addition *J. Crystal Growth* **353** 31–4
- [53] Radusovska M, Diko P, Piovarci S, Park S-D, Jun B-H and Kim C-J 2017 Microstructure and trapped field of YBCO bulk single-grain superconductors prepared by interior seeding *Supercond. Sci. Technol.* **30** 105013
- [54] Devendra Kumar N, Shi Y-H and Cardwell D A 2015 Fabrication of bulk (RE)BCO superconductors by the infiltration and growth process: past, present and future *Superconductivity: Applications Today and Tomorrow* ed M Muralidhar (New York: Nova Publishers) pp 1–35
- [55] Li T Y, Cheng L, Yan S B, Sun L J, Yao X, Yoshida Y and Ikuta H 2010 Growth and superconductivity of REBCO bulk processed by a seed/buffer layer/precursor construction *Supercond. Sci. Technol.* **23** 125002
- [56] Chen Y, Cui X and Yao X 2015 Peritectic melting of thin films, superheating and applications in growth of REBCO superconductors *Prog. Mater. Sci.* **68** 97–159
- [57] Namburi D K, Shi Y H, Zhai W, Dennis A R, Durrell J H and Cardwell D A 2015 Buffer pellets for high-yield, top-seeded melt growth of large grain Y–Ba–Cu–O superconductors *Cryst. Growth Des.* **15** 1472–80
- [58] Shi Y, Namburi D K, Zhao W, Durrell J H, Dennis A R and Cardwell D A 2016 The use of buffer pellets to pseudo hot seed (RE)–Ba–Cu–O–(Ag) single grain bulk superconductors *Supercond. Sci. Technol.* **29** 015010
- [59] Zhou D, Xu K, Hara S, Li B, Deng Z, Tsuzuki K and Murakami M 2012 MgO buffer-layer-induced texture growth of RE–Ba–Cu–O bulk *Supercond. Sci. Technol.* **25** 025022
- [60] Zhu Y, Mu Y, Zeng L, Wang M and Yao X 2020 Progress in buffer-supported seeding architectures for reliable epitaxial growth of $REBa_2Cu_3O_{7-\delta}$ bulk cryomagnets with superior properties *Cryst. Growth Des.* **20** 7533–49
- [61] Shi Y H, Hari Babu N and Cardwell D A 2005 Development of a generic seed crystal for the fabrication of large grain (RE)–Ba–Cu–O bulk superconductors *Supercond. Sci. Technol.* **18** L13–L16
- [62] Hari Babu N, Shi Y-H, Iida K and Cardwell D A 2005 A practical route for the fabrication of large single-crystal (RE)–Ba–Cu–O superconductors *Nat. Mater.* **4** 476–80
- [63] Peng B, Cheng L, Zhuang Y, Xu H and Yao X 2014 Large size and high T_c , J_c SmBCO bulk superconductor with addition of Sm242 particles grown in air *Physica C* **496** 11–3
- [64] Xu H H, Chen Y Y, Cheng L, Yan S B, Yu D J, Guo L S and Yao X 2013 YBCO-buffered NdBCO films with higher thermal stability in seeding REBCO growth and recycling failed bulk superconductors *J. Supercond. Nov. Magn.* **26** 919–22
- [65] Shi Y, Hari Babu N, Iida K and Cardwell D A 2007 Properties of GdBCO bulk superconductors melt-processed in air using a Mg-doped Nd–Ba–Cu–O generic seed crystal *Supercond. Sci. Technol.* **20** 38–43
- [66] Shi Y, Hari Babu N, Iida K and Cardwell D A 2008 Superconducting properties of Gd–Ba–Cu–O single grains processed from a new, Ba-rich precursor compound *J. Phys. Conf. Ser.* **97** 012250
- [67] Shi Y, Hari Babu N, Iida K and Cardwell D A 2009 The effect of very high barium content in the precursor on the properties of GdBCO single grain bulk superconductors *J. Mater. Res.* **24** 10–18
- [68] Li Z, Ida T, Miki M and Izumi M 2017 Trapped flux behaviour in melt-growth GdBCO bulk superconductor under off-axis field-cooled magnetisation *IEEE Trans. Appl. Supercond.* **27** 6800604
- [69] Li J, Shi Y-H, Dennis A R, Namburi D K, Durrell J H, Yang W and Cardwell D A 2017 A novel pre-sintering technique for the growth of Y–Ba–Cu–O superconducting single grains from raw metal oxides *Supercond. Sci. Technol.* **30** 095001
- [70] Pathak L C and Mishra S K 2005 A review on the synthesis of Y–Ba–Cu–Oxide powder *Supercond. Sci. Technol.* **18** R67
- [71] Nariki S, Sakai N, Murakami M and Hirabayashi I 2006 Effect of RE_2BaCuO_5 refinement on the critical current density and trapped field of melt-textured (Gd, Y)–Ba–Cu–O bulk superconductors *Physica C* **439** 62–6
- [72] Muralidhar M, Jirsa M, Sakai N and Murakami M 2003 Progress in melt-processed (Nd–Sm–Gd) $Ba_2Cu_3O_y$ superconductors *Supercond. Sci. Technol.* **16** R1–R16
- [73] Muralidhar M, Koblischka M R, Diko P and Murakami M 2000 Enhancement of J_c by 211 particles in ternary (Nd_{0.33}Eu_{0.33}Gd_{0.33}) $Ba_2Cu_3O_y$ melt-processed superconductors *Appl. Phys. Lett.* **76** 91–3
- [74] Muralidhar M, Chauhan H S, Saitoh T, Segawa K, Kamada K and Murakami M 1997 Grain growth and superconducting properties of (Sm, Eu, Gd)–Ba–Cu–O *Physica C* **280** 200–4
- [75] Kim S-J 2006 Characterization and superconducting properties of (YSN)BCO composites made a top-seeded melt growth process *J. Ceram. Process. Res.* **7** 230–4
- [76] Reddy E S and Rajasekharan T 1998 Fabrication of textured $REBa_2Cu_3O_7/RE_2BaCuO_5$ (RE=Y, Gd) composites by infiltration and growth of RE_2BaCuO_5 pre-forms by liquid phases *Supercond. Sci. Technol.* **11** 523–34
- [77] Kim C-J, Jee Y A and Hong G-W 2000 Variables affecting the fabrication of single grain $YBa_2Cu_3O_{7-y}$ superconductors by the top-seeded melt growth process *Supercond. Sci. Technol.* **13** 709
- [78] Jiao Y L, Xiao L, Ren H T, Zheng M H and Chen Y X 2003 J_c – B characteristics for bulk single domain YBCO superconductors *Physica C* **386** 266–70
- [79] Devendra Kumar N, Rajasekharan T, Muraleedharan K, Banerjee A and Seshubai V 2010 Unprecedented current density to high fields in $YBa_2Cu_3O_{7-\delta}$ superconductor through nano-defects generated by pre-form optimization in infiltration growth process *Supercond. Sci. Technol.* **23** 105020
- [80] Fang H, Zhou Y X, Ravi-Chandar K and Salama K 2004 On the study of the liquid infiltration and seeded growth process *Supercond. Sci. Technol.* **17** 269–73
- [81] Cloots R, Koutzarova T, Mathieu J-P and Ausloos M 2005 From RE-211 to RE-123. How to control the final microstructure of superconducting single-domains *Supercond. Sci. Technol.* **18** R9–R23
- [82] Devendra Kumar N, Rajasekharan T and Seshubai V 2013 Pre-form optimization in infiltration growth process: an

- efficient method to improve the superconducting properties of $\text{YBa}_2\text{Cu}_3\text{O}_{7-\delta}$ *Physica C* **495** 55–65
- [83] Meslin S and Noudem J G 2004 Infiltration and top seeded grown mono-domain $\text{YBa}_2\text{Cu}_3\text{O}_{7-x}$ bulk superconductor *Supercond. Sci. Technol.* **17** 1324–8
- [84] Hari Babu N, Rajasekharan T, Menon L and Malik S K 1999 Infiltration-growth processing of $\text{NdBa}_2\text{Cu}_3\text{O}_{7-\delta}$ superconductor *J. Am. Ceram. Soc.* **82** 2978–84
- [85] Viswanath N V N and Rajasekharan T 1998 Refinement of insulating $\text{Sm}_2\text{BaCuO}_5$ phase and its effect on J_c in melt processed $\text{SmBa}_2\text{Cu}_3\text{O}_y$ system *Physica C* **298** 173–7
- [86] Sudhakar Reddy E, Rajasekharan T, Ravi Kumar G, Chandrasekhar Rao T V and Shani V C 1999 Microstructural and magnetic properties of textured $\text{GdBa}_2\text{Cu}_3\text{O}_y/\text{Gd}_2\text{BaCuO}_5$ composites fabricated from $\text{Gd}_2\text{BaCuO}_5$ preforms *Mat. Sci. Eng. B* **57** 179–85
- [87] Li G Z, Yang W M, Cheng X F, Fan J and Guo X 2009 A modified TSIG technique for simplifying the fabrication process of single-domain GdBCO bulks with a new kind of liquid source *J. Mater. Sci.* **44** 6423–6
- [88] Namburi D K, Shi Y H, Palmer K G, Dennis A R, Durrell J H and Cardwell D A 2016 An improved top seeded infiltration growth method for the fabrication of Y–Ba–Cu–O bulk superconductors *J. Eur. Ceram. Soc.* **36** 615–24
- [89] Namburi D K, Shi Y, Palmer K G, Dennis A R, Durrell J H and Cardwell D A 2016 Control of Y-211 content in bulk YBCO superconductors fabricated by a buffer-aided, top seeded infiltration and growth melt process *Supercond. Sci. Technol.* **29** 034007
- [90] Namburi D K, Shi Y H, Palmer K G, Dennis A R, Durrell J H and Cardwell D A 2016 A novel, two-step top seeded infiltration and growth process for the fabrication of single grain, bulk (RE)BCO superconductors *Supercond. Sci. Technol.* **29** 095010
- [91] Wang M, Yang P-T, Yang W-M, Li J-W and Hassan Q U 2015 The fabrication process of a high performance and pure *c*-axis grown GdBCO bulk superconductor with the TSMT-IG technique *Supercond. Sci. Technol.* **28** 105011
- [92] Naik S P K, Muralidhar M and Murakami M 2018 Optimization of the Dy content in single crystalline GdBCO bulk superconductors fabricated in air via top-seeded infiltration growth process *J. Supercond. Nov. Magn.* **31** 981–7
- [93] Wang M, Yang W-M, Li J-W, Feng Z-L and Yang P-T 2015 Comparison of the superconducting properties in GdBCO bulk superconductors fabricated with two different solid phases *Supercond. Sci. Technol.* **28** 035004
- [94] Li Q and Yang W-M 2015 Preparation of high quality single domain SmBCO bulks by modified TSIG method in air with new solid phase of $\text{Sm}_2\text{O}_{3+x}\text{BaCuO}_2$ *J. Alloys Compd.* **650** 610–5
- [95] Das D, Muralidhar M, Ramachandra Rao M S and Murakami M 2017 Top-seeded infiltration growth of (Y, Gd) $\text{Ba}_2\text{Cu}_3\text{O}_y$ bulk superconductors with high critical current densities *Supercond. Sci. Technol.* **30** 105015
- [96] Namburi D K, Shi Y H, Dennis A R, Durrell J H and Cardwell D A 2018 A robust seeding technique for the growth of single grain (RE)BCO and (RE)BCO–Ag bulk superconductors *Supercond. Sci. Technol.* **31** 044003
- [97] Congreve J V J, Shi Y-H, Dennis A R, Durrell J H and Cardwell D A 2017 Improvements in the processing of large grain, bulk Y–Ba–Cu–O superconductors via the use of additional liquid phase *Supercond. Sci. Technol.* **30** 015017
- [98] Abrikosov A 1957 The magnetic properties of superconducting alloys *J. Phys. Chem. Solids* **2** 199–208
- [99] Devendra Kumar N, Rajasekharan T, Gundakaram R C and Seshubai V 2011 Extensive nanotwinning: origin of high current density to high fields in preform-optimized infiltration-growth-processed $\text{YBa}_2\text{Cu}_3\text{O}_{7-x}$ superconductor *IEEE Trans. Appl. Supercond.* **21** 3612–20
- [100] Goyal A *et al* 2005 Irradiation-free, columnar defects comprised of self-assembled nanodots and nanorods resulting in strongly enhanced flux-pinning in $\text{YBa}_2\text{Cu}_3\text{O}_{7-\delta}$ films *Supercond. Sci. Technol.* **18** 1533–8
- [101] Matsumoto K and Mele P 2010 Artificial pinning center technology to enhance vortex pinning in YBCO coated conductors *Supercond. Sci. Technol.* **23** 014001
- [102] Chen S-Y, Hseih P-C, Chen I-G and Wu M-K 2004 Effect of nano-sized $\text{Sm}_2\text{BaCuO}_5$ particles addition on the pinning mechanism of Sm–Ba–Cu–O materials *J. Mater. Res.* **19** 843–50
- [103] Ullmaier H 1975 *Irreversible Properties of Type II Superconductors* ed H Ullmaier (Berlin: Springer) 41–53 Ch 3
- [104] Campbell A M and Evetts J E 1972 Flux vortices and transport currents in type II superconductors *Adv. Phys.* **21** 199–428
- [105] Rotta M, Namburi D K, Shi Y-H, Pessoa A L, Carvalho C L, Durrell J H, Cardwell D A and Zadorosny R 2019 Synthesis of Y_2BaCuO_5 nano-whiskers by a solution blow spinning technique and their successful introduction into single-grain, YBCO bulk superconductors *Ceram. Int.* **45** 3948–53
- [106] Pinmangkorn S, Miryala M, Arvapalli S S and Murakami M 2020 Enhancing the superconducting performance of melt grown bulk $\text{YBa}_2\text{Cu}_3\text{O}_y$ via ultrasonically refined Y_2BaCuO_5 without PtO_2 and CeO_2 *Mater. Chem. Phys.* **244** 122721
- [107] Cardwell D A and Hari Babu N 2008 Improved magnetic flux pinning in bulk (RE)BCO superconductors *AIP Conf. Proc.* **986** 543–50
- [108] Koblishka M R, Muralidhar M and Murakami M 2000 Flux pinning sites in melt-processed $(\text{Nd}_{0.33}\text{Eu}_{0.33}\text{Gd}_{0.33})\text{Ba}_2\text{Cu}_3\text{O}_y$ superconductors *Physica C* **337** 31–8
- [109] Muralidhar M, Sakai N, Jirsa M and Koshizuka N 2003 Vortex pinning by mesoscopic defects: a way to levitation at liquid oxygen temperature *Appl. Phys. Lett.* **83** 5005–7
- [110] Muralidhar M, Sakai N, Jirsa M, Murakami M and Koshizuka N 2003 Levitation of NEG-123 at the temperature of liquid oxygen (90.2 K) *Supercond. Sci. Technol.* **16** L46–L48
- [111] Muralidhar M, Sakai N, Jirsa M and Koshizuka N 2004 Direct observation and analysis of nanoscale precipitates in $(\text{Sm},\text{Eu},\text{Gd})\text{Ba}_2\text{Cu}_3\text{O}_y$ *Appl. Phys. Lett.* **85** 3504
- [112] Muralidhar M, Sakai N, Jirsa M, Murakami M and Hirabayashi I 2008 Record flux pinning in melt-textured NEG-123 doped by Mo and Nb nanoparticles *Appl. Phys. Lett.* **92** 162512
- [113] Muralidhar M, Tomita M, Jirsa M, Sakai N, Murakami M and Hirabayashi I 2009 Observation of record flux pinning in melt-textured NEG-123 superconductor doped by Nb, Mo, and Ti nanoparticles *Physica C* **469** 1196–9
- [114] Bartunek V, Luxa J, Sedmidubsky D, Hlasek T and Jankovsky O 2019 Microscale and nanoscale pinning centres in single-domain REBCO superconductors *J. Mater. Chem. C* **7** 13010
- [115] Dew Hughes D 1974 Flux pinning mechanisms in type II superconductors *Phil. Mag.* **30** 293–305
- [116] Nakamura M, Hirayama T, Yamada Y, Ikuhara Y and Shiohara Y 1996 Correlation between anomalous peak effects in magnetic hysteresis loop and nanoscale structure for $\text{NdBa}_2\text{Cu}_3\text{O}_{7-x}$ single-crystal superconductor *Japan. J. Appl. Phys.* **35** 3882–6

- [117] Koblishka M R, Koblishka-Veneva A and Murakami M 2004 Nanosized pinning sites in HTSC compounds *J. Supercond. Nov. Magn.* **17** 373–7
- [118] Shi Y, Durrell J H, Dennis A R, Zhang Z, Zhai W, Hari Babu N and Cardwell D A 2013 A comparison of 0°–0° and 45°–45° bridge-seeded, YBCO single grains *J. Am. Ceram. Soc.* **96** 1757–62
- [119] Tang T-W, Cao Y, Wu D-J and Xu K-X 2016 A modified multi-seeding approach for YBCO bulk superconductors using Y₂BaCuO₅ buffer process *J. Alloys Compd.* **673** 170–4
- [120] Kim C-J, Kim H-J, Jee Y A, Hong G-W, Joo J-H, Han S-C, Han Y-H, Sung T-H and Kim S-J 2000 Multiseeding with (100)/(100) grain junctions in top-seeded melt growth processed YBCO superconductors *Physica C* **338** 205–12
- [121] Sawamura M, Mortia M and Hirano H 2002 New multi-seeding method of RE–Ba–Cu–O superconductor *Physica C* **378–381** 617–21
- [122] Shi Y, Dennis A R, Zhou D, Namburi D K, Huang K, Durrell J H and Cardwell D A 2016 Factors affecting the growth of multi-seeded superconducting single grains *Cryst. Growth Des.* **16** 5110–7
- [123] Shi Y, Durrell J H, Dennis A R, Huang K, Namburi D K, Zhou D and Cardwell D A 2017 Multiple seeding for the growth of bulk GdBCO–Ag superconductors with single grain behaviour *Supercond. Sci. Technol.* **30** 015003
- [124] Werfel F N, Floegel-Delor U, Rothfeld R, Riedel T, Goebel B, Wippich D and Schirrmeister P 2012 Superconductor bearings, flywheels and transportation *Supercond. Sci. Technol.* **25** 014007
- [125] Sawamura M, Morita M and Hirano H 2004 A new method for multiseeding RE–Ba–Cu–O superconductor *Supercond. Sci. Technol.* **17** S418
- [126] Namburi D K, Shi Y-H, Ainslie M, Dennis A R, Durrell J H and Cardwell D A 2020 Buffer-assisted top-seeded infiltration and growth for fabricating dense, single-grain (RE)–Ba–Cu–O bulk superconductors *IEEJ Trans. Power Energy* **140** 148–53
- [127] Shi Y-H, Dennis A R, Huang K, Zhou D, Durrell J H and Cardwell D A 2018 Advantages of multi-seeded (RE)–Ba–Cu–O superconductors for magnetic levitation applications *Supercond. Sci. Technol.* **31** 095008
- [128] Kim C-J, Park S-D, Park H-W and Jun B-H 2016 Interior seeding for the fabrication of single-grain REBCO bulk superconductors *Supercond. Sci. Technol.* **29** 034003
- [129] Lee J-H, Park S-D, Jun B-H, Lee J S, Han S C, Han Y H and Kim C-J 2011 A buffer bridge process for growing multiple YBa₂Cu₃O_{7–y} grains from one top seed *Supercond. Sci. Technol.* **24** 055019
- [130] Shi Y, Hari Babu N, Iida K, Yeoh W K, Dennis A R, Pathak S K and Cardwell D A 2010 Batch-processed GdBCO–Ag bulk superconductors fabricated using generic seeds with high trapped fields *Physica C* **470** 685–8
- [131] Muralidhar M, Suzuki K, Fukumoto Y, Ishihara A and Tomita M 2013 Recent progress on batch processed large size LRE-123 bulk superconductors using a novel thin film Nd-123 seed *Physica C* **484** 108–11
- [132] Muralidhar M, Suzuki K, Ishihara A, Jirsa M, Fukumoto Y and Tomita M 2010 Novel seeds applicable for mass processing of LRE-123 single-grain bulks *Supercond. Sci. Technol.* **23** 124003
- [133] Plechacek V, Jirsa M, Rames M and Muralidhar M 2012 Batch production of YBCO disks for levitation applications *Phys. Proc.* **36** 538–43
- [134] Werfel F N, Floegel-Delor U, Rothfeld R, Riedel T, Wippich D, Goebel B and Schirrmeister P 2012 Bulk superconductors in mobile application *Phys. Proc.* **36** 948–52
- [135] Werfel F N, Floegel-Delor U, Riedel T, Goebel B, Rothfeld R, Schirrmeister P and Wippich D 2013 Large-scale HTS bulks for magnetic application *Physica C* **484** 6–11
- [136] Iida K, Löwe K, Kühn L, Nenkov K, Fuchs G, Krabbes G, Behr G, Holzapfel B and Schultz L 2009 Recycling process for 123-type bulk superconductors *Physica C* **469** 1153–6
- [137] Xu H H, Cheng L, Yan S B, Yu D J, Guo L S and Yao X 2012 Recycling failed bulk YBCO superconductors using the NdBCO/YBCO/MgO film-seeded top-seeded melt growth method *J. Appl. Phys.* **111** 103910
- [138] Shi Y, Namburi D K, Wang M, Durrell J H, Dennis A R and Cardwell D A 2015 A reliable method for recycling (RE)–Ba–Cu–O (RE: Sm, Gd, Y) bulk superconductors *J. Am. Ceram. Soc.* **98** 2760–6
- [139] Cardwell D A, Shi Y and Namburi D K 2020 Reliable single grain growth of (RE)BCO bulk superconductors with enhanced superconducting properties *Supercond. Sci. Technol.* **33** 024004
- [140] Pathak S K, Babu N H, Dennis A R, Iida K, Strasik M and Cardwell D A 2010 Recycling of multi-grain, melt processed bulk (RE)BCO superconductors *Supercond. Sci. Technol.* **23** 065012
- [141] Congreve J V J, Shi Y, Dennis A R, Durrell J H and Cardwell D A 2016 Microstructure and composition of primary and recycled single grains of YBCO, GdBCO–Ag, and SmBCO–Ag bulk superconductors *J. Am. Ceram. Soc.* **99** 3111–9
- [142] Di Bernardo A, Komori S, Livanas G, Divitini G, Gentile P, Cuoco M and Robinson J W A 2019 Nodal superconducting exchange coupling *Nat. Mater.* **18** 1194–200
- [143] Krabbes G, Fuchs G, Canders W-R, May H and Palka R 2006 *High Temperature Superconductor Bulk Materials: Fundamentals-Processing-Properties Control-Application Aspects* (Weinheim: Wiley-VCH) pp 68, 106
- [144] Endo A, Chauhan H S, Egi T and Shiohara Y 1996 Macrosegregation of Y₂Ba₁Cu₁O₅ particles in Y₁Ba₂Cu₃O_{7–d} crystals grown by an undercooling method *J. Mater. Res.* **11** 795–803
- [145] Diko P 2000 Growth-related microstructure of melt-grown REBa₂Cu₃O_y bulk superconductors *Supercond. Sci. Technol.* **13** 1202–13
- [146] Murakami M 1992 Processing of bulk YBaCuO *Supercond. Sci. Technol.* **5** 185–203
- [147] Chow J C L, Leung H T, Lo W and Cardwell D A 1998 Analysis of the spatial distribution of Y₂BaCuO₅ inclusions in large-grain YBa₂Cu₃O_{7–δ} *J. Mater. Sci.* **33** 1083–9
- [148] Santos L D L V, Bustamante A D, Gonzalez J C, Feijoo J L, Osorio A A, Mitrelias T, Majima Y and Barnes C H W 2010 Magnetic properties of the superconductor LaCaBaCu₃O₇ *Open Supercond. J.* **2** 19–27
- [149] Rossat-Mignod J, Regnault L P, Vettier C, Burlet P, Henry J Y and Lapertot G 1991 Investigation of the spin dynamics in YBa₂Cu₃O_{6+x}, by inelastic neutron scattering *Physica B* **169** 58–65
- [150] Breit V, Schweiss P, Hauff R, Wühl H, Claus H, Rietschel H, Erb A and Müller-Vogt G 1995 Evidence for chain superconductivity in near-stoichiometric YBa₂Cu₃O_x single crystals *Phys. Rev. B* **52** 15727–30
- [151] Zmorayova K, Diko P, Šeřčiková M, Granados X, Sandiumenge F and Obradors X 2004 Oscillation of Y₂BaCuO₅ particle concentration in the melt-grown YBaCuO bulk superconductors *J. Cryst. Growth* **270** 685–90
- [152] Diko P, Šeřčiková M, Zmorayová K, Kalmanová M, Volochová D and Piovarčí S 2012 Blocky and spheroidal

- growth in $Y_{1.5}Ba_2Cu_3O_x$ system *J. Cryst. Growth* **338** 239–43
- [153] Zmorayova K, Diko P and Krabbes G 2006 Oxygenation cracks in top seeded melt growth Y–Ba–Cu–O bulk superconductors *Physica C* **445–448** 436–9
- [154] Mei L, Boyko V S and Chan S-W 2006 Twin engineering for high critical current densities in bulk $YBa_2Cu_3O_{7-x}$ *Physica C* **439** 78–84
- [155] Antal V, Zmorayová K, Kováč J, Kavečanský V, Diko P, Eisterer M and Weber H W 2010 The influence of annealing in flowing argon on the microstructural and superconducting properties of Al doped YBCO bulks *Supercond. Sci. Technol.* **23** 065014
- [156] Dias D H N, Sotelo G G, Moysés L A, Telles L G T, Bernstein P, Kenfaui D, Aburas M, Chaud X and Noudem J G 2015 Application of textured YBCO bulks with artificial holes for superconducting magnetic bearing *Supercond. Sci. Technol.* **28** 075005
- [157] Noudem J G, Meslin S, Horvath D, Harnois C, Chateigner D, Eve S, Gomina M, Chaud X and Murakami M 2007 Fabrication of textured YBCO bulks with artificial holes *Physica C* **463–465** 301–7
- [158] Bean C P 1962 Magnetization of hard superconductors *Phys. Rev. Lett.* **8** 250–3
- [159] Gyorgy E M, Van Dover R B, Jackson K A, Schneemeyer L F and Waszczak J V 1989 Anisotropic critical currents in $Ba_2YCu_3O_7$ analyzed using an extended Bean model *Appl. Phys. Lett.* **55** 283–5
- [160] Chen D X and Goldfarb R B 1988 Magnetic susceptibility of sintered and powdered Y–Ba–Cu–O *J. Appl. Phys.* **63** 980–3
- [161] Rush J P, May-Miller C J, Palmer K G B, Rutter N A, Dennis A R, Shi Y-H, Cardwell D A and Durrell J H 2016 Transport J_c in bulk superconductors: a practical approach? *IEEE Trans. Appl. Supercond.* **26** 6800904
- [162] Vanderbemden P, Misson V, Ausloos M and Cloots R 2002 Magnetic and transport measurements on melt-textured DyBCO single domains *Physica C* **372–376** 1225–8
- [163] Kikegawa T S *et al* 2005 Measurement of critical current for bulk superconductors by transport method *Physica C* **426–431** 649–53
- [164] Fuchs G, Schatzle P, Krabbes G, Groß S, Verges P, Müller K-H, Fink J and Schultz L 2000 Trapped magnetic fields larger than 14 T in bulk $YBa_2Cu_3O_{7-x}$ *Appl. Phys. Lett.* **76** 2107–9
- [165] Durrell J H *et al* 2014 A trapped field of 17.6 T in melt-processed, bulk Gd–Ba–Cu–O reinforced with shrink-fit steel *Supercond. Sci. Technol.* **27** 082001
- [166] Fuchs G, Gruss S, Krabbes G, Schätzle P, Verges P, Müller K-H, Fink J and Schultz L 2000 High trapped fields in bulk YBCO superconductors *Advances in Solid State Physics* vol 40, ed B Kramer (Berlin: Springer) pp 685–96
- [167] Nariki S, Sakai N and Murakami M 2004 Melt-processed Gd–Ba–Cu–O superconductor with trapped field of 3 T at 77 K *Supercond. Sci. Technol.* **18** S126–30
- [168] Fujishiro H, Tateiwa T, Fujiwara A, Oka T and Hayashi H 2006 Higher trapped field over 5 T on HTSC bulk by modified pulse field magnetizing *Physica C* **445–448** 334–8
- [169] Sander M, Sutter U, Adam M and Klaser M 2002 Comparison of pulsed magnetization processes for HTS bulk parts *Supercond. Sci. Technol.* **15** 748–53
- [170] Watasaki M, Miki M, Felder B, Tsuzuki K, Sato R, Kase S, Izumi M and Ida T 2013 Trapped magnetic flux of bulk HTS magnets in the external AC magnetic field at low temperatures *IEEE Trans. Appl. Supercond.* **23** 8201604
- [171] Fujishiro H, Yokoyama K, Kaneyama M, Ikebe M, Oka T and Noto K 2005 Approach from temperature measurement to trapped field enhancement in HTSC bulks by pulse field magnetizing *Physica C* **426–431** 594–601
- [172] Fujishiro H, Hiyama T, Naito T, Yanagi Y and Itoh Y 2009 Enhancement of trapped field and total trapped flux on GdBaCuO bulk by the MMPSC + IMRA method *Supercond. Sci. Technol.* **22** 095006
- [173] Weinstein R, Liu J, Ren Y, Sawh R P, Parks D, Foster C and Obot V 1996 *Proc. 10th Anniversary HTS Workshop on Physics, Materials, and Applications* ed B Batlogg, C W Chu, W K Chu, D U Gubser and K A Muller (Singapore: World Scientific) p 625
- [174] Ainslie M D, Fujishiro H, Ujiie T, Zou J, Dennis A R, Shi Y and Cardwell D A 2014 Modelling and comparison of trapped fields in (RE)BCO bulk superconductors for activation using pulsed field magnetization *Supercond. Sci. Technol.* **27** 065008
- [175] Wipf S L 1967 Magnetic instabilities in type-II superconductors *Phys. Rev.* **161** 404–16
- [176] Yanagi Y, Itoh Y, Yoshikawa M, Oka T, Ikuta H and Mizutani U 2005 Pulsed field magnetization of a 36 mm diameter single-domain Sm–Ba–Cu–O bulk superconductor at 30, 35 and 77 K *Supercond. Sci. Technol.* **18** 839–49
- [177] Zhou D, Ainslie M D, Shi Y, Dennis A R, Huang K, Hull J R, Cardwell D A and Durrell J H 2017 A portable magnetic field of >3 T generated by the flux jump assisted, pulsed field magnetization of bulk superconductors *Appl. Phys. Lett.* **110** 062601
- [178] Gruss S, Fuchs G, Krabbes G, Verges P, Stöver G, Müller K-H, Fink J and Schultz L 2001 Superconducting bulk magnets: very high trapped fields and cracking *Appl. Phys. Lett.* **79** 3131–3
- [179] Krabbes G, Fuchs G, Canders W-R, May H and Palka R 2006 *High Temperature Superconductor Bulk Materials: Fundamentals-Processing-Properties Control-Application Aspects* (Weinheim: Wiley-VCH) pp 110–5
- [180] Sawh R-P, Weinstein R, Carpenter K, Parks D and Davey K 2013 Production run of 2 cm diameter YBCO trapped field magnets with surface field of 2 T at 77 K *Supercond. Sci. Technol.* **26** 105014
- [181] Ikuta H, Mase A, Mizutani U, Yanagi Y, Yoshikawa M, Itoh Y and Oka T 1999 Very high trapped field in melt-processed Sm–Ba–Cu–O *IEEE Trans. Appl. Supercond.* **9** 2219–22
- [182] Teshima H, Morita M, Arayashiki T, Naito T and Fujishiro H 2013 10T class trapped field properties of a large Gd–Ba–Cu–O bulk superconductor *Phys. Proc.* **45** 61–64
- [183] Tomita M and Murakami M 2003 High-temperature superconductor bulk magnets that can trap magnetic fields of over 17 tesla at 29 K *Nature* **421** 517–20
- [184] Yokoyama K and Oka T 2020 Influence of the shape of soft-iron yoke on trapped field performance of HTS bulk *IEEE Trans. Appl. Supercond.* **30** 6800105
- [185] Namburi D K, Takahashi K, Hirano T, Kamada T, Fujishiro H, Shi Y-H, Cardwell D A, Durrell J H and Ainslie M D 2020 Pulsed-field magnetisation of Y–Ba–Cu–O bulk superconductors fabricated by the infiltration growth technique *Supercond. Sci. Technol.* **33** 115012
- [186] Huang K Y *et al* 2020 Composite stacks for reliable > 17 T trapped fields in bulk superconductor magnets *Supercond. Sci. Technol.* **33** 02LT01
- [187] Ren Y, Weinstein R, Liu J, Sawh R P and Foster C 1995 Damage caused by magnetic pressure at high trapped field in quasi-permanent magnets composed of melt-textured Y–Ba–Cu–O superconductor *Physica C* **251** 15–26

- [188] Murakami M 2014 A significant leap: a trapped field of 17.6 T in melt-processed, bulk Gd–Ba–Cu–O reinforced with shrink-fit steel *Supercond. Sci. Technol.* **27** 080501
- [189] Miyamoto T, Nagashima K, Sakai N and Murakami M 2000 Mechanical properties of bulk superconductors *Supercond. Sci. Technol.* **13** 816–9
- [190] Sakai N, Mase A, Ikuta H, Seo S J, Mizutani U and Murakami M 2000 Mechanical properties of Sm–Ba–Cu–O/Ag bulk superconductors *Supercond. Sci. Technol.* **13** 770–3
- [191] Joo J, Kim J G and Nah W 1998 Improvement of mechanical properties of YBCO–Ag composite superconductors made by mixing with metallic Ag powder and solution *Supercond. Sci. Technol.* **11** 645–9
- [192] Huang K Y *et al* 2018 Spatial distribution of flexural strength in Y–Ba–Cu–O bulk superconductors *IEEE Trans. Appl. Supercond.* **28** 6801505
- [193] Mathieu J P, Cano I G, Koutzarova T, Rulmont A, Vanderbenden P, Dew-Hughes D, Ausloos M and Cloots R 2003 The contribution of 211 particles to the mechanical reinforcement mechanism of 123 superconducting single domains *Supercond. Sci. Technol.* **17** 169–74
- [194] Nariki S, Sakai N, Murakami M and Hirabayashi I 2004 Effects of Dy₂BaCuO₅ contents on microstructure and mechanical strength of Ag-added Dy–Ba–Cu–O bulk superconductors *Physica C* **412–414** 651–6
- [195] Oka T, Itoh Y, Yanagi Y, Tanaka H, Takashima S, Yamada Y and Mizutani U 1992 Critical current density and mechanical strength of YBa₂Cu₃O_{7– δ} superconducting composites containing Zr, Ag and Y₂BaCuO₅ dispersions by melt-processing *Physica C* **200** 55–64
- [196] Murakami A, Katagiri K, Kasaba K, Shoji Y, Noto K, Teshima H, Sawamura M and Murakami M 2003 Mechanical properties of Gd123 bulk superconductors at room temperature *Cryogenics* **43** 345–50
- [197] Murakami A, Miyata H, Hashimoto R and Katagiri K 2007 Effects of Dy211 content on bending mechanical properties of Dy123 bulks at room temperature *IEEE Trans. Appl. Supercond.* **17** 3059–62
- [198] Kan R, Katagiri K, Murakami A, Kasaba K, Shoji Y, Noto K, Sakai N and Murakami M 2004 Deformation and fracture behavior of Sm123 bulk superconductors by compressive loading at room temperature *IEEE Trans. Appl. Supercond.* **14** 1114–7
- [199] Katagiri K, Murakami A, Sato T, Okudera T, Sakai N, Muralidhar M and Murakami M 2002 Stress–strain characteristics and fracture surface morphology of (Sm,Gd)–Ba–Cu–O bulk superconductor *Physica C* **378–381** 722–6
- [200] Murakami A, Katagiri K, Kasaba K, Miyata H and Shoji Y 2006 Bending mechanical properties of a single-grain Y123 bulk superconductor at liquid nitrogen temperature *Physica C* **445–448** 361–5
- [201] Murakami A, Katagiri K, Miyata H, Kasaba K and Shoji Y 2006 Distribution of mechanical properties in a single-grain Sm123 bulk superconductor at liquid nitrogen temperature *IEEE Trans. Appl. Supercond.* **16** 1003–6
- [202] Diko P 2004 Cracking in melt-grown RE–Ba–Cu–O single-grain bulk superconductors *Supercond. Sci. Technol.* **17** R45–R58
- [203] Miyamoto T, Katagiri J, Nagashima K and Murakami M 1999 Effect of Ag addition on the mechanical properties of bulk superconductors *IEEE Trans. Appl. Supercond.* **9** 2066–9
- [204] Joo J, Singh J P, Warzynski T, Grow A and Poeppel R B 1994 Role of silver addition on mechanical and superconducting properties of high- T_c superconductors *Appl. Supercond.* **2** 401–10
- [205] Katagiri K, Murakami A, Kan R, Kasaba K, Noto K, Muralidhar M, Sakai N and Murakami M 2003 Effects of Ag content on the mechanical properties of (Nd,Eu,Gd)–Ba–Cu–O bulk superconductors *Physica C* **392–396** 526–30
- [206] Konstantopoulou K, Shi Y H, Dennis A R, Durrell J H, Pastor J Y and Cardwell D A 2014 Mechanical characterization of GdBCO/Ag and YBCO single grains fabricated by top-seeded melt growth at 77 and 300 K *Supercond. Sci. Technol.* **27** 115011
- [207] Iida K, Hari Babu N and Cardwell D A 2007 Silver-doped Y–Ba–Cu–O bulk superconductors fabricated by seeded infiltration and growth *Supercond. Sci. Technol.* **20** 1065–70
- [208] Congreve J V J, Shi Y, Huang K Y, Dennis A R, Durrell J H and Cardwell D A 2019 Improving mechanical strength of YBCO bulk superconductors by addition of Ag *IEEE Trans. Appl. Supercond.* **29** 6802305
- [209] Nariki S, Sakai N, Kita M, Fujikura M, Murakami M and Hirabayashi I 2006 Advances in enlargement of melt-textured Gd–Ba–Cu–O superconductors *Supercond. Sci. Technol.* **19** S500–5
- [210] Murakami M, Miyata H, Hashimoto R and Katagiri K 2008 Fracture toughness of low porosity Dy123 bulks melt-processed in pure oxygen *J. Phys. Conf. Ser.* **97** 012138
- [211] Murakami A, Miyata H, Hashimoto R, Katagiri K and Iwamoto A 2009 Evaluations of mechanical properties in Dy123 single-grain bulk superconductors with low porosity *IEEE Trans. Appl. Supercond.* **19** 2995–8
- [212] Chaud X, Kenfau D, Louradour E and Noudem J G 2012 Thin-wall bulk high temperature superconductor as a permanent cryomagnet *IEEE Trans. Appl. Supercond.* **22** 6800304
- [213] Hlášek T, Huang K Y, Esnoz-Larraya J, Plecháček V, Durrell J, Valiente-Blanco I and Cardwell D A 2019 Enhanced mechanical properties of single-domain YBCO bulk superconductors processed with artificial holes *IEEE Trans. Appl. Supercond.* **29** 8400704
- [214] Katagiri K, Sato T, Murakami A, Kasaba K, Shoji Y, Noto K, Teshima H and Sawamura M 2005 Fracture toughness of REBaCuO bulk superconductor at liquid nitrogen temperature *Physica C* **426–431** 709–13
- [215] Tomita M and Murakami M 2000 Improvement of the mechanical properties and durability of bulk superconductors with resin impregnation *Physica C* **341–348** 2443–4
- [216] Tomita M, Murakami M, Sawa K and Tachi Y 2001 Effect of resin impregnation on trapped field and levitation force of large-grain bulk Y–Ba–Cu–O superconductors *Physica C* **357–360** 690–3
- [217] Murakami M 2007 Processing and applications of bulk RE–Ba–Cu–O superconductors *Int. J. Appl. Ceram. Technol.* **4** 225–41
- [218] Wang J *et al* 2002 The first man-loading high temperature superconducting Maglev test vehicle in the world *Physica C* **378–381** 809–14
- [219] Sotelo G G, Dias D H N, De Andrade R Jr and Stephan R M 2011 Tests on a superconductor linear magnetic bearing of a full-scale MagLev vehicle *IEEE Trans. Appl. Supercond.* **21** 1464–8
- [220] Sotelo G G, Dias D H N, Machado O J, David E D, De Andrade R Jr and Stephan R M 2010 Experiments in a real scale maglev vehicle prototype *J. Phys. Conf. Ser.* **234** 032054
- [221] Zheng J, Deng Z G, Wang L L, Liu L, Zhang Y, Wang S and Wang J 2007 Stability of the MagLev vehicle model using bulk high T_c superconductors at low speed *IEEE Trans. Appl. Supercond.* **17** 2103–6

- [222] Minami H and Yuyama J 1995 Construction and performance test of a magnetically levitated transport system in vacuum using high- T_c superconductors *Japan. J. Appl. Phys.* **34** 346–9
- [223] Koyama F, Akiyama S and Murakami M 2006 Developments of superconducting mixers for medical applications *Supercond. Sci. Technol.* **19** S572–4
- [224] Wang J S, Wang S Y, Ren Z Y, Jiang H, Zhu M, Wang X R, Shen X M and Song H H 2003 Experiment results of high temperature superconducting MagLev vehicle *Physica C* **386** 431–7
- [225] Sotelo G G, Dias D H N, Motta E S, Sass F, Ferreira A C, De Andrade R Jr and Stephan R M 2012 Operation tests of a full scale superconducting MagLev vehicle unit *Phys. Proc.* **36** 943–7
- [226] Ichihara T *et al* 2005 Application of superconducting magnetic bearings to a 10 kWh-class flywheel energy storage system *IEEE Trans. Appl. Supercond.* **15** 2245–8
- [227] Ogawa K, Nakamura T, Terada Y, Kose K and Haishi T 2011 Development of a magnetic resonance microscope using a high T_c bulk superconducting magnet *Appl. Phys. Lett.* **98** 234101
- [228] Hull J R, Mulcahy T M and Labataille J F 1997 Velocity dependence of rotational loss in Evershed-type superconducting bearings *Appl. Phys. Lett.* **70** 655–7
- [229] Strasik M *et al* 2007 Design, fabrication, and test of a 5-kWh/100-kW flywheel energy storage utilizing a high-temperature superconducting bearing *IEEE Trans. Appl. Supercond.* **17** 2133–7
- [230] Knoth K, Hühne R, Oswald S, Schultz L and Holzapfel B 2005 Highly textured $\text{La}_2\text{Zr}_2\text{O}_7$ buffer layers for YBCO-coated conductors prepared by chemical solution deposition *Supercond. Sci. Technol.* **18** 334–9
- [231] Majkic G, Pratap R, Xu A, Galstyan E, Higley H C, Prestemon S O, Wang X, Abraimov D, Jaroszynski J and Selvamannickam V 2018 Engineering current density over 5 kA mm^{-2} at 4.2 K, 14 T in thick film REBCO tapes *Supercond. Sci. Technol.* **31** 10LT01
- [232] Opherden L *et al* 2016 Large pinning forces and matching effects in $\text{YBa}_2\text{Cu}_3\text{O}_{7-\delta}$ thin films with $\text{Ba}_2\text{Y}(\text{Nb}/\text{Ta})\text{O}_6$ nano-precipitates *Sci. Rep.* **6** 21188
- [233] Noe M and Steurer M 2007 High-temperature superconductor fault current limiters: concepts, applications, and development status *Supercond. Sci. Technol.* **20** R15–R29
- [234] Kraemer H-P *et al* 2012 Superconducting fault current limiter for transmission voltage *Phys. Proc.* **36** 921–6
- [235] Kreutz R, Bock J, Breuer F, Juengst K-P, Kleimaier M, Klein H U, Krischel D, Noe M, Steingass R and Weck K H 2005 System technology and test of CURL 10, a 10 kV, 10 MVA resistive high- T_c superconducting fault current limiter *IEEE Trans. Appl. Supercond.* **15** 1961–4
- [236] Liu Y, Ou J, Schreiner F, Lao M, Noe M and Doppelbauer M 2018 Design of a superconducting DC demonstrator for wind generators *IEEE Trans. Energy Convers.* **33** 1955–64
- [237] Masson P J and Luongo C A 2005 High power density superconducting motor for all-electric aircraft propulsion *IEEE Trans. Appl. Supercond.* **15** 2226–9
- [238] Demko J A, Sauers I, James D R, Gouge M J, Lindsay D, Roden M, Tolbert J, Willen D, Traeholt C and Nielsen C T 2007 Triaxial HTS cable for the AEP Bixby project *IEEE Trans. Appl. Supercond.* **17** 2047–50
- [239] Lloberas J, Sumper A, Sanmarti M and Granados X 2014 A review of high temperature superconductors for offshore wind power synchronous generators *Renew. Sustain. Energy Rev.* **38** 404–14
- [240] Hellmann S, Abplanalp M, Elschner S, Kudymow A and Noe M 2019 Current limitation experiments on a 1MVA-class superconducting current limiting transformer *IEEE Trans. Appl. Supercond.* **29** 5501706
- [241] Stemmler M, Merschel F, Noe M and Hobl A 2013 AmpaCity-Installation of advanced superconducting 10 kV system in city center replaces conventional 110 kV cables *IEEE Int. Conf. on Applied Superconductivity and Electromagnetic Devices* p 14199323
- [242] Nakamura T, Itoh Y, Yoshikawa M, Oka T and Uzawa J 2007 Development of a superconducting magnet for nuclear magnetic resonance using bulk high-temperature superconducting materials *Concepts Magn. Reson. B* **31B** 65–70
- [243] Calvi M, Ainslie M D, Dennis A, Durrell J H, Hellmann S, Kittel C, Moseley D A, Schmidt T, Shi Y and Zhang K 2020 A GdBCO bulk staggered array undulator *Supercond. Sci. Technol.* **33** 014004
- [244] Nishijima S, Mishima F, Terada T and Takeda S 2007 A study on magnetically targeted drug delivery system using superconducting magnet *Physica C* **463–465** 1311–4
- [245] Hayashi S, Mishima F, Akiyama Y and Nishijima S 2011 Study on high gradient magnetic separation for selective removal of impurity from highly viscous fluid *IEEE Trans. Appl. Supercond.* **21** 2055–8
- [246] Saho N, Mizumori T, Nishijima N, Murakami M and Morita M 2012 High- T_c bulk-superconductor-based membrane-magnetic separation for water purification *Processing of High Temperature Superconductors* ed A Goyal, W Wong-Ng, M Murakami and P Judith Driscoll (New York: Wiley) p 325–35
- [247] Takeda S, Mishima F, Fujimoto S, Izumi Y and Nishijima S 2007 Development of magnetically targeted drug delivery system using superconducting magnet *J. Magn. Magn. Mater.* **311** 367–71
- [248] Denis S, Dusoulier L, Dirickx M, Vanderbemden P, Cloots R, Ausloos M and Vanderheyden B 2007 Magnetic shielding properties of high-temperature superconducting tubes subjected to axial fields *Supercond. Sci. Technol.* **20** 192
- [249] Wéra L, Fagnard J-F, Namburi D K, Shi Y, Vanderheyden B and Vanderbemden P 2017 Magnetic shielding above 1 T at 20 K with bulk, large grain YBCO tubes made by buffer-aided top seeded melt growth *IEEE Trans. Appl. Supercond.* **27** 6800305
- [250] Hirota Y, Mishima F, Akiyama Y and Nishijima S 2010 Drug delivery using an embedded ferromagnetic needle and external magnets *IEEE Trans. Appl. Supercond.* **20** 826–8
- [251] Minchenya V, Karcher C, Kolesnikov Y and Thess A 2011 Calibration of the Lorentz force flowmeter *Flow Meas. Instrum.* **22** 242–7
- [252] Niculescu H, Schmidmeier R, Topolski B and Gielisse P J 1994 Shielding effects in ceramic superconductors *Physica C* **229** 105–12
- [253] Claycomb J 1999 *Magnetic Shields Applied Superconductivity: Handbook on Devices and Applications* vol 1, ed P Seidel (New York: Wiley) pp 780–806
- [254] Fagnard J F, Elschner S, Bock J, Dirickx M, Vanderheyden B and Vanderbemden P 2010 Shielding efficiency and E(J) characteristics measured on large melt cast Bi-2212 hollow cylinders in axial magnetic fields *Supercond. Sci. Technol.* **23** 095012
- [255] Rabbers J J, Oomen M P, Bassani E, Ripamonti G and Giunchi G 2010 Magnetic shielding capability of MgB_2 cylinders *Supercond. Sci. Technol.* **23** 125003
- [256] Tomkow L, Cizek M and Chorowski M 2015 Combined magnetic screen made of Bi-2223 bulk cylinder and YBCO tape rings: modeling and experiments *J. Appl. Phys.* **117** 043901
- [257] Devendra Kumar N, Closset R, Wera L, Cloots R, Vanderbemden P and Vertruyen B 2015 Magnetic

- shielding performances of $\text{YBa}_2\text{Cu}_3\text{O}_{7-\delta}$ -coated silver tubes obtained by electrophoretic deposition *Supercond. Sci. Technol.* **28** 015007
- [258] Closset R, Kumar N D, Wera L, Dellicour A, Henrist C, Boschini F, Cloots R, Vanderbemden P and Vertruyen B 2014 $\text{YBa}_2\text{Cu}_3\text{O}_{7-\delta}$ thick films for magnetic shielding: electrophoretic deposition from butanol-based suspension *Mater. Lett.* **119** 154–6
- [259] Denis S, Grenzi G, Dusoulier L, Cloots R, Vanderbemden P, Vanderheyden B, Dirickx M and Ausloos M 2006 Characterisation of the magnetic shielding properties of YBaCuO thick films prepared by electrophoretic deposition on silver substrates *J. Phys.* **43** 509–12
- [260] Pavese F, Bianco M, Andreone D, Cresta R and Rellecati P 1992 Magnetic shielding properties of $\text{YBa}_2\text{Cu}_3\text{O}_{7-x}$ thick films deposited on silver cylinders with the continuous detonation spray technique *Physica C* **204** 1–7
- [261] Dusoulier L, Denis S, Vanderbemden P, Dirickx M, Ausloos M, Cloots R and Vertruyen B 2006 Preparation of $\text{YBa}_2\text{Cu}_3\text{O}_{7-x}$ superconducting thick films by the electrophoretic deposition method *J. Mater. Sci.* **41** 8109–14
- [262] Yntema G B 1955 Superconducting winding for electromagnets *Phys. Rev.* **98** 1197
- [263] Scanlan R M, Malozemoff A P and Larbalestier D C 2004 Superconducting materials for large scale applications *Proc. IEEE* **92** 1639–54
- [264] Quettier L *et al* 2017 Iseult/INUMAC whole body 11.7 T MRI magnet *IEEE Trans. Appl. Supercond.* **27** 4300204
- [265] (Available at: www.cea.fr/english/Pages/News/Iseult-MRI-Magnet-Record.aspx) 2019 11.7 teslas: The World-Record Magnetic Field Generated by a Human MRI Magnet
- [266] Nakashima T, Kobayashi S, Kagiya T, Yamazaki K, Kikuchi M, Yamade S, Hayashi K, Sato K, Osabe G and Fujikami J 2012 Overview of the recent performance of DI-BSCCO wire *Cryogenics* **52** 713–8
- [267] Goyal A *et al* 1997 Conductors with controlled grain boundaries: an approach to the next generation, high temperature superconducting wire *J. Mater. Res.* **12** 2924–40
- [268] Goyal A *et al* 1998 High critical current density $\text{YBa}_2\text{Cu}_3\text{O}_x$ tapes using the RABiTs approach *J. Supercond.* **11** 481–7
- [269] Malozemoff A P *et al* 2008 Progress in high temperature superconductor coated conductors and their applications *Supercond. Sci. Technol.* **21** 034005
- [270] Erbe M, Cayado P, Freitag W, Ackermann K, Langer M, Meledin A, Hänisch J and Holzapfel B 2020 Comparative study of CSD-grown REBCO films with different rare earth elements: processing windows and T_c *Supercond. Sci. Technol.* **33** 094002
- [271] Lao M *et al* 2019 In-field performance and flux pinning mechanism of pulsed laser deposition grown $\text{BaSnO}_3/\text{GdBa}_2\text{Cu}_3\text{O}_{7-\delta}$ nanocomposite coated conductors by SuperOx *Supercond. Sci. Technol.* **32** 094003
- [272] Rong C C, Barnes P N, Levin G A, Miller J D, Santosusso D J and Fitzpatrick B K 2015 Investigation of the relaxation of persistent current in superconducting closed loops made out of YBCO coated conductors *IEEE Trans. Appl. Supercond.* **25** 8200805
- [273] Goyal A (ed) 2005 *Second-Generation HTS Conductors* (New York, Boston: Kluwer Academic Publishers)
- [274] Kang S *et al* 2006 High-performance high- T_c superconducting wires *Science* **311** 1911–4
- [275] Obradors X and Puig T 2014 Coated conductors for power applications: materials challenges *Supercond. Sci. Technol.* **27** 044003
- [276] Muzzi L, De Marzi G, Di Zenobio A and Della Corte A 2015 Cable-in-conduit conductors: lessons from the recent past for future developments with low and high temperature superconductors *Supercond. Sci. Technol.* **28** 053001
- [277] Senatore C, Alessandrini M, Lucarelli A, Tediosi R, Uglietti D and Iwasa Y 2014 Progresses and challenges in the development of high-field solenoidal magnets based on RE123 coated conductors *Supercond. Sci. Technol.* **27** 103001
- [278] Miyajima T *et al* 2019 Microstructures of superconducting joint between $\text{GdBa}_2\text{Cu}_3\text{O}_y$ -coated conductors via additionally deposited precursor films *Japan. J. Appl. Phys.* **58** 050913
- [279] Patel A, Hahn S, Voccio J, Baskys A, Hopkins S C and Glowacki B A 2017 Magnetic levitation using a stack of high temperature superconducting tape annuli *Supercond. Sci. Technol.* **30** 024007
- [280] Ali M Z, Zheng J, Huber F, Zhang Z, Yuan W and Zhang M 2020 4.6 T generated by a high-temperature superconducting ring magnet *Supercond. Sci. Technol.* **33** 04LT01
- [281] Pahlke P *et al* 2016 Reduced J_c anisotropy and enhanced in-field performance of thick BaHfO_3 -doped $\text{YBa}_2\text{Cu}_3\text{O}_{7-\delta}$ films on ABAD-YSZ templates *IEEE Trans. Appl. Supercond.* **26** 6603104
- [282] Erbe M *et al* 2015 BaHfO_3 artificial pinning centres in TFA-MOD-derived YBCO and GdBCO thin films *Supercond. Sci. Technol.* **28** 114002
- [283] Namburi D K 2020 (RE)BCO coated conductors with BHO exhibiting promising in-field critical current performance up to fields of 31.2 T: a significant step forward towards the development of all (RE)BCO large field magnets *Supercond. Sci. Technol.* **33** 090502
- [284] Hazelton D W and Selvamanickam V 2009 SuperPower's YBCO coated high-temperature superconducting (HTS) wire and magnet applications *Proc. IEEE* **97** 1831–6
- [285] NHMFL press release 2017 New world-record magnet fulfills superconducting promise: 32 T All-Superconducting magnet (available at: <https://nationalmaglab.org/news-events/news/new-world-record-magnet-fulfills-superconducting-promise>)
- [286] Hahn S *et al* 2019 45.5-tesla direct-current magnetic field generated with a high-temperature superconducting magnet *Nature* **570** 496–9
- [287] Lvovsky Y, Stautner E-W and Zhang T 2013 Novel technologies and configurations of superconducting magnets for MRI *Supercond. Sci. Technol.* **26** 093001
- [288] Parizh M, Lvovsky Y and Sumption M 2016 Conductors for commercial MRI magnets beyond NbTi: requirements and challenges *Supercond. Sci. Technol.* **30** 014007
- [289] Borgnolutti F, Badel A, Benkel T, Chaud X, Debray F, Fazilleau P, Lecrevisse T and Tixador P 2016 Design study of a 10-T REBCO insert solenoid *IEEE Trans. Appl. Supercond.* **26** 4600405
- [290] Song J-B, Chaud X, Borgnic B, Debray F, Fazilleau P and Lecrevisse T 2019 Construction and test of a 7 T metal-as-insulation HTS insert under a 20 T high background magnetic field at 4.2 K *IEEE Trans. Appl. Supercond.* **29** 4601705
- [291] Benkel T, Miyoshi Y, Chaud X, Badel A and Tixador P 2017 REBCO tape performance under high magnetic field *Eur. Phys. J. Appl. Phys.* **79** 30601
- [292] Nishijima G *et al* 2018 International round robin test for critical current measurement of RE–Ba–Cu–O superconducting tapes *IEEE Trans. Appl. Supercond.* **28** 6601205
- [293] Van Der Laan D C *et al* 2020 A CORC® cable insert solenoid: the first high-temperature superconducting insert

- magnet tested at currents exceeding 4 kA in 14 T background magnetic field *Supercond. Sci. Technol.* **33** 05LT03
- [294] Brittles G D, Mousavi T, Grovenor C R M, Aksoy C and Speller S C 2015 Persistent current joints between technological superconductors *Supercond. Sci. Technol.* **28** 093001
- [295] Mousavi T, Aksoy C, Grovenor C R M and Speller S C 2015 Microstructure and superconducting properties of Sn–In and Sn–In–Bi alloys as Pb-free superconducting solders *Supercond. Sci. Technol.* **29** 015012
- [296] Mousavi T, Davies T, Melhem Z, Grovenor C R M and Speller S C 2018 Development of superconducting soldered joints between Bi-2212/Ag wires *IEEE Trans. Appl. Supercond.* **28** 6400303
- [297] Tsui Y, Surrey E and Hampshire D 2016 Soldered joints—an essential component of demountable high temperature superconducting fusion magnets *Supercond. Sci. Technol.* **29** 075005
- [298] Shin H-S, Nisay A, De Leon M B and Dedicataria M J 2015 Joining of REBCO coated conductor tapes using ultrasonic welding method *IEEE Trans. Appl. Supercond.* **25** 6602205
- [299] Park Y, Lee M, Ann H, Choi Y H and Lee H 2014 A superconducting joint for $\text{GdBa}_2\text{Cu}_3\text{O}_{7-\delta}$ -coated conductors *NPG Asia Mater.* **6** 98